

DIPLOMARBEIT

Correlations in multi-orbital electronic systems: parquet equations

ausgeführt zur Erlangung
des akademischen Grades des

Diplomingenieurs (Dipl.-Ing.)

im Rahmen des Studiums der
Technischen Physik

am Institut für Festkörperphysik
an der Technischen Universität Wien

unter der Anleitung von
Univ. Prof. Dr. Karsten Held
Univ. Ass. Dr. Anna Kauch

durch

Julian Mangott, BSc

Matrikelnummer 01627716

Serfaus, März 2022

Unterschrift Verfasser

Unterschrift Betreuer

Eidesstattliche Erklärung

Hiermit erkläre ich an Eides statt, dass ich die vorliegende Arbeit selbständig verfasst, andere als die angegebenen Quellen sowie Hilfsmittel nicht benutzt, und die den benutzten Quellen wörtlich und inhaltlich entnommenen Stellen als solche kenntlich gemacht habe.

Datum, Ort

Unterschrift

Statutory declaration

Hereby I declare in lieu of oath, that I wrote this thesis myself, using only literature cited in this volume. If text passages from sources are used literally, they are marked as such.

Date, Place

Signature

KURZFASSUNG

In vorliegender Arbeit wird der Parkettformalismus auf das Hubbardmodell im multi-orbitalen Fall angewendet. Dieser aus den 1960er-Jahren stammende Formalismus [2, 3] ermöglicht die selbstkonsistente Berechnung von Zwei-Teilchen-Korrelationsfunktionen ohne Annahme eines dominanten Streukanals.

Die Parkettmethode besteht im Wesentlichen aus der Iteration vierer Gleichungen, nämlich der Bethe-Salpeter-, Parkett-, Schwinger-Dyson- und der Dyson-Gleichung. Da letztlich Zwei-Teilchen-Korrelationsfunktionen berechnet werden, die von vier Spin-Orbitalen und je drei Frequenzen und Wellenvektoren abhängen, sind die Anforderungen hinsichtlich Speicherbedarf einer Implementierung enorm. Erst in den letzten Jahren wurden nennenswerte Fortschritte hinsichtlich Parallelisierung und Speichereffizienz erzielt und erste physikalische Systeme mit dem Parkettformalismus etwa mit *victory* [13], einer Implementierung für das Hubbardmodell für ein einzelnes Orbital, behandelt.

Für den allgemeineren Fall des multi-orbitalen Hubbardmodells gibt es nach Wissen des Verfassers noch keine Implementierung. Die Gleichungen für den Fall der zeitlichen Translations- und der $SU(2)$ -Symmetrie werden in dieser Diplomarbeit erstmals abgeleitet und in einem Fortran-Programm namens `multi-orbital-parquet` implementiert. Abschließend wird das Programm auf einfache physikalische Systeme angewendet: auf das Hubbardmodell im atomaren Limes und das Benzenmolekül. `multi-orbital-parquet` wurde so konzipiert, dass eine Erweiterung auf Gittersysteme, die eine zusätzliche Wellenvektor-Abhängigkeit erforderlich macht, möglichst einfach durchführbar ist.



Die approbierte gedruckte Originalversion dieser Diplomarbeit ist an der TU Wien Bibliothek verfügbar
The approved original version of this thesis is available in print at TU Wien Bibliothek.

ABSTRACT

In the present thesis, the parquet formalism is applied to the multi-orbital Hubbard model. This formalism dating from the 1960s [2, 3] enables the self-consistent calculation of two-particle correlation functions without assuming a dominant scattering channel.

The parquet method essentially consists of the iteration of four equations, namely the Bethe-Salpeter, Parquet, Schwinger-Dyson and Dyson equations. Since two-particle correlation functions are calculated, which depend on four spin orbitals and three frequencies and momenta, the memory requirements of an implementation are substantial. Only in the last few years significant progress has been made in terms of parallelization and memory efficiency. First physical systems have been studied for example with *victory* [13], an implementation for the single-orbital Hubbard model.

To the author's knowledge, there is still no implementation for the general case of the multi-orbital Hubbard model. The required equations for time-translational and SU(2) symmetry are derived for the first time in this thesis and are implemented in a Fortran program called `multi-orbital-parquet`. Finally, this program is tested on simple physical systems: the atomic-limit Hubbard model and the benzene molecule. The structure of the code allows for direct extension to lattice systems which requires including the momentum dependence.



Die approbierte gedruckte Originalversion dieser Diplomarbeit ist an der TU Wien Bibliothek verfügbar
The approved original version of this thesis is available in print at TU Wien Bibliothek.

CONTENTS

*Sections marked with * contain the author's original research.*

Kurzfassung	I
Abstract	III
1 Introduction	1
2 Correlation functions and vertices	5
2.1 Multi-orbital Hubbard model	5
2.2 Green's function	9
2.2.1 Properties	10
2.2.2 Symmetry relations	12
2.3 Dyson equation	16
2.4 Full two-particle vertex	17
2.4.1 Properties	18
2.4.2 Symmetry relations*	19
2.5 Generalized susceptibility	22
3 Multi-orbital parquet equations	25
3.1 General case	25
3.1.1 Two-particle reducibility	25
3.1.2 Schwinger-Dyson equation	31
3.2 Time-translation symmetry*	34
3.3 SU(2) symmetry*	37
3.4 Parquet method	40
3.5 Implementation*	40
3.5.1 General remarks	40
3.5.2 Technical remarks	42

4 Results	45
4.1 Atomic limit*	45
4.2 Benzene molecule	50
5 Outlook	55
Appendices	57
A Channel-wise Schwinger-Dyson equation	59
A.1 Time-translation symmetry*	59
A.2 SU(2) symmetry*	60
A.3 Asymptotic corrections*	61
B GitLab documentation	63
Bibliography	75
Acknowledgements	79

CHAPTER 1

INTRODUCTION

Materials with strongly correlated electrons are in the focus of condensed matter physics for their intriguing properties and strong reaction to external perturbations. Thermoelectricity, giant magnetoresistance and superconductivity are only some of the many fascinating effects they show that lead to prospective new functionalities. Yet, understanding the complex behaviour of interacting quantum particles has proved one of the most difficult and enduring challenges in computational science.

The basic theoretical tools to describe these phenomena are the n -particle correlation functions or Green's functions, which measure the correlation between n particles moving through an equilibrium system. They are also the starting point for the calculation of quantities which can be measured in experiment, the so-called response functions. Calculation of the one-particle response function (spectral function) for strongly correlated systems has become feasible after the introduction of the dynamical mean-field theory (DMFT) [7]. However, the computation of non-local two-particle Green's function and the associated response functions (for example susceptibilities and optical conductivity) still remains a major challenge.

The main reason is the highly unfavourable scaling of computational time and memory with the number of orbitals and inverse temperature. Non-local calculation of response functions in the two-particle extensions of DMFT [6, 8, 11, 14, 15, 20] are for multi-orbital models only feasible in the so-called ladder approximation based on the solution of the Bethe-Salpeter equation. For a full unbiased treatment of two-particle response the parquet method is needed, which is a self-consistent algorithm consisting of four equations, namely the Bethe-Salpeter, parquet, Schwinger-Dyson and the Dyson equation, that provide equal treatment of scattering channels. In systems where the physics is governed by competition of several types of fluctuations, high-temperature superconductors being a prominent example, approximations based on Bethe-Salpeter

equation alone induce a strong bias, already assuming dominance of one scattering channel.

However, the parquet method poses a computational challenge already from the sixties [2, 3]. Only recently the parquet equations could be solved with sufficient numerical efficiency with which interesting physical questions can be answered [1, 9, 16, 18]. Nonetheless, nothing beyond one orbital has been possible so far. The main problem is storage: two-particle quantities depend on four spin-orbital indices, three momenta, and three frequencies (two fermionic and one bosonic Matsubara frequency) due to momentum and energy conservation. Compared to the single-band parquet method, the multi-orbital implementation scales with an additional factor N_O^4 ; therefore, new ideas for reducing memory are needed. For the momentum indices the form-factor basis [5] has already been used in one-orbital models. For frequencies the newly developed sparse modeling technique [23] is very promising.

With these new techniques at hand, multi-orbital calculations will become feasible in the near future. In this thesis, we describe the equations needed for the multi-orbital parquet algorithm in detail and present an implementation of these equations for a multi-orbital impurity (or molecule) in Fortran called `multi-orbital-parquet` inspired by [13], which can be directly extended further with the aforementioned form-factor basis for momenta. In the one form-factor approximation the scaling in number of momenta and orbitals is similar to ladder approximations, which means that up to 5 orbitals could be possible at reasonably high temperature. In the future the application of sparse modelling methods will allow going to low temperatures.

The thesis is organised as follows. In chapter 2 we recapitulate basic concepts of solid-state physics and quantum field theory for many-body physics. First, we briefly touch the key points of the derivation of the multi-orbital Hubbard model from the general Hamiltonian for n electrons in a periodic potential (with Coulomb interaction between electrons) in section 2.1. Next, we summarize in section 2.2 the important concepts of correlation functions and their properties. The Dyson equation and the notion of one-particle reducibility are explained in section 2.3. Eventually, the full-two particle vertex F and its properties for multi-orbital systems and the generalized susceptibility X are described in sections 2.4 and 2.5.

Chapter 3 covers the concept of two-particle reducibility as well as the parquet and Bethe-Salpeter equation in section 3.1.1. After a short introduction of the Schwinger-Dyson equation in 3.1.2, explicit formulas for these three equations are derived in the

cases of time-translation and $SU(2)$ symmetry in sections 3.2 and 3.3. In 3.4 we give a short outline of the parquet method; remarks on the concrete implementation of the algorithm in multi-orbital-parquet can be found in section 3.5.

First benchmark results obtained with multi-orbital-parquet can be found in chapter 4. The thesis is concluded by a discussion of possible improvements for multi-orbital-parquet in chapter 5.



Die approbierte gedruckte Originalversion dieser Diplomarbeit ist an der TU Wien Bibliothek verfügbar
The approved original version of this thesis is available in print at TU Wien Bibliothek.

CORRELATION FUNCTIONS AND VERTICES

Note that throughout this thesis, we use natural units by setting Planck's reduced constant \hbar , the speed of light c , electrical permittivity ϵ_0 and Boltzmann's constant k_B as follows:

$$\hbar = 1, \quad c = 1, \quad \epsilon_0 = \frac{1}{4\pi} \quad \text{and} \quad k_B = 1.$$

2.1 Multi-orbital Hubbard model

In this section, we summarize the most important points of the derivation of the Hubbard model as stated in [19, pp. 12–21], but making some adaptations for the multi-orbital case.

Neglecting the motion of atomic nuclei (the so-called *Born-Oppenheimer approximation*) and relativistic effects, the general Hamiltonian describing the dynamics of N electrons in a crystal is given by

$$H = \sum_{i=1}^N \left(\frac{\mathbf{p}_i^2}{2m_e} + V(\mathbf{r}_i) \right) + \sum_{i=1}^N \sum_{j=i+1}^N \frac{e^2}{|\mathbf{r}_i - \mathbf{r}_j|}, \quad (2.1)$$

where \mathbf{r}_i is the position operator for the i -th electron, $\mathbf{p}_i = -i\frac{d}{d\mathbf{r}_i}$ the corresponding momentum operator, e the electron charge, m_e the electron mass and

$$V(\mathbf{r}) = V(\mathbf{r} + \mathbf{R}) \quad (2.2)$$

the lattice potential at position \mathbf{r} , being periodic for an arbitrary lattice vector \mathbf{R} .

We are not interested in the exact multi-particle wave function of the system, but only in the response of the system to particle excitations, which are related to measurable quantities as spin susceptibility or specific heat. Adding and removing particles is described best with second quantization, therefore we will continue within this formalism.

Thus we rewrite equation (2.1) as¹

$$\begin{aligned}
 H = & \underbrace{\sum_{\sigma} \int d^3r \psi_{\sigma}^{\dagger}(\mathbf{r}) \left[-\frac{1}{2m_e} \nabla^2 + V(\mathbf{r}) \right] \psi_{\sigma}(\mathbf{r})}_{=H_0} - \underbrace{\mu \sum_{\sigma} \int d^3r \psi_{\sigma}^{\dagger}(\mathbf{r}) \psi_{\sigma}(\mathbf{r})}_{=N} \\
 & + \frac{1}{2} \sum_{\sigma, \sigma'} \iint d^3r d^3r' \psi_{\sigma}^{\dagger}(\mathbf{r}) \psi_{\sigma'}^{\dagger}(\mathbf{r}') \frac{e^2}{|\mathbf{r} - \mathbf{r}'|} \psi_{\sigma'}(\mathbf{r}') \psi_{\sigma}(\mathbf{r}),
 \end{aligned} \tag{2.3}$$

where $\psi_{\sigma}^{(\dagger)}(\mathbf{r})$ annihilates (creates) an electron with spin σ at position \mathbf{r} and μ denotes the chemical potential.

Due to the periodicity condition (2.2), we can diagonalize the non-interacting Hamiltonian H_0 by using *Bloch's theorem* with orthonormal eigenfunctions (so-called *Bloch functions*) $\psi_{\mathbf{k}n}(\mathbf{r}) = e^{i\mathbf{k}\cdot\mathbf{r}} u_{\mathbf{k}n}(\mathbf{r})$, with $u_{\mathbf{k}n}(\mathbf{r})$ being \mathbf{R} -periodic, i. e.

$$H_0 \psi_{\mathbf{k}n}(\mathbf{r}) = \epsilon_{\mathbf{k}n} \psi_{\mathbf{k}n}(\mathbf{r}) \tag{2.4}$$

by means of *Bloch's theorem*. n is a discrete band index (bands stem from different orbitals as well as from multiple atoms in the unit cell), \mathbf{k} a vector from the first Brillouin zone and $\epsilon_{\mathbf{k}n}$ the eigenenergy for $\psi_{\mathbf{k}n}(\mathbf{r})$. Moreover, the functions $u_{\mathbf{k}n}(\mathbf{r})$ and energies $\epsilon_{\mathbf{k}n}$ are also periodic in \mathbf{k} -space, i. e. $u_{\mathbf{k}n}(\mathbf{r}) = u_{(\mathbf{k}+\mathbf{G})n}(\mathbf{r})$ and $\epsilon_{\mathbf{k}n}(\mathbf{r}) = \epsilon_{(\mathbf{k}+\mathbf{G})n}(\mathbf{r})$, where \mathbf{G} is an arbitrary reciprocal lattice vector, fulfilling $e^{i\mathbf{R}\cdot\mathbf{G}} = 1$. Thus, by using Bloch's theorem we transform the original non-interacting Hamiltonian H_0 of equation (2.1) with a continuous spectrum into a set of Hamiltonians $\{H_{0,\mathbf{k}}\}$, with a discrete spectrum indexed by n for every \mathbf{k} in the first Brillouin zone [12, p. 3]. Although this is only exact for the non-interacting system H_0 , it is also a good approximation for the case of *nearly-free electrons*, when $V(\mathbf{r}) \approx \text{const}$. Bloch functions can be obtained from *density-functional calculations* (DFT).

It is rather difficult to think about concepts in real space, for example chemical bonds stemming from localized atoms with overlapping orbitals, in terms of spread-out Bloch functions which “live” entirely in \mathbf{k} -space. To overcome this, an orthogonal basis in real space in which equation (2.1) is diagonal would be desirable. Unfortunately, we cannot get everything we want. The *Wannier basis* $\{\phi_n(\mathbf{r})\}$ provides an adequate orthonormal basis in real space. It is obtained by an orthogonal transformation (basically

¹Here we perform the replacement $H \rightarrow H - \mu N$ to obtain expectation values in the grand canonical ensemble, since the particle number is in general not constant for the interacting system.

a Fourier transformation) of the Bloch basis $\{\psi_{\mathbf{k}n}(\mathbf{r})\}$, such that

$$\psi_{\mathbf{k}n}(\mathbf{r}) = \sum_{\mathbf{R}} e^{i\mathbf{k}\cdot\mathbf{R}} \phi_n(\mathbf{r}-\mathbf{R}) \quad \text{and} \quad \phi_n(\mathbf{r}-\mathbf{R}) = \frac{V}{(2\pi)^3} \int_{1.BZ} d^3k e^{-i\mathbf{k}\cdot\mathbf{R}} \psi_{\mathbf{k}n}(\mathbf{r}), \quad (2.5)$$

V being the volume of the first Brillouin zone. However, as the Wannier functions are linear combinations of eigenfunctions of $H_{0,\mathbf{k}}$ with different \mathbf{k} , H_0 is in general no longer diagonal in the Wannier basis.

In the case of flat bands, i. e. $\epsilon_{\mathbf{k}n} \approx \epsilon_n$, where electrons are strongly localized, the Wannier functions are indeed approximately eigenfunctions, $H_0\phi_n(\mathbf{r}-\mathbf{R}) \approx \phi_n(\mathbf{r}-\mathbf{R})$. The potential $V(\mathbf{r})$ is then a linear combination of non-overlapping potentials of atomic orbitals and also the Wannier functions can be expressed in terms of atomic orbitals. Luckily, this is the case for strongly correlated systems (e. g. partially filled d- or f-shells of transition or rare-earth metals), which we are interested in.

For further investigation we therefore rewrite the Hamiltonian in the so-called *tight-binding representation*. Firstly, we perform an expansion of the operators in terms of Wannier functions,

$$\Psi_{\sigma}^{(\dagger)} = \sum_{\mathbf{R}_i, n} \phi_n^{(*)}(\mathbf{r}-\mathbf{R}_i) c_{i n \sigma}^{(\dagger)}, \quad (2.6)$$

where $c_{i n \sigma}^{(\dagger)}$ denotes the annihilation (creation) of an electron on lattice site i in “orbital” n with spin σ .² Secondly, we insert this expression into equation (2.3), which yields

$$\begin{aligned} H = & \sum_{\sigma} \sum_{ij} \sum_{nm} \tilde{t}_{ij}^{nm} c_{i n \sigma}^{\dagger} c_{j m \sigma} - \sum_{\sigma} \sum_i \sum_n \mu c_{i n \sigma}^{\dagger} c_{i n \sigma} \\ & + \frac{1}{2} \sum_{\sigma\sigma'} \sum_{nmop} \sum_{ijkl} \tilde{U}_{ikjl}^{n p m o} c_{i n \sigma}^{\dagger} c_{j m \sigma'}^{\dagger} c_{l o \sigma'} c_{k p \sigma}, \end{aligned} \quad (2.7)$$

with hopping amplitudes t_{ij}^{nm} and the two-body integrals $\tilde{U}_{ikjl}^{n p m o}$, which are defined as

$$\tilde{t}_{ij}^{nm} = \int d^3r \phi_n^*(\mathbf{r}-\mathbf{R}_i) \left[-\frac{1}{2m_e} \nabla^2 + V(\mathbf{r}) \right] \phi_m(\mathbf{r}-\mathbf{R}_j) \quad \text{and} \quad (2.8)$$

$$\tilde{U}_{ikjl}^{n p m o} = \iint d^3r d^3r' \phi_n^*(\mathbf{r}-\mathbf{R}_i) \phi_p(\mathbf{r}-\mathbf{R}_k) \frac{e^2}{|\mathbf{r}-\mathbf{r}'|} \phi_m^*(\mathbf{r}'-\mathbf{R}_j) \phi_o(\mathbf{r}'-\mathbf{R}_l). \quad (2.9)$$

²Remember that the band index n indexes orbitals as well as different atoms in the unit cell, so by “orbital” we actually mean orbital *or* atom in the unit cell.

We introduce the spin-dependent, fully anti-symmetrized two-body integrals

$$U_{ijkl,\sigma_i\sigma_k\sigma_j\sigma_l}^{npmo} = -U_{iljk,\sigma_i\sigma_l\sigma_j\sigma_k}^{nomp} = U_{jlik,\sigma_j\sigma_l\sigma_i\sigma_k}^{monp}, \quad (2.10)$$

demand the equality

$$\begin{aligned} \frac{1}{4} \sum_{\sigma\sigma'} \sum_{nmop} \sum_{ijkl} U_{ijkl,\sigma_i\sigma_l\sigma_j\sigma_k}^{npmo} c_{in\sigma_i}^\dagger c_{jm\sigma_j}^\dagger c_{lo\sigma_l} c_{kp\sigma_k} \\ \stackrel{!}{=} \frac{1}{2} \sum_{\sigma\sigma'} \sum_{nmop} \sum_{ijkl} \tilde{U}_{ijkl}^{npmo} c_{in\sigma}^\dagger c_{jm\sigma'}^\dagger c_{lo\sigma'} c_{kp\sigma} \end{aligned} \quad (2.11)$$

and find the following relations:

$$U_{ikjl,\uparrow\uparrow}^{npmo} = 2\tilde{U}_{ikjl}^{npmo} \quad \text{for } ((n,i) \neq (m,j)) \vee ((p,k) \neq (o,l)), \quad (2.12a)$$

$$U_{ikjl,\uparrow\downarrow}^{npmo} = \tilde{U}_{ikjl}^{npmo} \quad \text{and} \quad (2.12b)$$

$$U_{ikjl,\uparrow\downarrow}^{npmo} = -U_{iljk,\uparrow\downarrow}^{nomp} \quad \text{by anti-symmetry,} \quad (2.12c)$$

with the shorthand notation $\uparrow\uparrow = \uparrow\uparrow\uparrow\uparrow$, $\uparrow\downarrow = \uparrow\uparrow\downarrow\downarrow$ and $\uparrow\downarrow = \uparrow\downarrow\uparrow\downarrow$. All other elements of U have to be zero.

Analogously, we define spin-dependent hopping amplitudes $t_{ij,\sigma_i\sigma_j}^{nm} = \tilde{t}_{ij}^{nm} \delta_{\sigma_i,\sigma_j}$. We can write the Hamiltonian with both operators and matrix-elements depending on spin, orbital and site indices and thus obtain the *multi-orbital Hubbard model*:

$$H = - \sum_{ij} t_{ij} c_i^\dagger c_j - \sum_i \mu c_i^\dagger c_i + \frac{1}{4} \sum_{ijkl} U_{ijkl} c_i^\dagger c_j^\dagger c_l c_k, \quad (2.13)$$

where i, j, k, l denote now *spin-orbitals* collecting spin, orbital and site indices, i. e. $i = (o_i, \sigma_i, \mathbf{r}_i)$ – this notation was adapted from [23, p. 1]. The anti-symmetry condition can be written now concisely as $U_{ijkl} = -U_{iljk} = -U_{jkil}$. We note that all elements U_{ijkl} where i, j or k, l involve same spins, orbitals and sites must vanish. After a Fourier transform of real to momentum space, also the momentum dependence can be included (\mathbf{k}_i instead of \mathbf{r}_i).

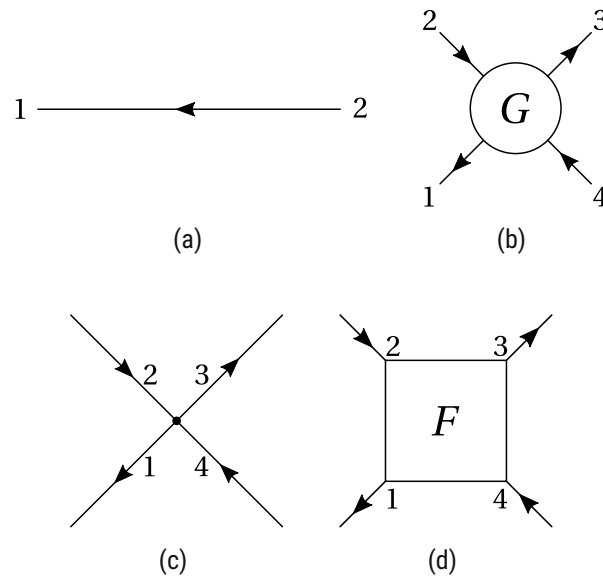


Figure 2.1: Building blocks of Feynman diagrams. Diagrams consist of (a) one-particle Green's functions $G(12)$, (b) two-particle Green's functions $G(1234)$, (c) bare interaction vertices $U(1234)$ and (d) other vertices (here the full interaction vertex $F(1234)$ is shown).

2.2 Green's function

Green's functions measure the correlation between the addition and removal of particles and are connected to quantities which can be directly observed in experiment, therefore they are also termed as *correlation functions*. The one- and two-particle Green's functions are given by

$$G(12) = -\langle \mathcal{T} c(1) c^\dagger(2) \rangle, \quad (2.14)$$

$$G(1234) = \langle \mathcal{T} c(1) c^\dagger(2) c(3) c^\dagger(4) \rangle, \quad (2.15)$$

respectively, where each bracketed number $\alpha = 1, 2, \dots$ is now shorthand for a tuple (i_α, τ_α) of a spin-orbital index i_α and a point in imaginary time τ_α . \mathcal{T} denotes the fermionic imaginary time-ordering operator and $\langle \dots \rangle = \text{Tr}(e^{-\beta H} \dots)$ the thermal expectation value with inverse temperature $\beta = \frac{1}{T}$.

Since we want to represent our equations as Feynman diagrams and all quantities must therefore depend on both spin-orbitals and imaginary times, we introduce an

imaginary time dependency for the interaction by writing [23, p. 1]

$$U(1234) = \sum_{ijkl} U_{ijkl} \delta(\tau_1 - \tau_2) \delta(\tau_2 - \tau_3) \delta(\tau_3 - \tau_4) \delta_{i_1, i} \delta_{i_2, k} \delta_{i_3, j} \delta_{i_4, l}. \quad (2.16)$$

This expression is the so-called *bare interaction vertex* and describes an instantaneous interaction. The order of indices 1...4 matches the order of indices in the U matrix, $ijkl$, to better match the convention of equation (2.15). One-particle Green's functions and bare interaction vertices are building blocks of Feynman diagrams and are depicted as such in figure 2.1. Furthermore, also a Feynman diagram for the two-particle Green's function is shown, which is not so frequently used, and a diagram for the full interaction vertex, which we will introduce in section 2.4.

2.2.1 Properties

Boundary conditions. As shown in [19, p. 26], if we assume that τ_1 is the largest and τ_4 the smallest imaginary time-argument of $G(1234)$, and require that the Green's function must be finite, we get

$$\tau_4 + \beta > \tau_1 > \tau_2, \tau_3 > \tau_4, \quad (2.17)$$

i. e. all imaginary time arguments have to be located in an interval of length β . Furthermore, one can show [19, pp. 27–28] that

$$G_{i_1 i_2 i_3 i_4}(\tau_1, \tau_2, \tau_3, \tau_4) = -G_{i_1 i_2 i_3 i_4}(\tau_1 - \beta, \tau_2, \tau_3, \tau_4) \quad (2.18)$$

$$G_{i_1 i_2 i_3 i_4}(\tau_1, \tau_2, \tau_3, \tau_4) = -G_{i_1 i_2 i_3 i_4}(\tau_1, \tau_2, \tau_3, \tau_4 + \beta) \quad (2.19)$$

if τ_1 is the largest and τ_4 the smallest imaginary time argument. Note that we deviate here from the concise notation introduced in equation (2.13) and write out explicitly imaginary time and spin-orbital dependencies. Whenever other dependencies are written explicitly, as for example \mathbf{k}_1 or σ_1 , then i_1 contains all remaining dependencies.

The same procedure for boundary conditions can be applied when the other two frequencies ν_2 and ν_3 are smallest or largest, yielding similar boundary conditions as eq. 2.18. Therefore, the two-particle Green's function can be expanded as a Fourier sum,

$$G_{i_1 i_2 i_3 i_4}(\tau_1, \tau_2, \tau_3, \tau_4) = \frac{1}{\beta^4} \sum_{\nu_1 \nu_2 \nu_3 \nu_4} e^{i(\nu_1 \tau_1 + \nu_2 \tau_2 + \nu_3 \tau_3 + \nu_4 \tau_4)} G_{i_1 i_2 i_3 i_4}(\nu_1, \nu_2, \nu_3, \nu_4), \quad (2.20)$$

$$G_{i_1 i_2 i_3 i_4}(\nu_1, \nu_2, \nu_3, \nu_4) = \int_0^\beta d\tau_1 \cdots \int_0^\beta d\tau_4 e^{-i(\nu_1 \tau_1 + \nu_2 \tau_2 + \nu_3 \tau_3 + \nu_4 \tau_4)} G_{i_1 i_2 i_3 i_4}(\tau_1, \tau_2, \tau_3, \tau_4), \quad (2.21)$$

where $\nu_i = (2n_i + 1)\frac{\pi}{\beta}$, $n_i \in \mathbb{Z}$ are fermionic Matsubara frequencies. Equation 2.20 extends the Green's function for arguments which lie outside condition 2.17. The same holds also for the one-particle Green's function.

Crossing symmetry. Exchange of fermionic operators yields a minus sign, i. e.

$$G(1234) = \langle \mathcal{T} c(1) c^\dagger(2) c(3) c^\dagger(4) \rangle = -\langle \mathcal{T} c(1) c^\dagger(4) c(3) c^\dagger(2) \rangle. \quad (2.22)$$

Therefore, the two-particle Green's function obeys the so-called *crossing symmetry*,

$$G(1234) = -G(1432) = -G(3214) = G(3412). \quad (2.23)$$

Note that this is a “symmetry” of crossing legs in Feynman diagrams stemming directly from Pauli's principle, it is not caused by a symmetry of H .

Complex conjugation. Complex conjugation switches order of the indices and imaginary times become negative:

$$\begin{aligned} G^*(1234) &= \langle \mathcal{T} c(1) c^\dagger(2) c(3) c^\dagger(4) \rangle^* = \\ &= \left(\sum_m \langle m | e^{\beta H} \mathcal{T} e^{\tau_1 H} c_{i_1} e^{-\tau_1 H} e^{\tau_2 H} c_{i_2}^\dagger e^{-\tau_2 H} e^{\tau_3 H} c_{i_3} e^{-\tau_3 H} e^{\tau_4 H} c_{i_4}^\dagger e^{-\tau_4 H} | m \rangle \right)^* \\ &= \text{Tr} \left(\mathcal{T} c_{i_4}(-\tau_4) c_{i_3}^\dagger(-\tau_3) c_{i_2}(-\tau_2) c_{i_1}^\dagger(-\tau_1) \right) \\ &= G_{i_4 i_3 i_2 i_1}(-\tau_4, -\tau_3, -\tau_2, -\tau_1), \end{aligned} \quad (2.24)$$

where the cyclic property of the trace, $\text{Tr}(AB) = \text{Tr}(BA)$ for operators A, B was used. Analogously we have for the two-particle Green's function:

$$G^*(12) = G_{i_2 i_1}(-\tau_2, -\tau_1). \quad (2.25)$$

2.2.2 Symmetry relations

Depending on the symmetries of the Hamiltonian H , the Green's function may obey additional symmetry relations. A *symmetry* of H is a unitary transformation U which fulfills $[H, U] = 0$. Then the Green's function $G'(1234) = \langle \mathcal{T}c'(1)c'^{\dagger}(2)c'(3)c'^{\dagger} \rangle$ of the transformed system $H' = U^{-1}HU$ with transformed operators $c'^{(\dagger)} = U^{-1}c^{(\dagger)}U$ must be the same as the original Green's function, i. e. $G'(1234) = G(1234)$ [19, p. 32].

Time- and space-translation symmetry. For a time-independent Hamiltonian $H(\tau) = H$, the imaginary time evolution operator $U = e^{-\tau H}$ is a symmetry of H . For the transformed two-particle Green's function we have

$$\begin{aligned} G'_{i_1 i_2 i_3 i_4}(\tau_1, \tau_2, \tau_3, \tau_4) &= \text{Tr}(e^{\beta H} \mathcal{T} e^{\tau_1 H} e^{\tau_2 H} c_{i_1} e^{-\tau_1 H} e^{-\tau_2 H} \dots e^{\tau_4 H} e^{\tau_3 H} c_{i_4}^{\dagger} e^{-\tau_4 H} e^{-\tau_3 H}) \\ &= \text{Tr}(e^{\beta H} \mathcal{T} e^{(\tau_1 + \tau) H} c_{i_1} e^{-(\tau_1 + \tau) H} \dots e^{(\tau_4 + \tau) H} c_{i_4}^{\dagger} e^{-(\tau_4 + \tau) H}). \end{aligned} \quad (2.26)$$

Setting $\tau = -\tau_4$ and requiring equality with the Green's function of the original system, we get

$$\underbrace{G_{i_1 i_2 i_3 i_4}(\tau_1 - \tau_4, \tau_2 - \tau_4, \tau_3 - \tau_4, 0)}_{=: G_{i_1 i_2 i_3 i_4}(\tau'_1, \tau'_2, \tau'_3)} = G(1234), \quad (2.27)$$

and for the one-particle Green's function

$$\underbrace{G_{i_1 i_2}(\tau_1 - \tau_2, 0)}_{=: G_{i_1 i_2}(\tau)} = G(12). \quad (2.28)$$

When we use equation (2.27) in the Fourier expansion equation (2.21) and perform a change of variables $\tau'_i = \tau_i - \tau_4$, $i = 1, 2, 3$, we have

$$\begin{aligned} G_{i_1 i_2 i_3 i_4}(v_1, v_2, v_3, v_4) &= \int_0^{\beta} d\tau_1 \dots \int_0^{\beta} d\tau_4 e^{i(v_1 \tau_1 + v_2 \tau_2 + v_3 \tau_3 + v_4 \tau_4)} \underbrace{G_{i_1 i_2 i_3 i_4}(\tau_1, \tau_2, \tau_3, \tau_4)}_{G_{i_1 i_2 i_3 i_4}(\tau_1 - \tau_4, \tau_2 - \tau_4, \tau_3 - \tau_4, 0)} \\ &= \int_0^{\beta} d\tau_4 \underbrace{\int_{-\tau_4}^{\beta - \tau_4} d\tau'_1 \dots \int_{-\tau_4}^{\beta - \tau_4} d\tau'_3}_{\int_0^{\beta} d\tau'_1 \dots \int_0^{\beta} d\tau'_3} e^{i(v_1 \tau'_1 - v_2 \tau'_2 + v_3 \tau'_3)} e^{i(v_1 - v_2 + v_3 - v_4) \tau_4} G_{i_1 i_2 i_3 i_4}(\tau'_1, \tau'_2, \tau'_3, 0) \\ &= \beta \delta_{v_1 - v_2 + v_3 - v_4, 0} \int_0^{\beta} d\tau'_1 \dots \int_0^{\beta} d\tau'_3 e^{i(v_1 \tau'_1 - v_2 \tau'_2 + v_3 \tau'_3)} G_{i_1 i_2 i_3 i_4}(\tau'_1, \tau'_2, \tau'_3, 0) \\ &=: \beta \delta_{v_1 - v_2 + v_3 - v_4, 0} G_{i_1 i_2 i_3 i_4}(v_1, v_2, v_3). \end{aligned} \quad (2.29)$$

The shift of integration limits in the second line is possible because

$$e^{i(v_1\tau'_1 - v_2\tau'_2 + v_3\tau'_3)} G_{i_1 i_2 i_3 i_4}(\tau'_1, \tau'_2, \tau'_3, 0) \quad (2.30)$$

is periodic with period β . Therefore the Green's function conserves energy and only three Matsubara frequencies are needed as arguments. This is a direct consequence of Noether's theorem for a system which is invariant under time-translation. Analogously, for the one-particle Green's function we find that only one frequency as argument is needed.

For space-translation symmetry we require invariance of H under translation by a lattice vector \mathbf{R} . The annihilation (creation) operators in real space transform as $c_{\mathbf{R}_i}^{(\dagger)} = T_{\mathbf{R}}^{-1} c_{\mathbf{R}_i}^{(\dagger)} T_{\mathbf{R}} = c_{\mathbf{R}_i + \mathbf{R}}^{(\dagger)}$. After a similar calculation as for time-translation symmetry, we find

$$G_{i_1 i_2 i_3 i_4}^{(\mathbf{R}_1 - \mathbf{R}_4)(\mathbf{R}_2 - \mathbf{R}_4)(\mathbf{R}_3 - \mathbf{R}_4)(\mathbf{R}_0)}(\tau_1, \tau_2, \tau_3, \tau_4) = G(1234) \quad (2.31)$$

with \mathbf{R}_0 being the null vector.

In Fourier space, where integration is now replaced by summation over discrete lattice vectors in the first Brillouin zone, the two-particle Green's function is due to momentum conservation fully determined with three \mathbf{k} -vector arguments,

$$G_{i_1 i_2 i_3 i_4}^{\mathbf{k}_1 \mathbf{k}_2 \mathbf{k}_3 \mathbf{k}_4}(\tau_1, \tau_2, \tau_3, \tau_4) = \frac{(2\pi)^3}{V} \delta(\mathbf{k}_1 - \mathbf{k}_2 + \mathbf{k}_3 - \mathbf{k}_4) G_{i_1 i_2 i_3 i_4}^{\mathbf{k}_1 \mathbf{k}_2 \mathbf{k}_3}(\tau_1, \tau_2, \tau_3, \tau_4), \quad (2.32)$$

and similarly for the one-particle Green's function.

SU(2) symmetry. Here we want to motivate the most important relations, for explicit proofs we refer to [19, pp. 37–42]. SU(2) symmetry simplifies the spin dependence of the Green's function, since total spin of ingoing and outgoing particles must be conserved along an arbitrary z -axis, so

$$G_{i_1 i_2 i_3 i_4}^{\sigma_1 \sigma_2 \sigma_3 \sigma_4}(\tau_1, \tau_2, \tau_3, \tau_4) = G_{i_1 i_2 i_3 i_4}^{\sigma_1 \sigma_2 \sigma_3 \sigma_4}(\tau_1, \tau_2, \tau_3, \tau_4) \delta_{\sigma_1 - \sigma_2 + \sigma_3 - \sigma_4, 0}. \quad (2.33)$$

For the one-particle Green's function this means it must be diagonal in the spin index and the diagonal elements have to be completely spin-independent,

$$G_{i_1 i_2}^{\sigma_1 \sigma_2}(\tau_1, \tau_2) = G_{i_1 i_2}(\tau_1, \tau_2) \delta_{\sigma_1, \sigma_2}. \quad (2.34)$$

Furthermore, the Green's function must be invariant under a total spin flip, i. e.

$$G_{i_1 i_2 i_3 i_4}^{\sigma_1 \sigma_2 \sigma_3 \sigma_4}(\tau_1, \tau_2, \tau_3, \tau_4) = G_{i_1 i_2 i_3 i_4}^{(-\sigma_1)(-\sigma_2)(-\sigma_3)(-\sigma_4)}(\tau_1, \tau_2, \tau_3, \tau_4). \quad (2.35)$$

Both relations imply that only 6 of the 2^4 combinations are non-vanishing, which are $\uparrow\uparrow, \uparrow\downarrow, \overline{\uparrow\downarrow}$ and $\downarrow\downarrow, \downarrow\uparrow, \overline{\downarrow\uparrow}$ (the latter three are not independent due to spin flip symmetry) with the shorthand notation already introduced in section 2.1, $\sigma\sigma' = \sigma\sigma'\sigma'$ and $\overline{\sigma\sigma'} = \sigma\sigma'\sigma$. Note that this symmetry relation affects only spin variables, therefore the same relations hold also for the Fourier transformed quantities. Applying equation (2.23),

$$\underbrace{G_{i_1 i_2 i_3 i_4}^{\sigma_1 \sigma_2 \sigma_3 \sigma_4}(\nu_1, \nu_2, \nu_3, \nu_4)}_{\beta G_{i_1 i_2 i_3 i_4}^{\sigma_1 \sigma_2 \sigma_3 \sigma_4} \delta_{\nu_1 - \nu_2 + \nu_3 - \nu_4, 0}} = - \underbrace{G_{i_1 i_4 i_3 i_2}^{\sigma_1 \sigma_4 \sigma_3 \sigma_2}(\nu_1, \nu_4, \nu_3, \nu_2)}_{\beta G_{i_1 i_4 i_3 i_2}^{\sigma_1 \sigma_4 \sigma_3 \sigma_2} \delta_{\nu_1 - \nu_4 + \nu_3 - \nu_2, 0}}, \quad (2.36)$$

we obtain

$$G_{i_1 i_2 i_3 i_4}^{\sigma\sigma'}(\nu_1, \nu_2, \nu_3) = -G_{i_1 i_2 i_3 i_4}^{\overline{\sigma\sigma'}}(\nu_1, \nu_2, \nu_3). \quad (2.37)$$

Thus, only two-particle Green's functions $G_{i_1 i_2 i_3 i_4}^{\uparrow\uparrow}(\nu_1, \nu_2, \nu_3)$ and $G_{i_1 i_2 i_3 i_4}^{\uparrow\downarrow}(\nu_1, \nu_2, \nu_3)$ are independent.

Finally, by analyzing a rotation of spins by $\frac{\pi}{2}$ about the y -axis (transforming spins in z - to spins in x -direction), we get the relation [19, p. 42]

$$G_{i_1 i_2 i_3 i_4}^{\uparrow\uparrow}(\nu_1, \nu_2, \nu_3) = G_{i_1 i_2 i_3 i_4}^{\uparrow\downarrow}(\nu_1, \nu_2, \nu_3) + G_{i_1 i_2 i_3 i_4}^{\overline{\uparrow\downarrow}}(\nu_1, \nu_2, \nu_3). \quad (2.38)$$

Using again crossing symmetry, this yields

$$G_{i_1 i_2 i_3 i_4}^{\uparrow\uparrow}(\nu_1, \nu_2, \nu_3) = G_{i_1 i_2 i_3 i_4}^{\uparrow\downarrow}(\nu_1, \nu_2, \nu_3) - G_{i_1 i_4 i_3 i_2}^{\uparrow\downarrow}(\nu_1, \nu_1 - \nu_2 + \nu_3, \nu_3), \quad (2.39)$$

so knowledge of $G^{\uparrow\downarrow}$ suffices to determine all other spin contributions.

Time- and space-reversal symmetry. For spin-independent systems, time reversal can be achieved by complex conjugation of the wave function.³ Therefore, for a time-reversal invariant system H must be a real function of creation and annihilation operators. Then, in occupation number basis the matrix elements of $c_i^{(\dagger)}$ and H are real and thus $G^*(1234) = G(1234)$. Writing out explicitly the imaginary time dependencies and using

³For a system with spin-dependent interaction a generalization is also possible [19, p. 42].

Table 2.1: Summary of the most important (symmetry) relations for one- and two-particle Green's functions. We use the notation defined in equations (2.27) and (2.28) and for Fourier space in equation (2.29), but with generalized frequencies $\nu = (\tilde{\nu}, \mathbf{k})$, therefore we implicitly assume time- and space-translation symmetry.

	One-particle Green's function	Two-particle Green's function
Anti-periodicity	$G_{i_1 i_2}(\tau) = -G_{i_1 i_2}(\tau \pm \beta)$	$G_{i_1 i_2 i_3 i_4}(-\tau_1, \tau_2, \tau_3) = -G_{i_1 i_2 i_3 i_4}(\tau_1 \pm \beta, \tau_2, \tau_3)$, similarly for τ_2, τ_3
Crossing symmetry	—	$G(1234) = -G(1432) = -G(3214) = G(3412)$
Complex conjugation	$G_{i_1 i_2}^*(\tau) = G_{i_2 i_1}(\tau)$ $G_{i_1 i_2}^*(\nu) = G_{i_2 i_1}(-\nu)$	$G_{i_1 i_2 i_3 i_4}^*(\tau_1, \tau_2, \tau_3, \tau_4) = G_{i_4 i_3 i_2 i_1}(-\tau_4, -\tau_3, -\tau_2, -\tau_1)$ $G_{i_1 i_2 i_3 i_4}^*(\nu_1, \nu_2, \nu_3) = G_{i_4 i_3 i_2 i_1}(-\nu_1 + \nu_2 - \nu_3, -\nu_3, -\nu_2)$
SU(2) symmetry	—	$G_{i_1 i_2 i_3 i_4}^{\parallel}(\nu_1, \nu_2, \nu_3) = G_{i_1 i_2 i_3 i_4}^{\parallel}(\nu_1, \nu_2, \nu_3) - G_{i_1 i_2 i_3 i_4}^{\bar{\parallel}}(\nu_1, \nu_2, \nu_3)$
Time-reversal symmetry	$G_{i_1 i_2}(\nu) = G_{i_2 i_1}(\nu)$	$G_{i_1 i_2 i_3 i_4}(\nu_1, \nu_2, \nu_3) = G_{i_4 i_3 i_2 i_1}(\nu_1 - \nu_2 + \nu_3, \nu_3, \nu_2)$

equations (2.18) and (2.24), we have

$$G_{i_1 i_2 i_3 i_4}(\tau_1, \tau_2, \tau_3, \tau_4) = G_{i_4 i_3 i_2 i_1}(-\tau_4, -\tau_3, -\tau_2, -\tau_1) = G_{i_4 i_3 i_2 i_1}(\beta - \tau_4, \beta - \tau_3, \beta - \tau_2, \beta - \tau_1). \quad (2.40)$$

A similar expression can be derived for the one-particle Green's function.

When using this identity in a similar fashion as in equation (2.29), we obtain in Fourier space

$$G_{i_1 i_2 i_3 i_4}(\nu_1, \nu_2, \nu_3) = G_{i_4 i_3 i_2 i_1}(\nu_1 - \nu_2 + \nu_3, \nu_3, \nu_2). \quad (2.41)$$

For additional spacial Fourier transform, we arrive at

$$G_{i_1 i_2 i_3 i_4}^{\mathbf{k}_1 \mathbf{k}_2 \mathbf{k}_3}(\nu_1, \nu_2, \nu_3) = G_{i_4 i_3 i_2 i_1}^{(-\mathbf{k}_3 + \mathbf{k}_2 - \mathbf{k}_1)(-\mathbf{k}_3)(-\mathbf{k}_2)}(\nu_1 - \nu_2 + \nu_3, \nu_3, \nu_2). \quad (2.42)$$

If the system is also space-reversal symmetric, i. e. is invariant under transformation $\mathbf{R} \rightarrow -\mathbf{R}$, then signs of all \mathbf{k} -arguments can be flipped,

$$G_{i_1 i_2 i_3 i_4}^{\mathbf{k}_1 \mathbf{k}_2 \mathbf{k}_3}(\nu_1, \nu_2, \nu_3) = G_{i_4 i_3 i_2 i_1}^{(\mathbf{k}_3 - \mathbf{k}_2 + \mathbf{k}_1)(\mathbf{k}_3)(\mathbf{k}_2)}(\nu_1 - \nu_2 + \nu_3, \nu_3, \nu_2). \quad (2.43)$$

The most important properties and symmetry relations are summarized in table 2.1.

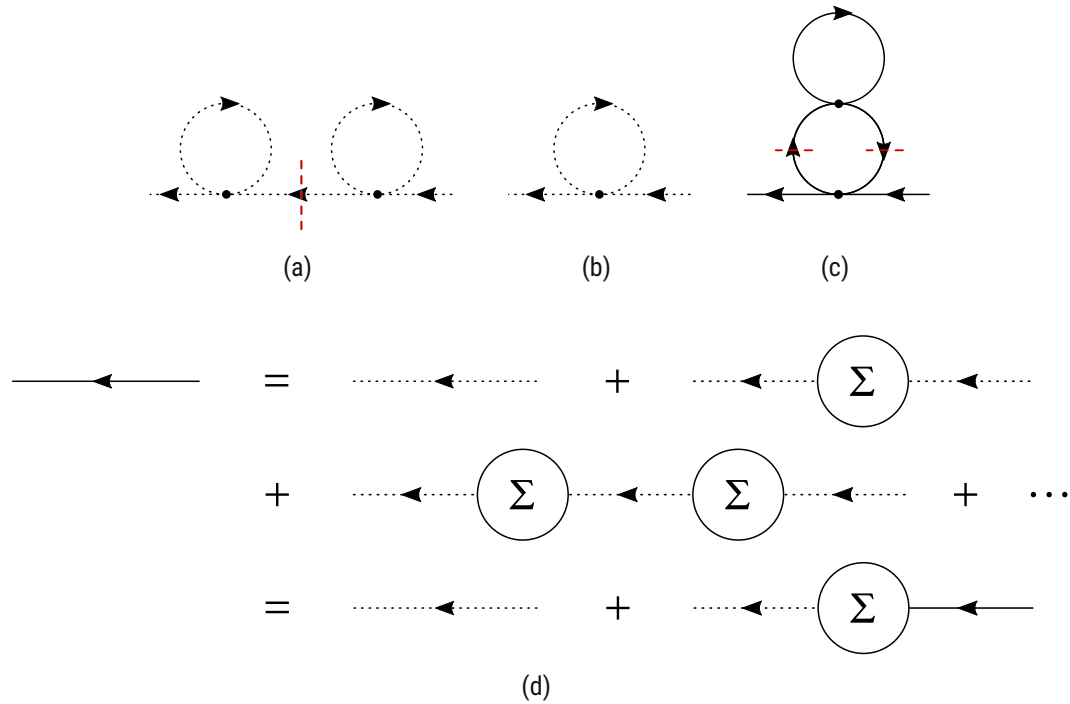


Figure 2.2: (a) One-particle reducible diagram (reducibility is indicated by the red, dashed line) and (b) irreducible one. (c) Non-skeleton diagram, as it can be separated by cutting the G lines along the red, dashed lines. (d) Feynman diagram of Dyson equation 2.44.

2.3 Dyson equation

The non-interacting one-particle Green's function is defined as $G_0(12) = -\langle \mathcal{T}c(1)c^\dagger(2) \rangle_0$. $\langle \dots \rangle_0 = \text{Tr}(e^{\beta H_0} \dots)$ denotes the expectation value with respect to the non-interacting system and H_0 is the non-interacting Hamiltonian. In Feynman diagrams we depict $G_0(12)$ as a dotted line.

We can classify all Feynman diagrams made of G_0 lines stemming from the perturbation series of G into *one-particle irreducible diagrams*, which do not separate into disconnected pieces if we cut one G_0 line, and *one-particle reducible* ones (see figures 2.2(a) and 2.2(b)). If we consider only diagrams which contribute to *self-energy* Σ , i. e. the diagrams where in- and outgoing lines were cut, we can reconstruct all Feynman diagrams for G by connecting one-particle irreducible Σ pieces with G_0 lines, as shown in figure 2.2(c). Irreducibility is required to avoid double-counting of Feynman diagrams. This reconstruction of G by means of Σ and G_0 is formulated mathematically by the *Dyson equation*,

$$G(12) = G_0(12) + G_0(13)\Sigma(34)G(42). \tag{2.44}$$

It is also possible to express diagrams of Σ in terms of the interacting one-particle Green's function G . To this end, *skeleton diagrams* have to be taken into account: these are diagrams which do not separate when cutting two G lines and therefore lack self-energy insertions (for a non-skeleton example, see figure 2.2(c)). The G lines contain already all self-energy corrections, so self-energy insertions would lead to double counting.

All diagrams which will be discussed from now on consist of interacting Green's function lines and are therefore skeleton diagrams.

2.4 Full two-particle vertex

For a non-interacting system, the two-particle Green's function can be represented as a sum of products of one-particle Green's functions by Wick's theorem,

$$G(1234) = G_0(12) G_0(34) - \underbrace{G_0(14) G_0(32)}_{=: X_0^{(U=0)}(4321)}, \quad (2.45)$$

where $X_0^{(U=0)}(4321)$ is the *bare susceptibility* in the non-interacting case, to which we get back in section 2.5.

When $U \neq 0$, an additional term arises describing the scattering process between two particles or a particle and a hole. This additional term is called *full two-particle* or *full interaction vertex* F , and the two-particle Green's function is related to F by

$$G(1234) = G(12) G(34) - G(14) G(32) - G(15) G(37) F(5678) G(62) G(84), \quad (2.46)$$

where for inner indices, summation over spin-orbitals and integration over imaginary time is implied. A representation of equation (2.46) in terms of Feynman diagrams is depicted in figure 2.3.

Note that vertices, as self-energy Σ , do not have in- and outgoing lines. This is the reason why in Feynman diagrams the indices are placed directly at the vertex corners, see for example figure 2.1(d) (nevertheless we draw in- and outgoing lines also for vertices in order to keep track how Green's function lines must be attached to vertex corners). Moreover, if we compare the line in figure 2.1 at point 1 for Green's functions and vertices, we notice that it is an incoming line for Green's functions and an outgoing

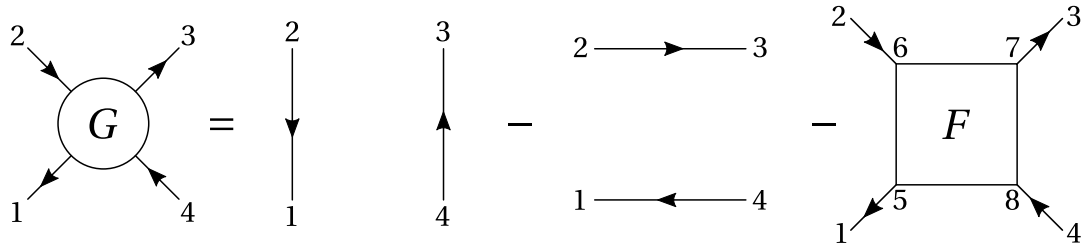


Figure 2.3: Feynman diagram of equation (2.46). $G(1234)$ consists of an disconnected part and an additional term with the full interaction vertex F , which describes a scattering process.

one for vertices. These different conventions are needed to attach Green’s function lines correctly to vertex corners – as an analogy one can think of a jigsaw puzzle, where for a given joint one part with a tab and one part with an indentation is needed.

The signs in equation (2.46) ensure that the lowest-order term in F is just the bare interaction U , which can be verified by expanding both equations (2.15) and (2.46) in their respective perturbation series and using Wick’s theorem:

$$\begin{aligned}
 G(1234) &= \langle c(1)c^\dagger(2)c(3)c^\dagger(4) \rangle_0 - \frac{1}{4}U(5678)\langle c(1)c^\dagger(2)c(3)c^\dagger(4)c^\dagger(5)c^\dagger(7)c(8)c(6) \rangle_0 + \mathcal{O}(U^2) \\
 &= G_0(12)G_0(34) - G_0(14)G_0(32) - U(5678)G_0(15)G_0(37)G_0(62)G_0(84) + \mathcal{O}(U^2).
 \end{aligned}
 \tag{2.47}$$

2.4.1 Properties

Anti-periodicity. Anti-periodicity with period β for F does not directly follow from anti-symmetry of one- and two-particle Green’s functions, but with the help of the Bethe-Salpeter equation for the susceptibility (not shown here) one can derive that also the vertices, including F , have the anti-symmetric property

$$F_{i_5 i_6 i_7 i_8}(\tau_5, \tau_6, \tau_7, \tau_8) = -F_{i_5 i_6 i_7 i_8}(\tau_5 \pm \beta, \tau_6, \tau_7, \tau_8),
 \tag{2.48}$$

and similarly for all other arguments. Then F can also be expanded as a Fourier sum in terms of fermionic Matsubara frequencies. As a consequence, all formulas with bracketed number notation are also valid for quantities depending on Matsubara frequencies, but integration over imaginary time has to be replaced by frequency summation including a normalization factor, for example $\int_0^\beta d\tau_1 \rightarrow \frac{1}{\beta} \sum_{\nu_1}$.

Crossing symmetry. We know from equation (2.23) that $G(1432) + G(1234) = 0$. Using now equation (2.46) for both terms, we have

$$-\underbrace{G(15)G(37)F(5678)G(64)G(82)}_{G(15)G(37)F(5876)G(84)G(62)} - G(15)G(37)F(5678)G(62)G(84) = 0, \quad (2.49)$$

where we relabeled indices which are summed over. This equation is fulfilled non-trivially when $F(1234) = -F(1432)$. By a similar argument, we find

$$F(1234) = -F(3214) = F(3412). \quad (2.50)$$

Complex conjugation. Equation 2.24 yields $G_{i_4 i_3 i_2 i_1}(-\tau_4, -\tau_3, -\tau_2, -\tau_1) - G^*(1234) = 0$. Inserting equation (2.46) for both terms gives

$$\begin{aligned} & G_{i_5 i_1}(-\tau_5, -\tau_1) G_{i_7 i_3}(-\tau_7, -\tau_3) F^*(5678) G_{i_2 i_6}(-\tau_2, -\tau_6) G_{i_4 i_8}(-\tau_4, -\tau_8) \\ &= G_{i_4 i_5}(-\tau_4, \tau_5) G_{i_2, i_7}(-\tau_2, \tau_7) F(5678) G_{i_6 i_3}(\tau_6, -\tau_3) G_{i_8 i_1}(\tau_8, -\tau_1) \\ &= G_{i_4 i_8}(-\tau_4, -\tau_8) G_{i_2 i_6}(-\tau_2, -\tau_6) F_{i_8 i_7 i_6 i_5}(-\tau_8, -\tau_7, -\tau_6, -\tau_5) G_{i_7 i_3}(-\tau_7, -\tau_3) G_{i_5 i_1}(-\tau_5, -\tau_1), \end{aligned} \quad (2.51)$$

where we performed the substitution $-\tau_j \rightarrow -\tau_j$, $j = 5, \dots, 8$, which changes also the integration limits $\int_0^\beta d\tau_j \rightarrow \int_0^{-\beta} d\tau_j$. However, when using equation (2.48), we can shift and flip integration limits back to the original ones and since we have to do this four times, no additional sign occurs. Thus, equation (2.51) can be fulfilled non-trivially only by

$$F^*(5678) = F_{i_8 i_7 i_6 i_5}(-\tau_8, -\tau_7, -\tau_6, -\tau_5). \quad (2.52)$$

2.4.2 Symmetry relations*

Time- and space-translation symmetry. We apply equation (2.28) on equation (2.46) and get

$$\begin{aligned} & G_{i_1 i_2 i_3 i_4}(\tau_1 - \tau, \tau_2 - \tau, \tau_3 - \tau, \tau_4 - \tau) = G_{i_1 i_2}(\tau_1, \tau_2) G_{i_3 i_4}(\tau_3, \tau_4) - G_{i_1 i_4}(\tau_1, \tau_4) G_{i_3 i_2}(\tau_3, \tau_2) \\ & - G_{i_1 i_5}(\tau_1 - \tau, \tau_5) G_{i_3 i_7}(\tau_3, \tau_7) F_{i_5 i_6 i_7 i_8}(\tau_5, \tau_6, \tau_7, \tau_8) G_{i_6 i_2}(\tau_6, \tau_2 - \tau) G_{i_8 i_4}(\tau_8, \tau_4 - \tau). \end{aligned} \quad (2.53)$$

If we demand this to be the same as equation (2.46), we only have to concentrate on the last term, which can be rewritten as

$$\begin{aligned}
 &= \tau'_5, \text{ etc.} \\
 &G_{i_1 i_5}(\tau_1, \tau_5 + \tau) G_{i_3 i_7}(\tau_3, \tau_7 + \tau) F_{i_5 i_6 i_7 i_8}(\tau_5, \tau_6, \tau_7, \tau_8) G_{i_6 i_2}(\tau_6, \tau_2) G_{i_8 i_4}(\tau_8, \tau_4) \\
 &= G_{i_1 i_5}(\tau_1, \tau'_5) G_{i_3 i_7}(\tau_3, \tau'_7) F_{i_5 i_6 i_7 i_8}(\tau'_5 - \tau, \tau'_6 - \tau, \tau'_7 - \tau, \tau'_8 - \tau) G_{i_6 i_2}(\tau'_6, \tau_2) G_{i_8 i_4}(\tau'_8, \tau_4).
 \end{aligned} \tag{2.54}$$

The substitution $\tau'_j = \tau_j + \tau$, $j = 5, \dots, 8$ shifts also the integration limits to $\int_{\tau}^{\beta + \tau} d\tau'_j$, but since the two-particle Green's functions and F are anti-periodic in β in all imaginary time arguments and thus the product is periodic, shifting the integration limits back to the original ones is possible. Comparing this with the last term of equation (2.46), we obtain

$$F_{i_5 i_6 i_7 i_8}(\tau_5, \tau_6, \tau_7, \tau_8) = \underbrace{F_{i_5 i_6 i_7 i_8}(\tau_5 - \tau_8, \tau_6 - \tau_8, \tau_7 - \tau_8, 0)}_{=: F_{i_5 i_6 i_7 i_8}(\tau'_5, \tau'_6, \tau'_7)}. \tag{2.55}$$

As for the two-particle Green's function in equation (2.29) energy is also conserved for F ,

$$F_{i_1 i_2 i_3 i_4}(\nu_1, \nu_2, \nu_3, \nu_4) = \beta \delta_{\nu_1 - \nu_2 + \nu_3 - \nu_4, 0} F_{i_1 i_2 i_3 i_4}(\nu_1, \nu_2, \nu_3). \tag{2.56}$$

If the system features also space-translation symmetry, a similar calculation as for time-translation symmetry yields

$$F_{i_1 i_2 i_3 i_4}^{\mathbf{R}_1 \mathbf{R}_2 \mathbf{R}_3 \mathbf{R}_4}(\tau_1, \tau_2, \tau_3, \tau_4) = F_{i_1 i_2 i_3 i_4}^{(\mathbf{R}_1 - \mathbf{R}_4)(\mathbf{R}_2 - \mathbf{R}_4)(\mathbf{R}_3 - \mathbf{R}_4)(\mathbf{R}_0)}(\tau_1, \tau_2, \tau_3, \tau_4) \tag{2.57}$$

and for the Fourier transform

$$F_{i_1 i_2 i_3 i_4}^{\mathbf{k}_1 \mathbf{k}_2 \mathbf{k}_3 \mathbf{k}_4}(\tau_1, \tau_2, \tau_3, \tau_4) = \frac{(2\pi)^3}{V} \delta_{\mathbf{k}_1 - \mathbf{k}_2 + \mathbf{k}_3 - \mathbf{k}_4} F_{i_1 i_2 i_3 i_4}^{\mathbf{k}_1 \mathbf{k}_2 \mathbf{k}_3}(\tau_1, \tau_2, \tau_3, \tau_4). \tag{2.58}$$

SU(2) symmetry. First, we check whether F fulfills spin conservation. To this end, we consider spin conservation for the two-particle Green's function and use equations (2.34) and (2.46):

$$\begin{aligned}
 &G(15) \delta_{\sigma_1, \sigma_5}, \text{ etc.} \\
 &\underbrace{G(15) G(37) F(5678) G(62) G(84)}_{\delta_{\sigma_1 - \sigma_2 + \sigma_3 - \sigma_4, 0}} \underbrace{\delta_{\sigma_5 - \sigma_6 + \sigma_7 - \sigma_8, 0}}_{\delta_{\sigma_1 - \sigma_2 + \sigma_3 - \sigma_4, 0}} \\
 &= G(15) G(37) F(5678) G(62) G(84) \delta_{\sigma_1, \sigma_5} \delta_{\sigma_3, \sigma_7} \delta_{\sigma_6, \sigma_2} \delta_{\sigma_8, \sigma_4}.
 \end{aligned} \tag{2.59}$$

It follows immediately that

$$F(1234) = F(1234) \delta_{\sigma_1 - \sigma_2 + \sigma_3 - \sigma_4}. \quad (2.60)$$

Secondly, for spin flip symmetry we get after a short calculation starting from equation (2.35) (without writing imaginary time/Matsubara frequency arguments for conciseness) the equality

$$G_{i_1 i_5}^{\sigma_1 \sigma_5} G_{i_3 i_7}^{\sigma_3 \sigma_7} F_{i_5 i_6 i_7 i_8}^{\sigma_5 \sigma_6 \sigma_7 \sigma_8} G_{i_6 i_2}^{\sigma_6 \sigma_2} G_{i_8 i_4}^{\sigma_8 \sigma_4} = G_{i_1 i_5}^{(-\sigma_1) \sigma_5} G_{i_3 i_7}^{(-\sigma_3) \sigma_7} F_{i_5 i_6 i_7 i_8}^{\sigma_5 \sigma_6 \sigma_7 \sigma_8} G_{i_6 i_2}^{(-\sigma_6) \sigma_2} G_{i_8 i_4}^{(-\sigma_8) \sigma_4}. \quad (2.61)$$

Performing a change of variables $\sigma_j \rightarrow -\sigma_j$, $j = 5, \dots, 8$ on the right-hand side of the equation and using equation (2.35) for the one-particle Green's function yields

$$F_{i_1 i_2 i_3 i_4}^{\sigma_1 \sigma_2 \sigma_3 \sigma_4} = F_{i_1 i_2 i_3 i_4}^{(-\sigma_1)(-\sigma_2)(-\sigma_3)(-\sigma_4)}. \quad (2.62)$$

Finally, we verify that equation (2.38) is also valid for F . Therefore, we start with the term on the left-hand side of equation (2.38) and use equation (2.46) to obtain

$$G_{i_1 i_2 i_3 i_4}^{\uparrow \uparrow} = G_{i_1 i_2}^{\uparrow \uparrow} G_{i_3 i_4}^{\uparrow \uparrow} - G_{i_1 i_4}^{\uparrow \uparrow} G_{i_3 i_2}^{\uparrow \uparrow} - G_{i_1 i_5}^{\uparrow \sigma_5} G_{i_3 i_7}^{\uparrow \sigma_7} F_{i_5 i_6 i_7 i_8}^{\sigma_5 \sigma_6 \sigma_7 \sigma_8} G_{i_6 i_2}^{\sigma_6 \uparrow} G_{i_8 i_4}^{\sigma_8 \uparrow}, \quad (2.63)$$

where imaginary time/Matsubara frequency arguments were neglected. Equally, for the right-hand side of equation (2.38) we get

$$G_{i_1 i_2 i_3 i_4}^{\uparrow \downarrow} + G_{i_1 i_2 i_3 i_4}^{\overline{\uparrow \downarrow}} = G_{i_1 i_2}^{\uparrow \uparrow} G_{i_3 i_4}^{\downarrow \downarrow} - G_{i_1 i_4}^{\uparrow \uparrow} G_{i_3 i_2}^{\downarrow \downarrow} - G_{i_1 i_5}^{\uparrow \sigma_5} G_{i_3 i_7}^{\uparrow \sigma_7} F_{i_5 i_6 i_7 i_8}^{\sigma_5 \sigma_6 \sigma_7 \sigma_8} G_{i_6 i_2}^{\sigma_6 \uparrow} G_{i_8 i_4}^{\sigma_8 \uparrow} - G_{i_1 i_5}^{\uparrow \sigma_5} G_{i_3 i_7}^{\downarrow \sigma_7} F_{i_5 i_6 i_7 i_8}^{\sigma_5 \sigma_6 \sigma_7 \sigma_8} G_{i_6 i_2}^{\sigma_6 \downarrow} G_{i_8 i_4}^{\sigma_8 \uparrow}, \quad (2.64)$$

where we used spin conservation 2.34 for the one-particle Green's function. Thus equation (2.38) can be written as

$$\underbrace{G_{i_1 i_5}^{\uparrow \sigma_5} \delta_{\uparrow, \sigma_5}}_{\text{etc.}} G_{i_3 i_7}^{\uparrow \sigma_7} F_{i_5 i_6 i_7 i_8}^{\sigma_5 \sigma_6 \sigma_7 \sigma_8} G_{i_6 i_2}^{\sigma_6 \uparrow} G_{i_8 i_4}^{\sigma_8 \uparrow} = G_{i_1 i_5}^{\uparrow \sigma_5} G_{i_3 i_7}^{\uparrow \sigma_7} F_{i_5 i_6 i_7 i_8}^{\sigma_5 \sigma_6 \sigma_7 \sigma_8} G_{i_6 i_2}^{\sigma_6 \uparrow} G_{i_8 i_4}^{\sigma_8 \uparrow} - G_{i_1 i_5}^{\uparrow \sigma_5} G_{i_3 i_7}^{\downarrow \sigma_7} F_{i_5 i_6 i_7 i_8}^{\sigma_5 \sigma_6 \sigma_7 \sigma_8} G_{i_6 i_2}^{\sigma_6 \downarrow} G_{i_8 i_4}^{\sigma_8 \uparrow}, \quad (2.65)$$

thus we find that

$$F_{i_1 i_2 i_3 i_4}^{\uparrow \uparrow} = F_{i_1 i_2 i_3 i_4}^{\uparrow \downarrow} + F_{i_1 i_2 i_3 i_4}^{\overline{\uparrow \downarrow}}. \quad (2.66)$$

Table 2.2: Summary of the most important (symmetry) relations for full interaction vertex F . We use the notation defined in equation (2.55) and for Fourier space in equation (2.56), but with generalized frequencies $\nu = (\tilde{\nu}, \mathbf{k})$, therefore we implicitly assume time- and space-translation symmetry.

Anti-periodicity	$F_{i_1 i_2 i_3 i_4}(\tau_1, \tau_2, \tau_3) = -F_{i_1 i_2 i_3 i_4}(\tau_1 \pm \beta, \tau_2, \tau_3)$, similarly for τ_2, τ_3
Crossing symmetry	$F(1234) = -F(1432) = -F(3214) = F(3412)$
Complex conjugation	$F_{i_1 i_2 i_3 i_4}^*(\tau_1, \tau_2, \tau_3, \tau_4) = F_{i_4 i_3 i_2 i_1}(-\tau_4, -\tau_3, -\tau_2, -\tau_1)$ $F_{i_1 i_2 i_3 i_4}^*(\nu_1, \nu_2, \nu_3) = F_{i_4 i_3 i_2 i_1}(-\nu_1 + \nu_2 - \nu_3, -\nu_3, -\nu_2)$
SU(2) symmetry	$F_{i_1 i_2 i_3 i_4}^{\uparrow\downarrow}(\nu_1, \nu_2, \nu_3) = F_{i_1 i_2 i_3 i_4}^{\uparrow\downarrow}(\nu_1, \nu_2, \nu_3) - F_{i_1 i_2 i_3 i_4}^{\overline{\uparrow\downarrow}}(\nu_1, \nu_2, \nu_3)$
Time-reversal symmetry	$F_{i_1 i_2 i_3 i_4}(\nu_1, \nu_2, \nu_3) = F_{i_4 i_3 i_2 i_1}(\nu_1 - \nu_2 + \nu_3, \nu_3, \nu_2)$

Time- and space-reversal symmetry. In order to find a time-reversal symmetry relation for F we apply equation (2.46) to equation (2.41),

$$\begin{aligned} & G_{i_1 i_5}(\nu_1, \nu_5) G_{i_3 i_7}(\nu_3, \nu_7) F_{i_5 i_6 i_7 i_8}(\nu_5, \nu_6, \nu_7, \nu_8) G_{i_6 i_2}(\nu_6, \nu_2) G_{i_8 i_4}(\nu_8, \nu_4) \\ & \quad \underbrace{G_{i_5 i_4}(\nu_5, \nu_4), \text{ etc.}}_{= G_{i_4 i_5}(\nu_4, \nu_5)} \\ & = G_{i_4 i_5}(\nu_4, \nu_5) G_{i_2 i_7}(\nu_2, \nu_7) F_{i_5 i_6 i_7 i_8}(\nu_5, \nu_6, \nu_7, \nu_8) G_{i_6 i_3}(\nu_6, \nu_3) G_{i_8 i_1}(\nu_8, \nu_1) \end{aligned} \quad (2.67)$$

which yields after renaming of summed over variables

$$F_{i_1 i_2 i_3 i_4}(\nu_1, \nu_2, \nu_3) = F_{i_4 i_3 i_2 i_1}(\nu_1 - \nu_2 + \nu_3, \nu_3, \nu_2). \quad (2.68)$$

After a similar calculation we obtain for space-reversal symmetry

$$F_{i_1 i_2 i_3 i_4}^{\mathbf{k}_1 \mathbf{k}_2 \mathbf{k}_3}(\nu_1, \nu_2, \nu_3) = F_{i_4 i_3 i_2 i_1}^{(\mathbf{k}_1 - \mathbf{k}_2 - \mathbf{k}_3) \mathbf{k}_2 \mathbf{k}_3}(\nu_1 - \nu_2 + \nu_3, \nu_3, \nu_2). \quad (2.69)$$

In table 2.2 the most important relations for the full-interaction vertex F are summarized.

2.5 Generalized susceptibility

The *generalized susceptibility* can be obtained by adding the two-particle vertex with reattached legs to the bare susceptibility $X_0(1234)$:

$$X(1234) = \underbrace{G(23) G(41)}_{X_0(1234)} + G(25) G(61) F(5678) G(83) G(47). \quad (2.70)$$

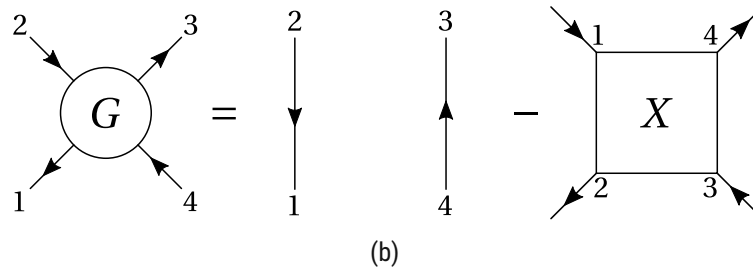
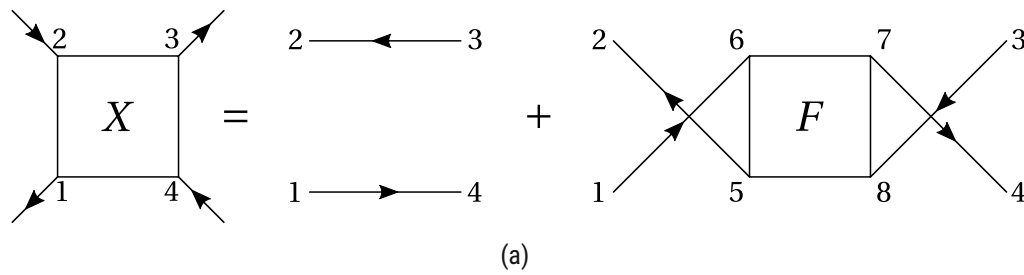


Figure 2.4: (a) Feynman diagram of equation (2.70), which is the sum of a bare susceptibility X_0 and full interaction vertex F with attached Green's function lines. (b) Diagram of equation (2.71). One can clearly see the difference in index conventions for Green's function $G(1234)$ and vertex X .

Figure 2.4(a) shows equation (2.70) in terms of Feynman diagrams.

Note that with this definition, the creation and annihilation operators in X are in the “vertex” convention (2.46) rather than the “Green's function” convention, i.e., one has to permute indices when moving from G to X :

$$G(1234) = G(12)G(34) - X(2143). \quad (2.71)$$

This convention (see figure 2.4(b) for a diagrammatical representation) for X and X_0 from [23, p. 2] is more natural for two reasons: Firstly, *physical* susceptibilities, depending on one frequency argument only, can be obtained by gluing together legs 1 and 2 as well as 3 and 4, which amounts to taking limits $\tau_2 \rightarrow \tau_1^-$, $\tau_3 \rightarrow \tau_4^-$ and $\tau_4 \rightarrow 0$. Secondly, this definition leads to a more straightforward composition rule in the Bethe-Salpeter equation, as we will see in chapter 3. The general susceptibility defined in [19, p. 65] would correspond to $X(2143)$ in our convention.

Due to equation (2.71) adaptation of properties and symmetry relations of $G(1234)$ for X is straightforward.



Die approbierte gedruckte Originalversion dieser Diplomarbeit ist an der TU Wien Bibliothek verfügbar
The approved original version of this thesis is available in print at TU Wien Bibliothek.

MULTI-ORBITAL PARQUET EQUATIONS

3.1 General case

3.1.1 Two-particle reducibility

All contributions to F must be one-particle irreducible, which can be seen from following argument: if a contribution would be one-particle reducible, then one would have either a bare interaction vertex violating particle number conservation (figure 3.1(a)) or a self-energy insertion, which would contradict the fact that we exclusively work with skeleton diagrams (figure 3.1(b)). One-particle irreducibility is an intrinsic property of two-particle diagrams; three-particle diagrams for example can be one-particle irreducible [19, p. 67].

However, contributions to F can be classified into *two-particle irreducible digrams*, which do not separate into disconnected pieces when cutting two Green's function lines, and into *two-particle reducible* ones.

Unlike in the single-particle case there are three notions of two-particle reducibility: labelling the outer legs of our diagram by 1, 3 as outgoing and 2, 4 as ingoing lines, we call the vertex *reducible with respect to the longitudinal particle-hole channel* (ph) when 1, 2 can be separated from 3, 4 (figure 3.2(a)), *reducible with respect to the transversal particle-hole channel* ($\overline{\text{ph}}$) when 1, 4 can be separated from 2, 3 (figure 3.2(b)), and *reducible with respect to the particle-particle channel* (pp) when 1, 3 can be separated from 2, 4 (figure 3.2(c)).

In each of the channels, the full vertex F decomposes into a reducible part Φ and an irreducible part Γ :

$$F(1234) = \Gamma^r(1234) + \Phi^r(1234), \quad r = \text{ph}, \overline{\text{ph}}, \text{pp}. \quad (3.1)$$

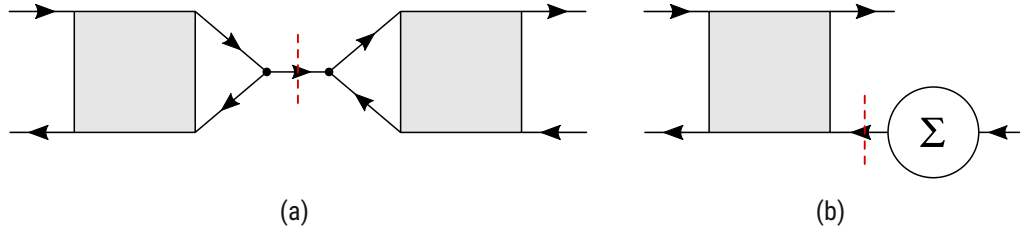


Figure 3.1: (a) Hypothetical one-particle reducible diagram, which violates particle number conservation and (b) diagram with a self-energy insertion, which contradicts the fact that we use skeleton diagrams only.

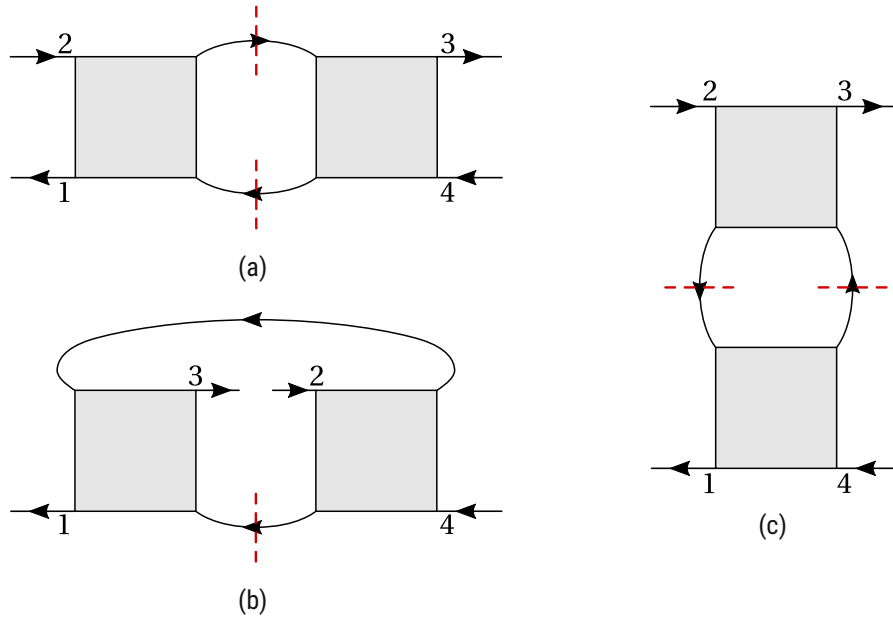


Figure 3.2: Two-particle reducible diagrams with respect to (a) ph -, (b) \overline{ph} -, and (c) pp -channel.

The irreducible and reducible parts in each channel are related by the *Bethe-Salpeter equations*:

$$\Phi^{ph}(1234) = \Gamma^{ph}(1256) G(67) G(85) F(7834), \quad (3.2a)$$

$$\Phi^{\overline{ph}}(1234) = -\Gamma^{\overline{ph}}(1654) G(67) G(85) F(7238), \quad (3.2b)$$

$$\Phi^{pp}(1234) = \frac{1}{2}\Gamma^{pp}(1536) G(67) G(58) F(7284). \quad (3.2c)$$

We can interpret the Bethe-Salpeter equations as follows: For a given channel r , F is the sum of all diagrams that are reducible in r and all diagrams that are irreducible

in r (3.1). Every r -reducible diagram of Φ^r can be represented by splitting it into two subdiagrams connected by two Green's function lines, where one diagram is irreducible and the other diagram is in the set of F . To make this decomposition of Φ^r unique, we require that the leftmost subdiagram has to be the irreducible one [19, p. 70]. Therefore, the Bethe-Salpeter equations are the two-particle counterpart of the Dyson equation.

The signs of equation (3.2) can be computed by attaching operators to each of the quantities, e. g., $G(67) \rightarrow G(67)c(6)c^\dagger(7)$, and then permuting the operators until they lie in the sequence generated by the perturbation series for $F(1234)$ [23, p. 3].

The factor $\frac{1}{2}$ of equation (3.2c) is of topological nature: we notice that relabelling the outer legs $1 \leftrightarrow 3$ and $2 \leftrightarrow 4$ does not change the Bethe-Salpeter equation for pp-channel, therefore this factor is needed for compensating overcounting. Moreover, relabelling the legs for ph- yields the Bethe-Salpeter equation for $\overline{\text{ph}}$ -channel up to a sign – this is the reason for the peculiar crossing symmetry for channels, which will be described below.

Each diagram in F can only be reducible in at most one channel: a diagram reducible in two channels would allow us to sever a single external point from two others. This would require terms violating particle number conservation to be present in the interaction. The *parquet equation* expresses this fact by classifying all diagrams by reducibility:

$$F(1234) = \Lambda(1234) + \Phi^{\text{ph}}(1234) + \Phi^{\overline{\text{ph}}}(1234) + \Phi^{\text{pp}}(1234), \quad (3.3)$$

where Λ is the fully irreducible vertex collecting terms irreducible in all channels.

Crossing symmetry. While the full vertex is crossing symmetric, the situation for the channels is slightly more involved. By applying equation (2.50) to equation (3.1) and equation (3.2a) and relabelling, we obtain for ph-channel

$$F(1234) = -\Gamma^{\text{ph}}(1432) + \Gamma^{\text{ph}}(1456) G(67) G(85) F(7238), \quad (3.4)$$

and for $\overline{\text{ph}}$ -channel

$$F(1234) = \Gamma^{\overline{\text{ph}}}(1234) - \Gamma^{\overline{\text{ph}}}(1654) G(67) G(85) F(7238). \quad (3.5)$$

Comparing the two equations and using again (3.1) to get relations for Φ , we have

$$\Gamma^{\overline{\text{ph}}}(1234) = -\Gamma^{\text{ph}}(1432), \quad \Phi^{\overline{\text{ph}}}(1234) = -\Phi^{\text{ph}}(1432), \quad (3.6)$$

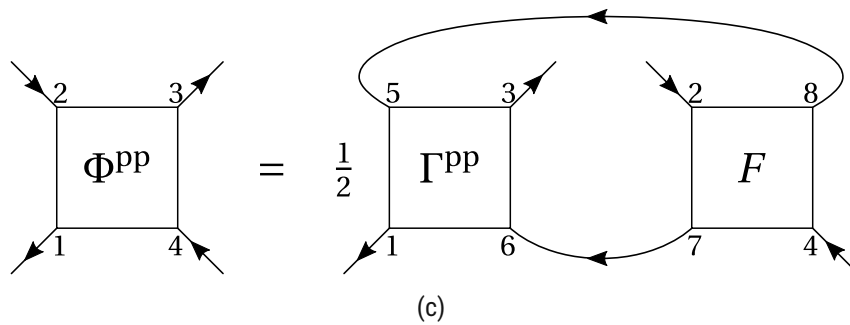
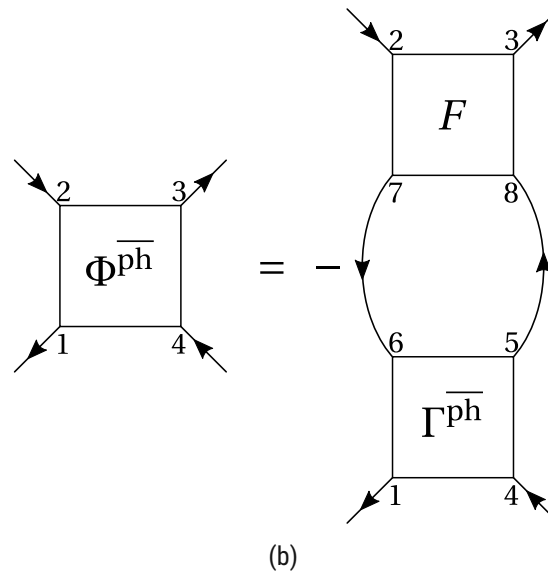
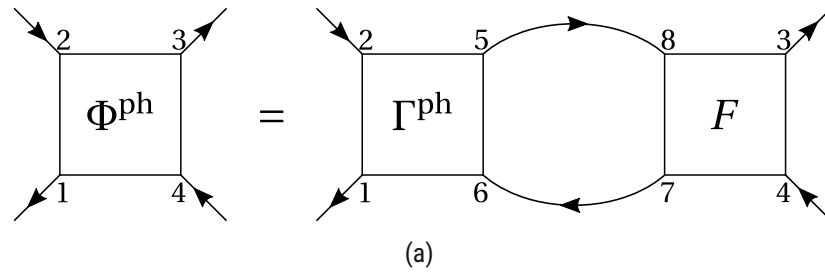


Figure 3.3: Bethe-Salpeter equations for (a) ph-, (b) \bar{ph} - and (c) pp-channel. Note that the crossing symmetry for Φ can be explained by the fact that the diagrams of side of the Bethe-Salpeter equations for ph- and \bar{ph} -channel can be transformed into each other up to a sign by relabelling $1 \leftrightarrow 3$ or $2 \leftrightarrow 4$. For pp the diagrams remain the same under relabelling – this is the reason why an additional factor of $\frac{1}{2}$ for compensating overcounting is needed.

$$F = \Lambda + \Phi^{\text{ph}} + \Phi^{\overline{\text{ph}}} + \Phi^{\text{pp}}$$

e. g.

Figure 3.4: Parquet equation and exemplary first order diagrams of each channel. Red, dashed lines indicate two-particle reducibility for the corresponding channel.

i. e., under crossing the ph- and $\overline{\text{ph}}$ -channel trade place.

The parquet equation (3.3) then dictates that the pp-channel must be crossing symmetric:

$$\Gamma^{\text{pp}}(1234) = -\Gamma^{\text{pp}}(1432), \quad \Phi^{\text{pp}}(1234) = -\Phi^{\text{pp}}(1432), \quad (3.7)$$

which alternatively can also be verified by inserting (2.50) into (3.2c) and relabelling.

Bethe-Salpeter picture. Equations (3.1), (3.2) and (3.3) are formulated in the “parquet picture”, where all channels share a global incoming and outgoing convention. This makes it easy to sum them up through the parquet equation (3.3) in order to obtain the full vertex. However, it comes at the cost of channel-dependent Bethe-Salpeter equations (3.2). An alternative formulation can be obtained by introducing F in each of the channels:

$$F(1234) = F^{\text{ph}}(12|34) = F^{\overline{\text{ph}}}(14|32) = F^{\text{pp}}(13|24). \quad (3.8)$$

By replacing each channel vertex by its “channel-native” convention, e.g., by replacing $\Gamma^{\overline{\text{ph}}}(1234)$ with $\Gamma^{\overline{\text{ph}}}(14|32)$, for all channels the Bethe-Salpeter equation has the same structure:

$$\Phi^r(12|34) = \kappa_r \Gamma^r(12|56) X_0^r(56|78) F^r(78|34), \quad (3.9)$$

with the channel-dependent bare susceptibilities

$$X_0^{\text{ph}}(12|34) = G(23)G(41), \quad \kappa_{\text{ph}} = 1, \quad (3.10a)$$

$$X_0^{\overline{\text{ph}}}(12|34) = G(23)G(41), \quad \kappa_{\overline{\text{ph}}} = -1, \quad (3.10b)$$

$$X_0^{\text{pp}}(12|34) = -G(23)G(14), \quad \kappa_{\text{pp}} = -\frac{1}{2}. \quad (3.10c)$$

Note the extra bar separating the “incoming” and “outgoing” side in the channel-native convention.

In each of the channel conventions, the parquet equation then reads:

$$F^{\text{ph}}(12|34) = \Lambda^{\text{ph}}(12|34) + \Phi^{\text{ph}}(12|34) + \overline{\Phi^{\text{ph}}}(14|32) + \Phi^{\text{pp}}(13|24), \quad (3.11a)$$

$$F^{\overline{\text{ph}}}(12|34) = \Lambda^{\overline{\text{ph}}}(12|34) + \Phi^{\text{ph}}(14|32) + \overline{\Phi^{\text{ph}}}(12|34) + \Phi^{\text{pp}}(13|42), \quad (3.11b)$$

$$F^{\text{pp}}(12|34) = \Lambda^{\text{pp}}(12|34) + \Phi^{\text{ph}}(13|24) + \overline{\Phi^{\text{ph}}}(14|23) + \Phi^{\text{pp}}(12|34). \quad (3.11c)$$

In the “parquet picture” we had one parquet equation (3.3) and distinct Bethe-Salpeter equations (3.2) for each channel, while in this picture there are distinct parquet equations for each channel but all Bethe-Salpeter equations have the same structure [23, pp. 4–5].

Frequency convention. When applying time- and space-translation symmetry, it is convenient to depart from our bracketed-number notation and write frequency and momentum dependencies explicitly. We introduce the following convention with generalized frequencies, $\nu = (\tilde{\nu}, \mathbf{k})$, which inherently guarantees energy and momentum conservation:

$$\text{ph and } \overline{\text{ph}} \left\{ \begin{array}{ll} \nu_1 = \nu & \nu_1 = \nu \\ \nu_2 = \nu + \omega & \nu_2 = \omega - \nu' \\ \nu_3 = \nu' + \omega & \nu_3 = \omega - \nu \\ \nu_4 = \nu' & \nu_4 = \nu' \end{array} \right\} \text{pp} \quad (3.12)$$

Here $\tilde{\nu}$ and $\tilde{\nu}_1$ denote fermionic Matsubara frequencies, whereas $\tilde{\omega}$ denotes a bosonic Matsubara frequency, $\tilde{\omega} = 2n\frac{\pi}{\beta}$, $n \in \mathbb{Z}$. With this convention ph- and $\overline{\text{ph}}$ -reducible diagrams describe an interaction of a particle propagating forward in time with energy $\tilde{\nu}$ and a hole propagating backward in time with energy $-\tilde{\nu}'$, whereas pp-reducible diagrams describe an interaction of two particles with energies $\tilde{\nu}$ and $\tilde{\nu}'$ (see also the lowest order diagrams of figure 3.4), thus justifying the channel names.

We introduce also the following shorthand notation for the vertices showing frequency dependence,

$$\Phi_{(i_1 i_2 | i_3 i_4)}^{\text{ph}, \nu \nu' \omega} := \Phi_{i_1 i_2 i_3 i_4}^{\text{ph}}(\nu, \nu + \omega, \nu' + \omega, \nu'), \quad (3.13a)$$

$$\Phi_{(i_1 i_2 | i_3 i_4)}^{\overline{\text{ph}}, \nu \nu' \omega} := \Phi_{i_1 i_4 i_3 i_2}^{\overline{\text{ph}}}(\nu, \nu', \nu' + \omega, \nu + \omega), \quad (3.13b)$$

$$\Phi_{(i_1 i_2 | i_3 i_4)}^{\text{pp}, \nu \nu' \omega} := \Phi_{i_1 i_3 i_2 i_4}^{\text{pp}}(\nu, \omega - \nu, \omega - \nu', \nu'), \quad (3.13c)$$

analogously for F^r , Γ^r and Λ^r . Then two important crossing symmetry relations in this notation are

$$\Phi_{(i_1 i_2 | i_3 i_4)}^{\text{ph}, \nu \nu' \omega} = +\Phi_{(i_3 i_2 | i_1 i_4)}^{\text{ph}, (\nu'+\omega)(\nu+\omega)(-\omega)}, \quad (3.14a)$$

$$\overline{\Phi}_{(i_1 i_2 | i_3 i_4)}^{\text{ph}, \nu \nu' \omega} = -\overline{\Phi}_{(i_1 i_2 | i_3 i_4)}^{\text{ph}, \nu(\nu'+\omega)(\nu'-\nu)}. \quad (3.14b)$$

According to the second equation, the vertices for ph- and $\overline{\text{ph}}$ -channel are not independent – therefore it is sufficient to restrict calculations to ph- and pp-channel vertices only. For the channel-dependent bare susceptibilities we introduce a similar shorthand notation showing frequency dependence:

$$X_{0(i_1 i_2 | i_3 i_4)}^{\text{ph}, \nu \nu' \omega} = \beta G_{i_2 i_3}(\nu) G_{i_4 i_1}(\nu' + \omega) \delta_{\nu, \nu'}, \quad (3.15a)$$

$$X_{0(i_1 i_2 | i_3 i_4)}^{\text{pp}, \nu \nu' \omega} = -\beta G_{i_2 i_3}(\nu) G_{i_1 i_4}(\omega - \nu') \delta_{\nu, \nu'}. \quad (3.15b)$$

3.1.2 Schwinger-Dyson equation

In this section we are going to derive an equation which relates the one-particle quantity Σ to the full interaction vertex $F(1234)$.

We start by taking the derivative of the one-particle Green's function,

$$\frac{d}{d\tau_1} G_{i_1 i_2}(\tau_1, \tau_2) = -\frac{d}{d\tau_1} \langle \mathcal{T} c_{i_1}(\tau_1) c_{i_2}^\dagger(\tau_2) \rangle. \quad (3.16)$$

Using the definition of the imaginary time-ordering operator we obtain for the thermal expectation value

$$\langle \mathcal{T} c_{i_1}(\tau_1) c_{i_2}^\dagger(\tau_2) \rangle = \langle c_{i_1}(\tau_1) c_{i_2}^\dagger(\tau_2) \rangle \theta(\tau_1 - \tau_2) - \langle c_{i_2}^\dagger(\tau_2) c_{i_1}(\tau_1) \rangle \theta(\tau_2 - \tau_1). \quad (3.17)$$

The derivative is

$$\begin{aligned} \frac{d}{d\tau_1} \langle \mathcal{T} c_{i_1}(\tau_1) c_{i_2}^\dagger(\tau_2) \rangle &= \underbrace{\langle c_{i_1}(\tau_1) c_{i_2}^\dagger(\tau_2) + c_{i_2}(\tau_2) c_{i_1}^\dagger(\tau_1) \rangle}_{=\langle c_{i_1}(\tau_1), c_{i_2}^\dagger(\tau_1) \rangle = \langle \delta_{i_1, i_2} \rangle = \delta_{i_1, i_2}} \delta(\tau_1 - \tau_2) + \langle \mathcal{T} \frac{d}{d\tau_1} c_{i_1}(\tau_1) c_{i_2}^\dagger(\tau_2) \rangle. \end{aligned} \quad (3.18)$$

Therefore, we have

$$\frac{d}{d\tau_1} G_{i_1 i_2}(\tau_1, \tau_2) = -\delta_{i_1, i_2} \delta(\tau_1 - \tau_2) - \langle \mathcal{T} \frac{d}{d\tau_1} c_{i_1}(\tau_1) c_{i_2}^\dagger(\tau_2) \rangle. \quad (3.19)$$

Consider the Heisenberg equation

$$\frac{d}{d\tau_1} c_{i_1}(\tau_1) = \frac{d}{d\tau_1} e^{H\tau_1} c_{i_1} e^{-H\tau_1} = [H, c_{i_1}(\tau_1)] = [H, c_{i_1}](\tau_1), \quad (3.20)$$

if H has no explicit time dependence. In the following we consider our multi-orbital Hubbard Hamiltonian (2.13), where this is certainly the case.

With the commutation relations

$$[AB, C] = A[B, C] + [A, C]B = A\{B, C\} - \{A, C\}B,$$

$$[ABXY] = AB[XY, C] + [AB, C]XY = AB(X\{Y, C\} - \{X, C\}Y) + (A\{B, C\} - \{A, C\}B)XY$$

we get for the one- and two-particle terms in our Hamiltonian

$$\begin{aligned} [c_i^\dagger c_j, c_{i_1}] &= -\delta_{i, i_1} c_j \\ [c_i^\dagger c_j^\dagger c_l c_k, c_{i_1}] &= (c_i^\dagger \delta_{j, i_1} - \delta_{i, i_1} c_j^\dagger) c_l c_k. \end{aligned}$$

Thus we can write the commutator in the Heisenberg equation (3.20) as

$$[H, c_{i_1}] = \sum_j (t_{i_1 j} c_j + \mu \delta_{i_1, j} c_j) + \frac{1}{2} \sum_{ikl} U_{i_1 lik} c_i^\dagger c_l c_k. \quad (3.21)$$

Using this for equation (3.19), we find

$$\begin{aligned} \frac{d}{d\tau_1} G_{i_1 i_2}(\tau_1, \tau_2) &= -\delta_{i_1, i_2} \delta(\tau_1 - \tau_2) + \sum_j (t_{i_1 j} + \mu \delta_{i_1, j}) G_{j i_2}(\tau_1, \tau_2) \\ &\quad + \frac{1}{2} \sum_{ikl} U_{i_1 lik} G_{lik i_2}(\tau_1, \tau_1 + 0^+, \tau_1 + 0^+, \tau_2). \end{aligned} \quad (3.22)$$

Next we Fourier transform this equation and use time-translation symmetry (2.28):

$$\sum_j ((i\nu_1 + \mu) \delta_{i_1, j} + t_{i_1 j}) G_{j i_2}(\nu_1) = \delta_{i_1, i_2} - \frac{1}{2} \sum_{ikl} U_{i_1 lik} G_{lik i_2}(\nu_1, \nu_1, \nu_1), \quad (3.23)$$

which can be interpreted as a BBGKY-hierarchy, relating one- to two-particle Green's functions. For the non-interacting one-particle Green's function G_0 we find in (3.23) by setting $U_{i_1 lik} = 0$

$$\sum_j ((i\nu_1 + \mu) \delta_{i_1, j} + t_{i_1 j}) G_{0, j i_2}(\nu_1) = \delta_{i_1, i_2}. \quad (3.24)$$

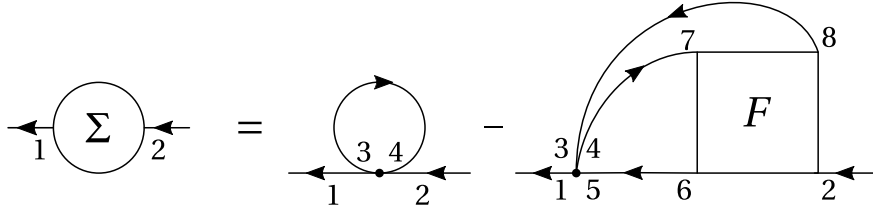


Figure 3.5: Feynman diagram of the Schwinger-Dyson equation.

Inserting the Dyson equation (2.44) into the left side of (3.23) and using (3.24) yields

$$\sum_j ((i\nu_1 + \mu) \delta_{i_1, j} + t_{i_1 j}) G_{0, j i_2}(\nu_1) = \delta_{i_1, i_2} + \sum_j \Sigma_{i_1 j}(\nu_1) G_{j i_2}(\nu_1). \quad (3.25)$$

Comparing this with the right side of equation (3.23), we find

$$(\Sigma G)_{i_1 i_2}(\nu_1) = \frac{1}{2} U_{i_1 i_3 i_4 i_5} G_{i_5 i_4 i_3 i_2}(\nu_1, \nu_1, \nu_1) \quad (3.26)$$

and for imaginary times

$$(\Sigma G)_{i_1 i_2}(\tau_1, \tau_2) = \frac{1}{2} U_{i_1 i_3 i_4 i_5} G_{i_5 i_4 i_3 i_2}(\tau_1, \tau_1 + 0^+, \tau_1 + 0^-, \tau_2). \quad (3.27)$$

As a last step, we insert equation (2.46) into (3.27),

$$\begin{aligned} (\Sigma G)_{i_1 i_2}(\tau_1, \tau_2) &= U_{i_1 i_3 i_4 i_5} (\langle c_{i_4}^\dagger(\tau_1) c_{i_5}(\tau_1) \rangle G_{i_3 i_2}(\tau_1, \tau_2) \\ &\quad - \frac{1}{2} G_{i_5 i_6}(\tau_1, \tau_6) G_{i_3 i_7}(\tau_1, \tau_7) F_{i_6 i_8 i_7 i_9}(\tau_6, \tau_8, \tau_7, \tau_9) G_{i_8 i_4}(\tau_8, \tau_1) G_{i_9 i_2}(\tau_9, \tau_2)), \end{aligned} \quad (3.28)$$

and after relabelling summed over indices and factoring out $G_{i_9 i_2}(\tau_9, \tau_2)$ on both sides we obtain the *Schwinger-Dyson equation*,

$$\begin{aligned} \Sigma_{i_1 i_2}(\tau_1, \tau_2) &= -U_{i_1 i_4 i_3 i_2} \overbrace{\langle c_{i_3}^\dagger(\tau_1) c_{i_4}(\tau_1) \rangle}^{G_{i_4 i_3}(\tau_1 + 0^-, \tau_1)} \delta(\tau_2 - \tau_1) \\ &\quad - \frac{1}{2} U_{i_1 i_3 i_4 i_5} G_{i_5 i_6}(\tau_1, \tau_6) G_{i_3 i_8}(\tau_1, \tau_8) F_{i_6 i_7 i_8 i_2}(\tau_6, \tau_7, \tau_8, \tau_2) G_{i_7 i_4}(\tau_7, \tau_1), \end{aligned} \quad (3.29)$$

which is shown as a Feynman diagram in figure 3.5.

3.2 Time-translation symmetry*

In this and the next section we will apply symmetries to the equations needed in the parquet formalism, in order to obtain the formulas which are actually implemented in multi-orbital-parquet. We consider only equations in ph- and pp-channel, since $\overline{\text{ph}}$ is related to ph by crossing symmetry (3.14).

Bethe-Salpeter equation. We start from equation (3.9) and explicitly write the frequency dependencies. For ph-channel, we obtain

$$\begin{aligned} & \kappa_{\text{ph}} \Gamma^{\text{ph}}(12|56) X_0^{\text{ph}}(56|78) F^{\text{ph}}(78|34) \\ & = \kappa_{\text{ph}} \Gamma_{i_1 i_2 i_3 i_4}^{\text{ph}}(\nu_1, \nu_2, \nu_5, \nu_6) G_{i_6 i_7}(\nu_6, \nu_7) G_{i_8 i_7}(\nu_8, \nu_7) F_{i_7 i_8 i_3 i_4}^{\text{ph}}(\nu_7, \nu_8, \nu_3, \nu_4). \end{aligned} \quad (3.30)$$

Using time- and space-translation symmetry for Φ and G , the frequency convention (3.12) and the notation defined in equations (3.13) and (3.15), we have

$$\Phi_{(i_1 i_2 | i_3 i_4)}^{\text{ph}, \nu \nu' \omega} = \frac{1}{\beta^2} \sum_{\nu_1 \nu_2} \kappa_{\text{ph}} \Gamma_{(i_1 i_2 | i_5 i_6)}^{\text{ph}, \nu \nu_1 \omega} \underbrace{X_{0(i_5 i_6 | i_7 i_8)}^{\text{ph}, \nu_1 \nu_2 \omega} F_{(i_7 i_8 | i_3 i_4)}^{\text{ph}, \nu_2 \nu' \omega}}_{=:\tilde{F}_{(i_5 i_6 | i_3 i_4)}^{\text{ph}, \nu_1 \nu' \omega}}, \quad (3.31)$$

where we wrote the frequency summations explicitly for keeping track of the normalization factors, but summation over repeated spin-orbitals is still implicit.

A similar calculation yields for the pp-channel

$$\Phi_{(i_1 i_2 | i_3 i_4)}^{\text{pp}, \nu \nu' \omega} = \frac{1}{\beta^2} \sum_{\nu_1 \nu_2} \kappa_{\text{pp}} \Gamma_{(i_1 i_2 | i_5 i_6)}^{\text{pp}, \nu \nu_1 \omega} \underbrace{X_{0(i_5 i_6 | i_7 i_8)}^{\text{pp}, \nu_1 \nu_2 \omega} F_{(i_7 i_8 | i_3 i_4)}^{\text{pp}, \nu_2 \nu' \omega}}_{=:\tilde{F}_{(i_5 i_6 | i_3 i_4)}^{\text{pp}, \nu_1 \nu' \omega}}. \quad (3.32)$$

Parquet equation. We take equation (3.11) and use the vertex notation equation (3.13) which inherently respects time-translation symmetry. In order to get rid of $\Phi^{\overline{\text{ph}}}$ in equations (3.11), we have to apply crossing symmetry (3.14b). As the left-hand side of equation (3.11a) has frequencies in ph-convention (3.12), Φ^{pp} on the right-hand side however in pp-convention, the latter has to be expressed also with ph-channel frequencies. The relation between the two different convention can be read off from equation (3.13). We get for the ph-channel the parquet equation

$$F_{(i_1 i_2 | i_3 i_4)}^{\text{ph}, \nu \nu' \omega} = \Lambda_{(i_1 i_2 | i_3 i_4)}^{\text{ph}, \nu \nu' \omega} + \Phi_{(i_1 i_2 | i_3 i_4)}^{\text{ph}, \nu \nu' \omega} - \Phi_{(i_1 i_4 | i_3 i_2)}^{\text{ph}, \nu(\nu+\omega)(\nu'-\nu)} + \Phi_{(i_1 i_3 | i_2 i_4)}^{\text{pp}, \nu \nu'(\omega+\nu+\nu')} \quad (3.33)$$

and for the pp-channel

$$F_{(i_1 i_2 | i_3 i_4)}^{\text{pp}, \nu \nu' \omega} = \Lambda_{(i_1 i_2 | i_3 i_4)}^{\text{pp}, \nu \nu' \omega} + \Phi_{(i_1 i_2 | i_3 i_4)}^{\text{pp}, \nu \nu' \omega} + \Phi_{(i_1 i_3 | i_2 i_4)}^{\text{ph}, \nu \nu' (\omega - \nu - \nu')} - \Phi_{(i_1 i_4 | i_2 i_3)}^{\text{ph}, \nu (\omega - \nu') (\nu' - \nu)}. \quad (3.34)$$

Schwinger-Dyson equation. Assuming time-translation symmetry for G and Σ and using the notations defined in equations (3.13) and (3.15), Fourier transformation of equation (3.29) yields

$$\Sigma_{i_1 i_2}(\nu) = -\frac{1}{\beta} \sum_{\nu'} U_{i_1 i_4 i_3 i_2} G_{i_4 i_3}(\nu') e^{i\nu' 0^-} - \frac{1}{2\beta^3} \sum_{\nu' \nu'' \omega} U_{i_1 i_3 i_4 i_5} G_{i_3 i_8}(\nu + \omega) \underbrace{X_{0(i_4 i_5 | i_6 i_7)}^{\text{ph}, \nu' \nu'' \omega} F_{(i_6 i_7 | i_8 i_2)}^{\text{ph}, \nu' \nu \omega}}_{=\bar{F}_{(i_4 i_5 | i_8 i_2)}^{\text{ph}, \nu' \nu \omega}}, \quad (3.35)$$

where summation over repeated spin-orbitals is again implicit.

We can improve results for Schwinger-Dyson equation by using Fourier transformed quantities for both terms and considering the asymptotic behaviour of F for the second term.

Let us start with the first, so called ‘tadpole’ term (due to the form of the Feynman diagram in figure 3.5). This term is numerically problematic, as can be seen by considering the non-interacting Green’s function for a system without hopping (e. g. atomic limit in section 4.1). Then the tadpole diagram is proportional to $\sum_{\nu'} \frac{1}{i\nu' - \mu}$ and summing the terms naively in a loop would lead to almost equal negative and positive imaginary contributions and a vanishing result, whereas analytically one would get the non-zero occupation number n . Note that due to the fully anti-symmetric definition of the interaction used here, the tadpole diagram contains both the Hartree and Fock contributions.

We rewrite the tadpole (Hartree-Fock) term as

$$\begin{aligned} \frac{1}{\beta} \sum_{\nu'} U_{i_1 i_3 i_4 i_2} G_{i_3 i_4}(\nu') e^{i\nu' 0^-} &= \frac{1}{\beta} \sum_{\nu'} U_{i_1 i_3 i_4 i_2} \int_0^\beta d\tau G_{i_3 i_4}(\tau) e^{-i\nu'(\tau - 0^-)} \\ &= \frac{1}{\beta} U_{i_1 i_3 i_4 i_2} \int_0^\beta d\tau \beta \delta(\tau - 0^-) G_{i_3 i_4}(\tau) = U_{i_1 i_3 i_4 i_2} G_{i_3 i_4}(0^-). \end{aligned} \quad (3.36)$$

Thus we have replaced the summation over infinitely many bosonic Matsubara frequencies by a evaluation of the imaginary time-dependent Green’s function at 0^- . The factor $e^{i\nu' 0^-}$ was crucial for the calculation here, taking the limit from the other side would change the order of operators in G .

For the second term we write

$$\begin{aligned}
& -\frac{1}{2\beta^3} \sum_{\nu'\nu''\omega} U_{i_1 i_3 i_4 i_5} G_{i_3 i_8}(\nu + \omega) X_{0(i_4 i_5 | i_6 i_7)}^{\text{ph}, \nu' \nu'' \omega} (F_{(i_6 i_7 | i_8 i_2)}^{\text{ph}, \nu'' \nu \omega} - (U_{i_6 i_7 i_8 i_2})_{\nu'' \nu \omega}) \\
& -\frac{1}{2\beta^2} \sum_{\nu'\omega} U_{i_1 i_3 i_4 i_5} G_{i_3 i_8}(\nu + \omega) G_{i_5 i_6}(\nu') G_{i_7 i_4}(\nu' + \omega) U_{i_6 i_7 i_8 i_2}.
\end{aligned} \tag{3.37}$$

The full interaction vertex is asymptotic to U , cf. [25, p. 4], therefore subtracting it and calculating a simpler expression for the U^2 -term in the second line yields better results for the summation over ν'' and ω , since in any implementation only limited frequency box sizes are available.

This simpler expression for the U^2 -term is obtained by replacing $G(\nu)$ again with the Fourier transformed $G(\tau)$, i. e.

$$\begin{aligned}
& \frac{1}{2\beta^2} \sum_{\nu'\omega} U_{i_1 i_3 i_4 i_5} U_{i_6 i_7 i_8 i_2} G_{i_3 i_8}(\nu + \omega) G_{i_4 i_6}(\nu') G_{i_7 i_5}(\nu' + \omega) \\
& = -\frac{1}{2} \int_0^\beta d\tau U_{i_1 i_3 i_4 i_5} U_{i_6 i_7 i_8 i_2} G_{i_3 i_8}(\tau) G_{i_4 i_6}(\tau) G_{i_7 i_5}(\beta - \tau) e^{-i\nu\tau}
\end{aligned} \tag{3.38}$$

Thus the double sum over infinitely many fermionic and bosonic Matsubara frequencies was replaced by a Fourier transformed multiplication of three imaginary time-dependent Green's functions.

Collecting all terms of equations (3.36) to (3.38) yields

$$\begin{aligned}
\Sigma_{i_1 i_2}(\nu) & = -U_{i_1 i_3 i_4 i_2} G_{i_3 i_4}(0^-) + \frac{1}{2} \int_0^\beta d\tau U_{i_1 i_3 i_4 i_5} U_{i_6 i_7 i_8 i_2} G_{i_3 i_8}(\tau) G_{i_4 i_6}(\tau) G_{i_7 i_5}(\beta - \tau) e^{-i\nu\tau} \\
& -\frac{1}{2\beta^3} \sum_{\nu'\nu''\omega} U_{i_1 i_3 i_4 i_5} G_{i_3 i_8}(\nu + \omega) X_{0(i_4 i_5 | i_6 i_7)}^{\text{ph}, \nu' \nu'' \omega} (F_{(i_6 i_7 | i_8 i_2)}^{\text{ph}, \nu'' \nu \omega} - (U_{i_6 i_7 i_8 i_2})_{\nu'' \nu \omega}).
\end{aligned} \tag{3.39}$$

3.3 SU(2) symmetry*

In addition to time-translation symmetry assumed in the last section, we will now also make use of SU(2) symmetry.

Bethe-Salpeter equation. We take the right-hand side of 3.30 and apply SU(2) symmetry relations (2.34) and (2.60):

$$\Phi_{\substack{(i_1 i_2 | i_3 i_4) \\ \sigma_1 \sigma_2 \sigma_3 \sigma_4}}^{\text{ph}, \nu \nu' \omega} = \kappa_{\text{ph}} \frac{1}{\beta} \sum_{\sigma} \sum_{\nu_1} \Gamma_{\substack{(i_1 i_2 | i_5 i_6) \\ \sigma_1 \sigma_2 \sigma (\sigma - \sigma_3 + \sigma_4)}}^{\text{ph}, \nu \nu_1 \omega} G_{i_6 i_7}(\nu_1) G_{i_8 i_5}(\nu_1 + \omega) F_{\substack{(i_7 i_8 | i_3 i_4) \\ (\sigma - \sigma_3 + \sigma_4) \sigma \sigma_3 \sigma_4}}^{\text{ph}, \nu_1 \nu' \omega} \delta_{\sigma_1 - \sigma_2 + \sigma_3 - \sigma_4, 0} \quad (3.40)$$

Inserting spin combinations $\uparrow\uparrow$ and $\uparrow\downarrow$, we find

$$\Phi_{\substack{(i_1 i_2 | i_3 i_4), \uparrow\uparrow}}^{\text{ph}, \nu \nu' \omega} = \kappa_{\text{ph}} \frac{1}{\beta^2} \sum_{\nu_1 \nu_2} \sum_{\sigma} \Gamma_{\substack{(i_1 i_2 | i_5 i_6), \uparrow\sigma}}^{\text{ph}, \nu \nu_1 \omega} X_{0(i_5 i_6 | i_7 i_8)}^{\text{ph}, \nu_1 \nu_2 \omega} F_{\substack{(i_7 i_8 | i_3 i_4), \sigma\uparrow}}^{\text{ph}, \nu_2 \nu' \omega} \quad (3.41a)$$

$$\Phi_{\substack{(i_1 i_2 | i_3 i_4), \uparrow\downarrow}}^{\text{ph}, \nu \nu' \omega} = \kappa_{\text{ph}} \frac{1}{\beta^2} \sum_{\nu_1 \nu_2} \sum_{\sigma} \Gamma_{\substack{(i_1 i_2 | i_5 i_6), \uparrow\sigma}}^{\text{ph}, \nu \nu_1 \omega} X_{0(i_5 i_6 | i_7 i_8)}^{\text{ph}, \nu_1 \nu_2 \omega} F_{\substack{(i_7 i_8 | i_3 i_4), \sigma\downarrow}}^{\text{ph}, \nu_2 \nu' \omega} \quad (3.41b)$$

with both spin combinations occurring in each of the two equations. These equations can be decoupled by introducing

$$\Phi_{\substack{(i_1 i_2 | i_3 i_4)}}^{\text{d}, \nu \nu' \omega} := \Phi_{\substack{(i_1 i_2 | i_3 i_4), \uparrow\uparrow}}^{\text{ph}, \nu \nu' \omega} + \Phi_{\substack{(i_1 i_2 | i_3 i_4), \uparrow\downarrow}}^{\text{ph}, \nu \nu' \omega} \quad (3.42)$$

$$\Phi_{\substack{(i_1 i_2 | i_3 i_4)}}^{\text{m}, \nu \nu' \omega} := \Phi_{\substack{(i_1 i_2 | i_3 i_4), \uparrow\uparrow}}^{\text{ph}, \nu \nu' \omega} - \Phi_{\substack{(i_1 i_2 | i_3 i_4), \uparrow\downarrow}}^{\text{ph}, \nu \nu' \omega} \quad (3.43)$$

and similarly for F and Γ . The Bethe-Salpeter equations in the *density*- and *magnetic*-channels are

$$\Phi_{\substack{(i_1 i_2 | i_3 i_4)}}^{\text{d}, \nu \nu' \omega} = \kappa_{\text{ph}} \frac{1}{\beta^2} \sum_{\nu_1 \nu_2} \Gamma_{\substack{(i_1 i_2 | i_5 i_6)}}^{\text{d}, \nu \nu_1 \omega} X_{0(i_5 i_6 | i_7 i_8)}^{\text{ph}, \nu_1 \nu_2 \omega} F_{\substack{(i_7 i_8 | i_3 i_4)}}^{\text{d}, \nu_2 \nu' \omega} \quad (3.44a)$$

$$\Phi_{\substack{(i_1 i_2 | i_3 i_4)}}^{\text{m}, \nu \nu' \omega} = \kappa_{\text{ph}} \frac{1}{\beta^2} \sum_{\nu_1 \nu_2} \Gamma_{\substack{(i_1 i_2 | i_5 i_6)}}^{\text{m}, \nu \nu_1 \omega} X_{0(i_5 i_6 | i_7 i_8)}^{\text{ph}, \nu_1 \nu_2 \omega} F_{\substack{(i_7 i_8 | i_3 i_4)}}^{\text{m}, \nu_2 \nu' \omega} \quad (3.44b)$$

For the pp-channel we apply again SU(2) symmetry and with the definitions

$$\Phi_{\substack{(i_1 i_2 | i_3 i_4)}}^{\text{t}, \nu \nu' \omega} := \Phi_{\substack{(i_1 i_2 | i_3 i_4), \uparrow\downarrow}}^{\text{pp}, \nu \nu' \omega} + \Phi_{\substack{(i_1 i_2 | i_3 i_4), \uparrow\uparrow}}^{\text{pp}, \nu \nu' \omega} \quad (3.45)$$

$$\Phi_{\substack{(i_1 i_2 | i_3 i_4)}}^{\text{s}, \nu \nu' \omega} := \Phi_{\substack{(i_1 i_2 | i_3 i_4), \uparrow\downarrow}}^{\text{pp}, \nu \nu' \omega} - \Phi_{\substack{(i_1 i_2 | i_3 i_4), \uparrow\uparrow}}^{\text{pp}, \nu \nu' \omega} \quad (3.46)$$

we obtain the Bethe-Salpeter equations in the *triplet*- and *singlet*-channels:

$$\Phi_{(i_1 i_2 | i_3 i_4)}^{t, vv'\omega} = \kappa_{pp} \frac{1}{\beta^2} \sum_{\nu_1 \nu_2} \Gamma_{(i_1 i_2 | i_5 i_6)}^{t, vv_1 \omega} X_{0(i_5 i_6 | i_7 i_8)}^{pp, \nu_1 \nu_2 \omega} F_{(i_7 i_8 | i_3 i_4)}^{t, \nu_2 \nu' \omega}, \quad (3.47a)$$

$$\Phi_{(i_1 i_2 | i_3 i_4)}^{s, vv'\omega} = -\kappa_{pp} \frac{1}{\beta^2} \sum_{\nu_1 \nu_2} \Gamma_{(i_1 i_2 | i_5 i_6)}^{s, vv_1 \omega} X_{0(i_5 i_6 | i_7 i_8)}^{pp, \nu_1 \nu_2 \omega} F_{(i_7 i_8 | i_3 i_4)}^{s, \nu_2 \nu' \omega}. \quad (3.47b)$$

Note the additional minus sign for the s-channel. The vertices for d-, m-, t and s-channels do not depend on spin, so the memory requirement for a single vertex is reduced by a factor of 16. However, now four instead of two channels are needed, therefore memory is reduced effectively by a factor of 8.

Parquet equation. To obtain a relation between F , Φ , Λ in d-channel, we start from definition (3.42) and use the more general parquet equation (3.33):

$$\begin{aligned} F_{(i_1 i_2 | i_3 i_4)}^{d, vv'\omega} &= \Lambda_{(i_1 i_2 | i_3 i_4) \uparrow \uparrow}^{ph, vv'\omega} + \Phi_{(i_1 i_2 | i_3 i_4) \uparrow \uparrow}^{ph, vv'\omega} - \Phi_{(i_1 i_4 | i_3 i_2) \uparrow \uparrow}^{ph, v(v+\omega)(v'-v)} + \Phi_{(i_1 i_3 | i_2 i_4) \uparrow \uparrow}^{pp, vv'(\omega+v+v')} \\ &+ \Lambda_{(i_1 i_2 | i_3 i_4) \uparrow \downarrow}^{ph, vv'\omega} + \Phi_{(i_1 i_2 | i_3 i_4) \uparrow \downarrow}^{ph, vv'\omega} - \Phi_{(i_1 i_4 | i_3 i_2) \uparrow \downarrow}^{ph, v(v+\omega)(v'-v)} + \Phi_{(i_1 i_3 | i_2 i_4) \uparrow \downarrow}^{pp, vv'(\omega+v+v')} \end{aligned} \quad (3.48)$$

Applying (2.66), we obtain a relation between ph-channel vertices with spin combination $\uparrow \downarrow$ and m-channel vertices:

$$\Phi_{(i_1 i_2 | i_3 i_4) \uparrow \downarrow}^{ph, vv'\omega} = \Phi_{(i_1 i_2 | i_3 i_4)}^{m, vv'\omega}. \quad (3.49)$$

With this equality and definitions (3.42), (3.43), (3.45) and (3.46) we obtain the parquet equation in the density-channel:

$$\begin{aligned} F_{(i_1 i_2 | i_3 i_4)}^{d, vv'\omega} &= \Lambda_{(i_1 i_2 | i_3 i_4)}^{d, vv'\omega} + \Phi_{(i_1 i_2 | i_3 i_4)}^{d, vv'\omega} - \frac{1}{2} \Phi_{(i_1 i_4 | i_3 i_2)}^{d, v(v+\omega)(v'-v)} - \frac{3}{2} \Phi_{(i_1 i_4 | i_3 i_2)}^{m, v(v+\omega)(v'-v)} \\ &+ \frac{3}{2} \Phi_{(i_1 i_3 | i_2 i_4)}^{t, vv'(\omega+v+v')} + \frac{1}{2} \Phi_{(i_1 i_3 | i_2 i_4)}^{s, vv'(\omega+v+v')}. \end{aligned} \quad (3.50)$$

A similar calculation yields for magnetic-channel

$$\begin{aligned} F_{(i_1 i_2 | i_3 i_4)}^{m, vv'\omega} &= \Lambda_{(i_1 i_2 | i_3 i_4)}^{m, vv'\omega} + \Phi_{(i_1 i_2 | i_3 i_4)}^{m, vv'\omega} - \frac{1}{2} \Phi_{(i_1 i_4 | i_3 i_2)}^{d, v(v+\omega)(v'-v)} + \frac{1}{2} \Phi_{(i_1 i_4 | i_3 i_2)}^{m, v(v+\omega)(v'-v)} \\ &+ \frac{1}{2} \Phi_{(i_1 i_3 | i_2 i_4)}^{t, vv'(\omega+v+v')} - \frac{1}{2} \Phi_{(i_1 i_3 | i_2 i_4)}^{s, vv'(\omega+v+v')}. \end{aligned} \quad (3.51)$$

For triplet-channel we obtain

$$F_{(i_1 i_2 | i_3 i_4)}^{t, \nu \nu' \omega} = \Lambda_{(i_1 i_2 | i_3 i_4)}^{t, \nu \nu' \omega} + \Phi_{(i_1 i_2 | i_3 i_4)}^{t, \nu \nu' \omega} + \frac{1}{2} \Phi_{(i_1 i_3 | i_2 i_4)}^{d, \nu \nu' (\omega - \nu - \nu')} + \frac{1}{2} \Phi_{(i_1 i_3 | i_2 i_4)}^{m, \nu \nu' (\omega - \nu - \nu')} - \frac{1}{2} \Phi_{(i_1 i_4 | i_2 i_3)}^{d, \nu (\omega - \nu') (\nu' - \nu)} - \frac{1}{2} \Phi_{(i_1 i_4 | i_2 i_3)}^{m, \nu (\omega - \nu') (\nu' - \nu)}, \quad (3.52)$$

and for singlet-channel the parquet equation becomes

$$F_{(i_1 i_2 | i_3 i_4)}^{s, \nu \nu' \omega} = \Lambda_{(i_1 i_2 | i_3 i_4)}^{s, \nu \nu' \omega} + \Phi_{(i_1 i_2 | i_3 i_4)}^{s, \nu \nu' \omega} + \frac{1}{2} \Phi_{(i_1 i_3 | i_2 i_4)}^{d, \nu \nu' (\omega - \nu - \nu')} - \frac{3}{2} \Phi_{(i_1 i_3 | i_2 i_4)}^{m, \nu \nu' (\omega - \nu - \nu')} + \frac{1}{2} \Phi_{(i_1 i_4 | i_2 i_3)}^{d, \nu (\omega - \nu') (\nu' - \nu)} - \frac{3}{2} \Phi_{(i_1 i_4 | i_2 i_3)}^{m, \nu (\omega - \nu') (\nu' - \nu)}. \quad (3.53)$$

Schwinger-Dyson equation. We take equation (3.35) and apply SU(2) symmetry relations (2.34) and (2.60). For the first term we have

$$-\frac{1}{\beta} \sum_{\nu'} \sum_{\sigma} U_{i_1 i_3 i_4 i_2} G_{i_3 i_4}(\nu') e^{i\nu' 0^-} \delta_{\sigma_1, \sigma_2} \xrightarrow{(\sigma_1 \sigma_2) = \uparrow \uparrow} -\frac{1}{\beta} \sum_{\nu'} (U_{i_1 i_3 i_4 i_2, \uparrow \uparrow} + U_{i_1 i_3 i_4 i_2, \uparrow \downarrow}) G_{i_3 i_4}(\nu') e^{i\nu' 0^-}. \quad (3.54)$$

For the second term we obtain

$$-\frac{1}{2\beta^2} \sum_{\nu' \omega} \sum_{\sigma} U_{i_1 i_3 i_4 i_5} G_{i_3 i_8}(\nu + \omega) G_{i_5 i_6}(\nu') G_{i_7 i_4}(\nu' + \omega) F_{(i_6 i_7 | i_8 i_2)}^{\text{ph}, \nu' \nu \omega} \delta_{\sigma_1, \sigma_2} \xrightarrow{(\sigma_1 \sigma_2) = \uparrow \uparrow} -\frac{1}{2\beta^2} \sum_{\nu' \omega} G_{i_3 i_8}(\nu + \omega) G_{i_5 i_6}(\nu') G_{i_7 i_4}(\nu' + \omega) (U_{i_1 i_3 i_4 i_5, \uparrow \uparrow} F_{(i_6 i_7 | i_8 i_2), \uparrow \uparrow}^{\text{ph}, \nu' \nu \omega} + U_{i_1 i_3 i_4 i_5, \uparrow \downarrow} F_{(i_6 i_7 | i_8 i_2), \uparrow \downarrow}^{\text{ph}, \nu' \nu \omega}). \quad (3.55)$$

We perform the same numerical improvements for the bubble- and U^2 -term as described in the previous section and use definitions (3.42) and (3.43), which yields

$$\begin{aligned} \Sigma_{i_1 i_2, \uparrow \uparrow}(\nu) &= -(U_{i_1 i_3 i_4 i_2, \uparrow \uparrow} + U_{i_1 i_3 i_4 i_2, \uparrow \downarrow}) G_{i_3 i_4}(0^-) \\ &+ \frac{1}{2} \int_0^\beta d\tau (U_{i_1 i_3 i_4 i_5, \uparrow \uparrow} U_{i_6 i_7 i_8 i_2, \uparrow \uparrow} + U_{i_1 i_3 i_4 i_5, \uparrow \downarrow} U_{i_6 i_7 i_8 i_2, \uparrow \downarrow}) G_{i_3 i_8}(\tau) G_{i_4 i_6}(\tau) G_{i_7 i_5}(\beta - \tau) e^{-i\nu \tau} \\ &- \frac{1}{4\beta^3} \sum_{\nu' \nu'' \omega} G_{i_3 i_8}(\nu + \omega) \left(U_{i_1 i_3 i_4 i_5, \uparrow \uparrow} X_{0(i_4 i_5 | i_6 i_7)}^{\text{ph}, \nu' \nu'' \omega} (F_{(i_6 i_7 | i_8 i_2)}^{d, \nu'' \nu \omega} + F_{(i_6 i_7 | i_8 i_2)}^{m, \nu'' \nu \omega} - 2(U_{i_6 i_7 i_8 i_2, \uparrow \uparrow}) \nu'' \nu \omega) \right. \\ &\quad \left. + U_{i_1 i_3 i_4 i_5, \uparrow \downarrow} X_{0(i_4 i_5 | i_6 i_7)}^{\text{ph}, \nu' \nu'' \omega} (F_{(i_6 i_7 | i_8 i_2)}^{d, \nu'' \nu \omega} - F_{(i_6 i_7 | i_8 i_2)}^{m, \nu'' \nu \omega} - 2(U_{i_6 i_7 i_8 i_2, \uparrow \downarrow}) \nu'' \nu \omega) \right). \end{aligned} \quad (3.56)$$

3.4 Parquet method

The parquet formalism is a self-consistent method for calculating self-energies, full-interaction vertices and as a consequence response functions (e. g. generalized susceptibility X) for given Hamiltonian H , irreducible vertex Λ and suitable starting guesses for F , Φ , and Σ . Note that the method is a fix-point iteration, but neither convergence nor uniqueness of the solution is guaranteed [4, p. 38].

As described in section 2.1, the Hamiltonian (or more precisely, hopping amplitudes t_{ij} and two-body integrals U_{ijkl}) can be obtained by means of density-functional theory and Wannierization. The irreducible vertex can be approximated simply by the bare interaction,

$$\begin{aligned}\Lambda_{(i_1 i_2 | i_3 i_4)}^{\text{ph}, vv' \omega} &\approx (U_{i_1 i_2 i_3 i_4})_{vv' \omega}, \\ \Lambda_{(i_1 i_2 | i_3 i_4)}^{\text{pp}, vv' \omega} &\approx (U_{i_1 i_3 i_2 i_4})_{vv' \omega},\end{aligned}$$

which is called *parquet approximation* [4, p. 38] and was first suggested in [2, p. 44]. A more sophisticated approach would be the usage of Λ calculated by dynamical vertex approximation [10]. Λ does not change during the iteration – this approximation is the reason why only a subset of all possible diagrams is summed over in equation (3.3). For the parquet approximation we neglect all but one fully irreducible diagrams, which is a rather strong simplification (the next, neglected, fully irreducible diagram is of order U^4).

Algorithm 1 sketches the single steps for the parquet method. Details on how convergence is measured and how vertices and self-energy are initialized depend on the actual implementation – specific information for our multi-orbital Hubbard model implementation `multi-orbital-parquet` is found in appendix B.

3.5 Implementation*

3.5.1 General remarks

Algorithm 1 was implemented in the Fortran program `multi-orbital-parquet` with a core solver based on the Dyson equation (2.44) and on equations (3.31) to (3.34) and (3.39) for time-translation symmetry only, and, when input flag `SU2_BOOL` is activated, with additional SU(2) symmetry using equations (3.44), (3.47), (3.50) to (3.53)

Algorithm 1 Parquet method with equations using time-translation or additionally SU(2) symmetry.

```

1: Approximate  $\Lambda$ 
2: Initialize  $\Sigma^{(0)} \leftarrow 0$ ,  $F^{(0)}$ ,  $\Phi^{(0)}$  and  $\Gamma^{(0)} = F^{(0)} - \Phi^{(0)}$  depending on  $\Lambda$ 
3: Calculate  $G_0$  and  $G^{(0)}$  by (2.44)
4: for  $i = 1, i_{\max}$  do
5:   Calculate  $\Phi^{(i)}$  from  $F^{(i-1)}$ ,  $\Gamma^{(i-1)}$  &  $G^{(i-1)}$  by (3.31) & (3.32) or (3.44) & (3.47)
6:   Calculate  $F^{(i)}$  from  $\Lambda$  and  $\Phi^{(i)}$  by (3.33) & (3.34) or (3.50)–(3.53)
7:   Calculate  $\Gamma^{(i)} = F^{(i)} - \Phi^{(i)}$ 
8:   Calculate  $\Sigma^{(i)}$  from  $F^{(i)}$  and  $G^{i-1}$  by (3.39) or (3.56)
9:   Calculate  $G^{(i)}$  from  $G_0$  and  $\Sigma^{(i)}$  by (2.44)
10:  if  $F^{(i)}$ ,  $\Sigma^{(i)}$  converged then
11:    break
12:  end if
13: end for

```

and (3.56) for calculation.

Note that the current version of multi-orbital-parquet only handles frequencies, however, a generalization for generalized frequencies, $\nu = (\tilde{\nu}, \mathbf{k})$ with momenta \mathbf{k} , is straightforward. Another possibility to add momentum dependence would be the implementation of the truncated unity scheme, which is much more memory efficient than an implementation with generalized frequencies [4, p. 55]. The truncated unity scheme requires a Schwinger-Dyson equation with contributions from all channels, specific formulas for the multi-orbital Hubbard model are derived in appendix A.

The frequency range can be reduced due to symmetries. For fermionic Matsubara frequencies the range includes positive and negative frequencies, but only positive for bosonic ones due to complex conjugation (2.52) and time-reversal symmetry (2.68):

$$\left(\Phi_{(i_1 i_2 | i_3 i_4)}^{r, \nu \nu' \omega}\right)^* = \Phi_{(i_1 i_2 | i_3 i_4)}^{r, (-\nu)(-\nu')(-\omega)} \quad (3.57)$$

for an arbitrary channel r . So by using this symmetry relation, vertex values for negative bosonic frequencies can be obtained on demand and thus memory required for a vertex can be reduced approximately by a factor of two. The N_F fermionic frequencies in the code are spread symmetrically around zero, $\nu_i = (2n_i + 1)\frac{\pi}{\beta}$ with $n_i = -\frac{N_F}{2}, \dots, \frac{N_F}{2} - 1$; therefore, N_F has to be even. The N_B bosonic frequencies start from zero, so $\omega_j = 2m_j\frac{\pi}{\beta}$ with $m_j = 0, \dots, N_B - 1$.

Bottleneck of the code is memory consumption. Memory requirement for an entire vertex is tabulated in table 3.1. To reduce the size of arrays, the code uses the Message

Table 3.1: Memory consumption for an entire vertex with fermionic Matsubara frequency number N_F and number of orbitals N_O in GB (number of spins $N_S = 2$). Bosonic Matsubara frequency number is fixed as $N_B = 32$, SU(2) symmetry is not used.

N_O/N_F	4	8	16	32	64
2	0.002	0.008	0.034	0.134	0.537
6	0.170	0.679	2.718	10.872	43.487
10	1.310	5.243	20.972	83.886	335.544

Parsing Interface (MPI) and vertices are divided in ω -chunks between different nodes. All other quantities are stored on every node in order to avoid extensive communication. Therefore, the total memory consumption grows slightly larger than $\mathcal{O}(N_O^4 N_F^2 N_B)$, N_O denoting the number of orbitals used in the code. Calculation with SU(2) symmetry is enabled by an input flag, it reduces memory consumption (roughly) by a factor of 8, as mentioned in section 3.3. Before calculation `multi-orbital-parquet` prints the projected memory consumption.¹

The imaginary-time Green's function $G(\tau)$ required for asymptotic corrections is calculated from $G(\nu)$ with asymptotic flanks removed, $G(\tau) = \frac{1}{\beta} \sum_{\nu} (G(\nu) - \frac{1}{\nu}) e^{i\nu\tau}$ and then $G(\tau) \leftarrow G(\tau) - \frac{1}{2}$. Quantities which are Fourier transformed from imaginary time to frequency domain are approximated by a cubic spline and then integrated by using analytical formulas.²

3.5.2 Technical remarks

Numbers refer to lines in algorithm 1.

ad 5: Since the Bethe-Salpeter equations are diagonal in ω , every node can perform calculations independently and no communication is needed. By introducing combined indices $i = (i_1, i_2, \nu)$ the Bethe-Salpeter equations can be reformulated as a matrix-multiplication for a fixed value of ω , i. e. it can be written as $(\Phi_{ij})_{\omega} = \kappa(\Gamma_{ik})_{\omega} (\tilde{F}_{kj})_{\omega}$, with $(\tilde{F}_{kj})_{\omega} = (X_{0kl})_{\omega} (F_{lj})_{\omega}$. This matrix multiplication is implemented with LAPACK routine `zgemm`. Furthermore, over-relaxation for Φ is implemented to improve convergence, meaning that the new vertices Φ are mixed with the older ones by $\Phi^{(i)} \leftarrow (1 - \alpha) \Phi^{(i)} + \alpha \Phi^{(i-1)}$, with relaxation parameter $\alpha \geq 0$.

¹This feature was contributed by Kayran Schmidt.

²The code in `fourier_routines.f90`, `f_gamma_functions.f90` and `mpi_routines.f90` was contributed by Anna Kauch.

- ad 6: Due to the structure of parquet equations vertices from different ω -chunks and thus from different nodes have to be added. This requires extensive data exchange, making the parquet equations the computational bottleneck of the code. Data exchange is realized in `multi-orbital-parquet` with `MPI_Bcast` in the same way as in [13, pp. 6–7], which was originally proposed in [21, p. 13]. Due to crossing symmetry applied to $\overline{\text{ph}}$ -vertices in order to convert them to `ph`-notation, the second fermionic frequency argument is shifted as $v' \rightarrow (v + \omega)$ and values can exceed the frequency box. `multi-orbital-parquet` overcomes this problem by using Kernel functions which employ the scan-edge method [25, p. 7]: if $v + \omega$ exceeds the box, we approximate $\Phi^{v(v+\omega)(v'-v)} \approx \Phi^{v\tilde{v}(v'-v)}$ by taking the nearest value at the edge, i.e. $\tilde{v} = v_{-N_F/2}$ or $\tilde{v} = v_{N_F/2-1}$, as $\Phi^{vv'\omega}$ is asymptotically constant along v' for fixed v and ω . Note that for vertices with bosonic frequencies outside the box no approximation with Kernel functions is provided, they are set to 0.
- ad 8: Correction terms for the Schwinger-Dyson equation are computed only on the master node, whereas the terms with ω -summation are computed on all nodes in ω -chunks and summation is then performed by `MPI_Allreduce`, similarly as [13, p. 7]. For faster computation quantities which are summed over v' are evaluated first, i. e. $\tilde{F}_{ik}^{\text{red},v'v\omega} = \frac{1}{\beta} \sum_{v''} X_{0ij}^{v'v''\omega} (F_{jk}^{v''v\omega} - (U_{jk})_{v''v\omega})$, then the v' -summation is performed and subsequently `zgemm` used for multiplication of U_{ij} and $\frac{1}{\beta} \sum_{v'} \tilde{F}_{jk}^{\text{red},v'v\omega}$.
- ad 9: LAPACK routines `zgetrf` and `zgetri` are used for Dyson equation $G(v) = [G_0(v) - \Sigma(v)]^{-1}$, and also for $G_0 = [iv + \mu - H_0]^{-1}$. If $G(v)$ is needed for a value v outside the frequency box, the code approximates it by $G(v) \approx [iv - \mu - \Sigma_{\text{static}}]^{-1}$, where Σ_{static} is the Hartree-Fock term in the Schwinger-Dyson equation (3.39) or (3.56).



Die approbierte gedruckte Originalversion dieser Diplomarbeit ist an der TU Wien Bibliothek verfügbar
The approved original version of this thesis is available in print at TU Wien Bibliothek.

CHAPTER 4

RESULTS

4.1 Atomic limit*

Throughout the development of multi-orbital-parquet the code was tested with the atomic limit single-orbital Hubbard model with effective Coulomb interaction U ,

$$H = U n_{\uparrow} n_{\downarrow} - \mu (n_{\uparrow} + n_{\downarrow}), \quad (4.1)$$

where $n_{\sigma} = c_{\sigma}^{\dagger} c_{\sigma}$ and $\mu = \frac{U}{2}$ (half-filling). The built-in test option also uses the atomic-limit Hubbard model; results can be validated with the included Jupyter notebooks (see appendix B for more details).

Numerical results in this section were checked against analytical results derived in [22]. All calculations were performed on a MacBook Pro (2016) with a 2 GHz Dual-Core processor and 8 GB DDR3 RAM. The number of orbitals was set to $N_{\text{ORBITAL}} = 1$, and calculations were performed with $t_{ij} = 0$, $U_{\uparrow\uparrow\downarrow} = U_{\downarrow\downarrow\uparrow} = U$, $U_{\uparrow\downarrow\uparrow} = U_{\downarrow\uparrow\downarrow} = -U$ and otherwise 0. Except for general time-translation and time-reversal symmetry (and SU(2) symmetry for figure 4.5) no hard-coded symmetries were used for this problem.

We tested convergence of the parquet equation depending on the box size N_F by using analytic vertices $\Lambda_{\text{exact}}^{\text{ph}}$, $\Phi_{\text{exact}}^{\text{ph}}$ and $\Phi_{\text{exact}}^{\text{pp}}$ as input. The used parameters are demanding, as they lie slightly over the first divergence line [24, fig. 14]. The left diagram of figure 4.1 shows the results with and without usage of Kernel functions (scan edge procedure). Apparently they are crucial for convergence; this was also the problem which [21] was facing when implementing the parquet equations without Kernels.

Furthermore, the convergence of the Bethe-Salpeter equation was tested in a similar fashion, with analytic vertices $\Gamma_{\text{exact}}^{\text{ph}}$, $F_{\text{exact}}^{\text{ph}}$ and $X_{0\text{exact}}^{\text{ph}}$ as input. The full interaction vertex was calculated from the reducible vertex by $F^{\text{ph}} = \Gamma_{\text{exact}}^{\text{ph}} + \Phi^{\text{ph}}$, the right plot in figure 4.1 shows the results.

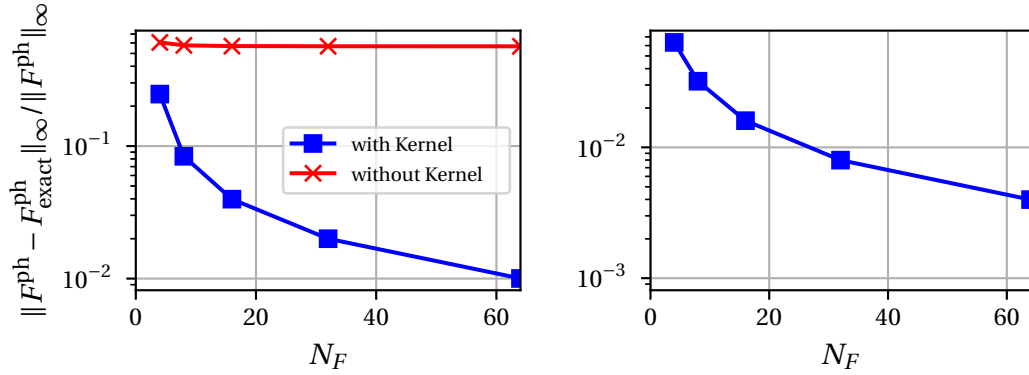


Figure 4.1: Convergence of parquet equation with and without Kernel functions for $N_B = N_F$ (left) and convergence of Bethe-Salpeter equation (right) for full-interaction vertex F^{ph} with $\omega = 0$ (no SU(2) symmetry used). Parameters $\beta = 2.3$, $U = 1.55$ (and $\mu = \frac{U}{2}$) are slightly above the first divergence line for $\frac{1}{\beta U} \approx 0.276$, as shown in [24, fig. 14]. Note that according to the plot, Kernel functions are crucial for the convergence of the parquet equations.

In figures 4.2 and 4.4 we show the real and imaginary parts of the converged self-energy in spin-sector $\uparrow\uparrow$ as well as the full interaction vertex F and reducible vertices Φ in spin-sector $(\uparrow\downarrow \mid \downarrow\uparrow)$ after a successful run of multi-orbital-parquet with default convergence parameters as tabulated in appendix B. Parameters were chosen as $N_F = N_B = 20$, $\beta = 1.0$, $U = 0.5$ and $\mu = \frac{U}{2}$; no SU(2) symmetry was used. The values for Σ and F are in good agreement with the analytic results, the offset of Φ stems from the rather small frequency box. The results for $N_F = N_B = 64$ in the right plot of figure 4.3) indicate that the discrepancies vanish for large frequency boxes.

The same calculation with parameters $N_F = N_B = 20$, $\beta = 1.0$, $U = 0.5$ and $\mu = \frac{U}{2}$ was repeated with SU(2) symmetry. We remark again the good agreement for F with the analytic results, whereas the offset for Φ is again present, except for the t-channel, which is in accordance with the analytical values (see figure 4.5).

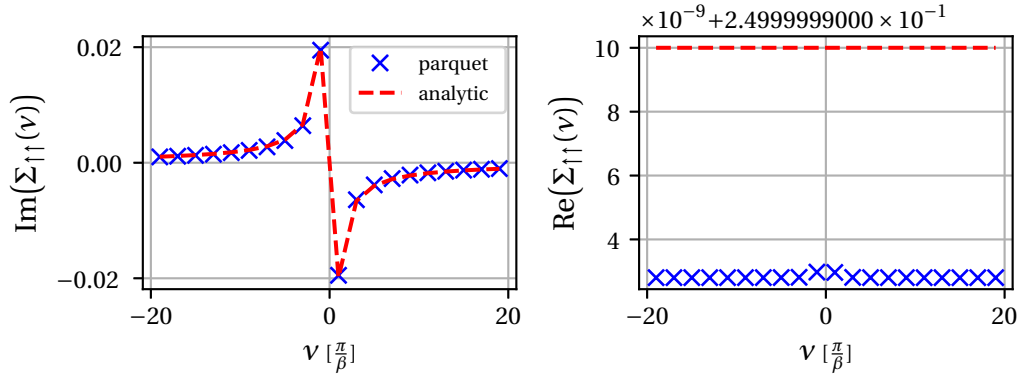


Figure 4.2: Imaginary and real parts of $\Sigma(v)$ in spin-sector $\uparrow\uparrow$ for $N_F = N_B = 20$, with $\beta = 1.0$, $U = 0.5$ and $\mu = \frac{U}{2}$. Blue crosses are results obtained by using multi-orbital-parquet, the red dashed line indicates analytic results from [22]. No $SU(2)$ symmetry was used.

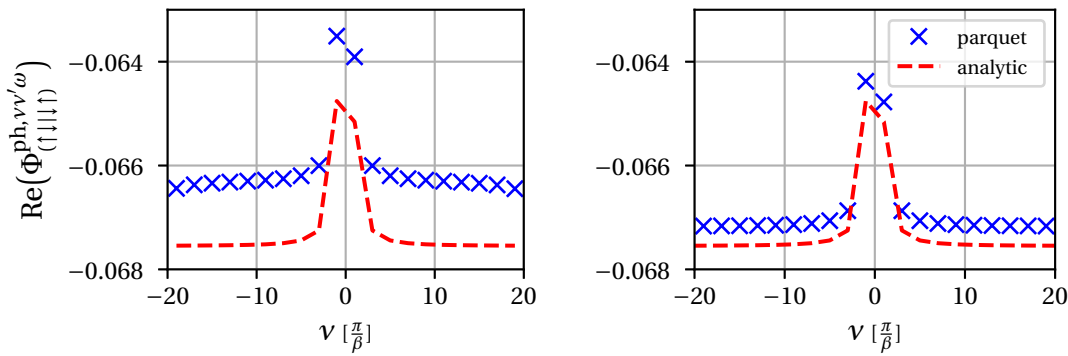


Figure 4.3: Real part of $\Phi^{\text{ph}, vv'\omega}$ in spin-sector $(\uparrow\downarrow | \downarrow\uparrow)$ with $N_F = N_B = 20$ (left) and $N_F = N_B = 64$ (right), both for $v' = \frac{\pi}{\beta}$ and $\omega = 0$. Parameters were chosen as $\beta = 1.0$, $U = 0.5$ and $\mu = \frac{U}{2}$, no $SU(2)$ symmetry was used. It is clearly visible that the offset between numerical and analytical results vanishes for larger frequency boxes.

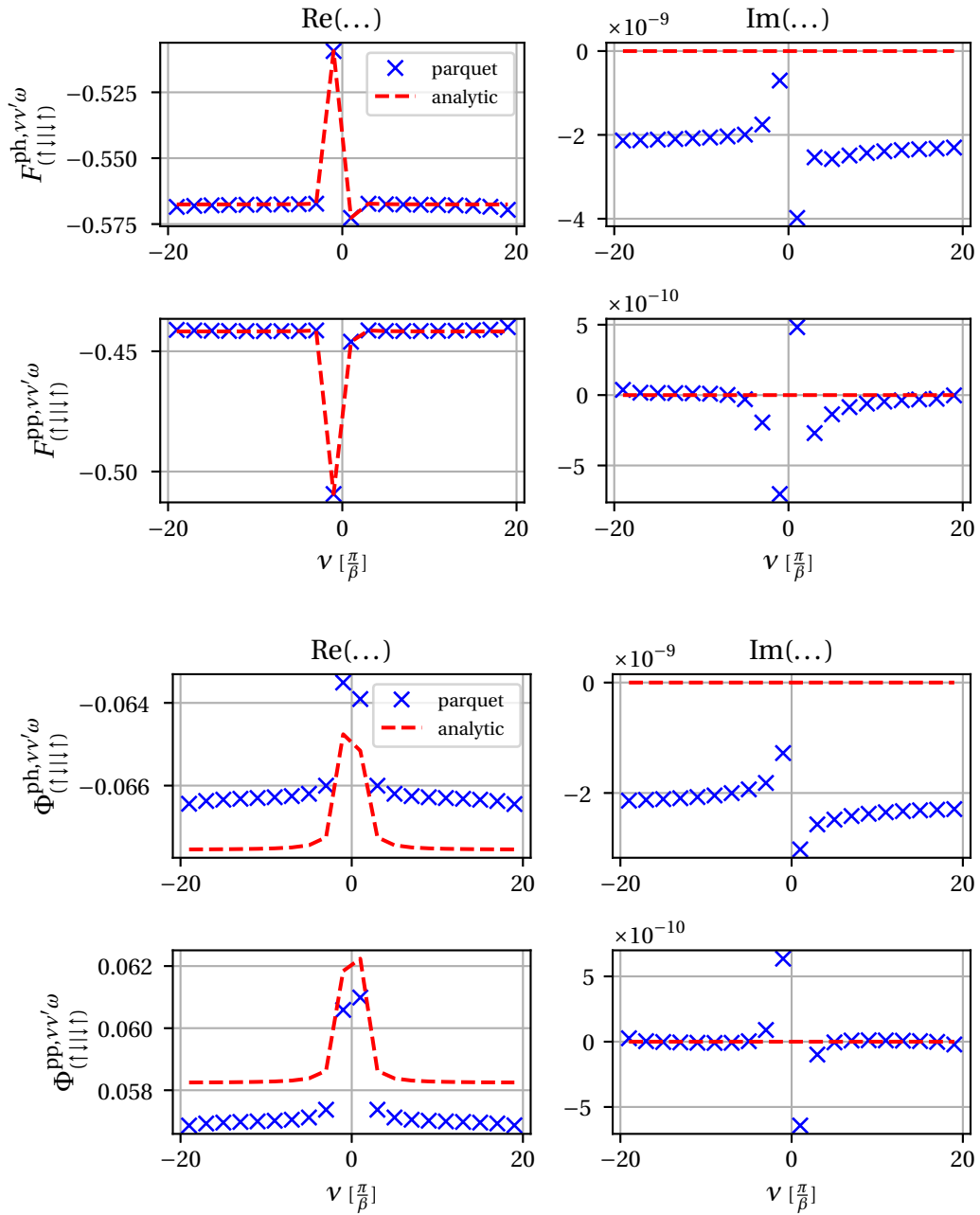


Figure 4.4: Real and imaginary parts of $F^{r, vv' \omega}$ (top) and $\Phi^{r, vv' \omega}$ (bottom), $r = (\text{ph}, \text{pp})$, in spin-sector $(\uparrow \downarrow | \downarrow \uparrow)$ for $v' = \frac{\pi}{\beta}$ and $\omega = 0$. Note the small imaginary parts for numerical values, which is in good agreement with the real analytical results. Same parameters as in figure 4.2.

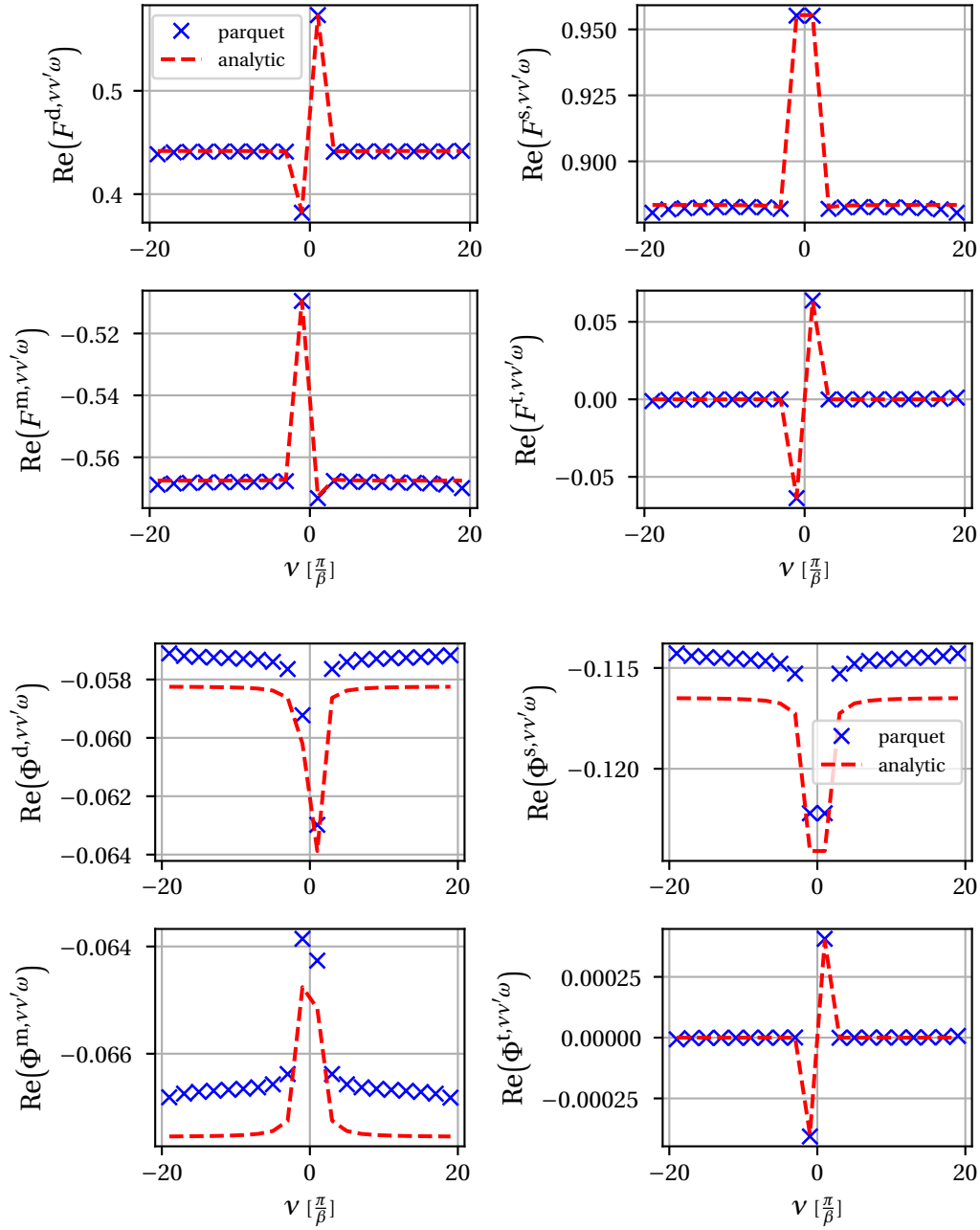


Figure 4.5: Real parts of $F^{r,vv'\omega}$ (top) and $\Phi^{r,vv'\omega}$ (bottom), $r = (d, m, t, s)$, for $v' = \frac{\pi}{\beta}$ and $\omega = 0$. Same parameters as in figure 4.2. For this plot SU(2) symmetry was used.

4.2 Benzene molecule

In this section we reproduce some results of Kayran Schmidt's project thesis on studying the benzene molecule with multi-orbital-parquet on Vienna Scientific cluster (VSC4).

Benzene (C_6H_6) is a molecule consisting of 6 carbon and 6 hydrogen atoms. The $1s$ -orbital of each hydrogen atom hybridizes with the $2s$ -, $2p_x$ - and $2p_y$ -orbitals of carbon, forming σ -bonds, which connect the carbon atoms by a hexagonal ring. The remaining p_z -orbitals of the carbon atoms also overlap and form π -bonds [17, pp. 6].

In the low-temperature regime the σ -bonds are completely filled and affect the system only by screening. Therefore, dynamics and correlations stem mainly from the unsaturated π -electrons. They are mapped in the Pariser-Parr-Pople (PPP) model to creation and annihilation operators $c_i^{(\dagger)}$, i denoting the carbon site [17, p. 6–7].

The system is described by a Hamiltonian with periodic boundary conditions,

$$\begin{aligned}
 H = & -t \sum_{i=1}^6 \sum_{\sigma} (c_{i\sigma}^{\dagger} c_{(i+1)\sigma} + c_{(i+1)\sigma}^{\dagger} c_{i\sigma}) - \mu \sum_{i=1}^6 \sum_{\sigma} c_{i\sigma}^{\dagger} c_{i\sigma} + \sum_{i=1}^6 U c_{i\uparrow}^{\dagger} c_{i\uparrow} c_{i\downarrow}^{\dagger} c_{i\downarrow} \\
 & + \frac{1}{2} \sum_{i=1}^6 \sum_{\sigma\sigma'} c_{i\sigma}^{\dagger} c_{i\sigma} \left[V_1 (c_{(i+1)\sigma'}^{\dagger} c_{(i+1)\sigma'} + c_{(i-1)\sigma'}^{\dagger} c_{(i-1)\sigma'}) \right. \\
 & \left. + V_2 (c_{(i+2)\sigma'}^{\dagger} c_{(i+2)\sigma'} + c_{(i-2)\sigma'}^{\dagger} c_{(i-2)\sigma'}) + V_3 c_{(i+3)\sigma'}^{\dagger} c_{(i+3)\sigma'} \right],
 \end{aligned} \tag{4.2}$$

with nearest-neighbor hopping amplitude t , on-site interaction $U = 3.962t$, non-local interaction $V_1 = 2.832t$, $V_2 = 2.014t$, $V_3 = 1.803t$ and chemical potential $\mu = (\frac{1}{2}U + 2V_1 + 2V_2 + V_3)$. Figure 4.6 depicts the structure of benzene and the interaction terms of the PPP model.

Calculations were performed on VSC4 for $\beta = 1.0$ and $\beta = 2.0$ with default convergence parameters and box sizes $N_F = 24$ and $N_B = 12$. Carbon atoms were treated as distinct orbitals, thus the number of orbitals was set as `N_ORBITAL = 6`. In order to fully test the code, no translational symmetry in space or $SU(2)$ symmetry were assumed. The hopping amplitude was set to $t = 1.0$, and all interactions were scaled by a factor 0.1 for figures 4.7 and 4.8 and by a factor 0.5 for figure 4.9 in order to reduce the number of iterations and the size of frequency box needed for convergence. The results are compared with values calculated by Anna Kauch using a parquet implantation for single-band Hubbard models called *victory* (see [13] for details). All resulting quantities (self-energy and vertices) were checked for fulfillment of translational, $SU(2)$ and particle-hole symmetries in the framework of Kayran Schmidt's project thesis. Figures 4.7 to 4.9 show that

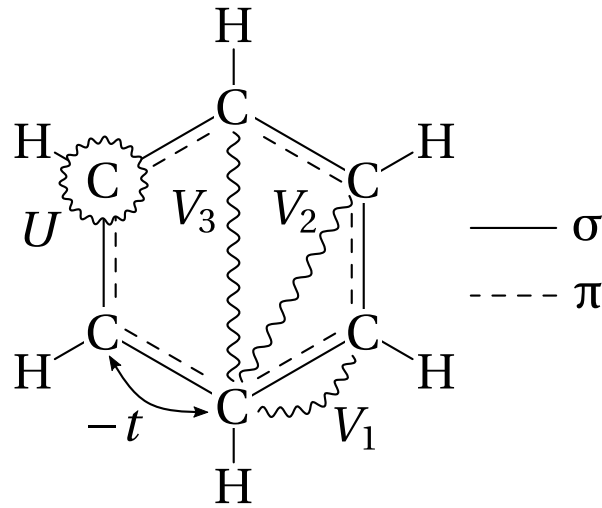


Figure 4.6: Schematic picture of benzene (C_6H_6) showing σ - and π -bonds, on-site interaction U , interaction terms V_i and hopping amplitude t for PPP model. Adapted from Kayran Schmidt.

indeed the results fulfill the translational and particle-hole symmetry relations

$$\operatorname{Re}(\Sigma_{k=0}(\nu)) + \operatorname{Re}(\Sigma_{k=\pi}(\nu)) = 2\mu,$$

$$\operatorname{Im}(\Sigma_{k=0}(\nu)) = \operatorname{Im}(\Sigma_{k=\pi}(\nu)),$$

$$\operatorname{Re}(\Sigma_{k=\frac{\pi}{3}}(\nu)) = \operatorname{Re}(\Sigma_{k=\frac{5\pi}{3}}(\nu)),$$

$$\operatorname{Im}(\Sigma_{k=\frac{\pi}{3}}(\nu)) = \operatorname{Im}(\Sigma_{k=\frac{5\pi}{3}}(\nu)).$$

The agreement between the results for interaction terms scaled by 0.1 obtained with the *victory* and multi-orbital-parquet codes is excellent. For interaction terms scaled by 0.5 differences in the asymptotic corrections of both codes and box size effects due to the rather high inverse temperature $\beta = 3.0$ are the reasons for the small quantitative discrepancies in figure 4.9; they should vanish for larger box sizes.

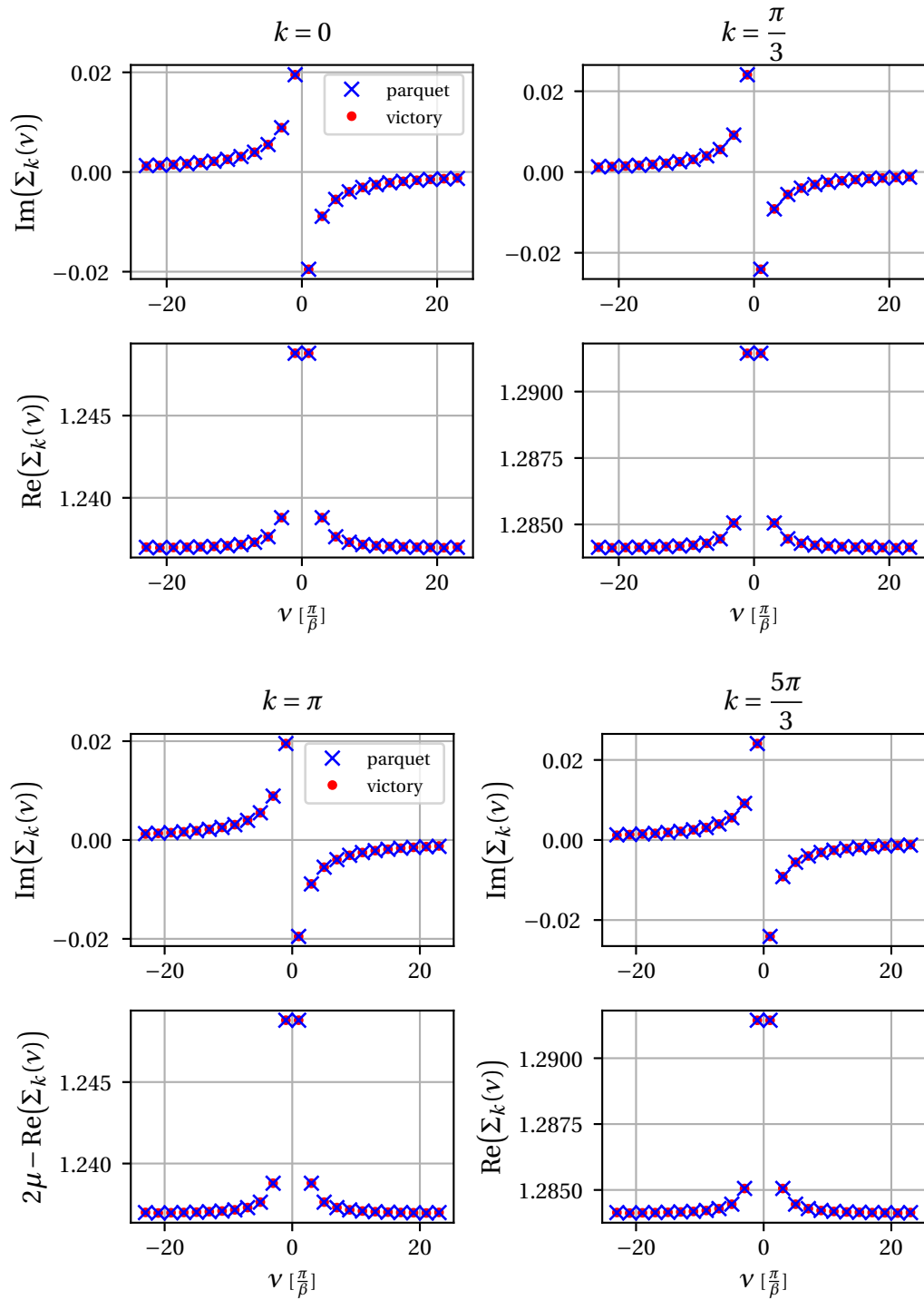


Figure 4.7: $\Sigma_k(\nu)$ with $k = 0$ (top, left) and $k = \frac{\pi}{3}$ (top, right), $k = \pi$ (bottom, left) and $k = \frac{5\pi}{3}$ (bottom, right) for $\beta = 1.0$, with interaction terms scaled by a factor 0.1. Blue crosses are results obtained by Kayran Schmidt using multi-orbital-parquet on VSC4, red dots were calculated by Anna Kauch using victory code.

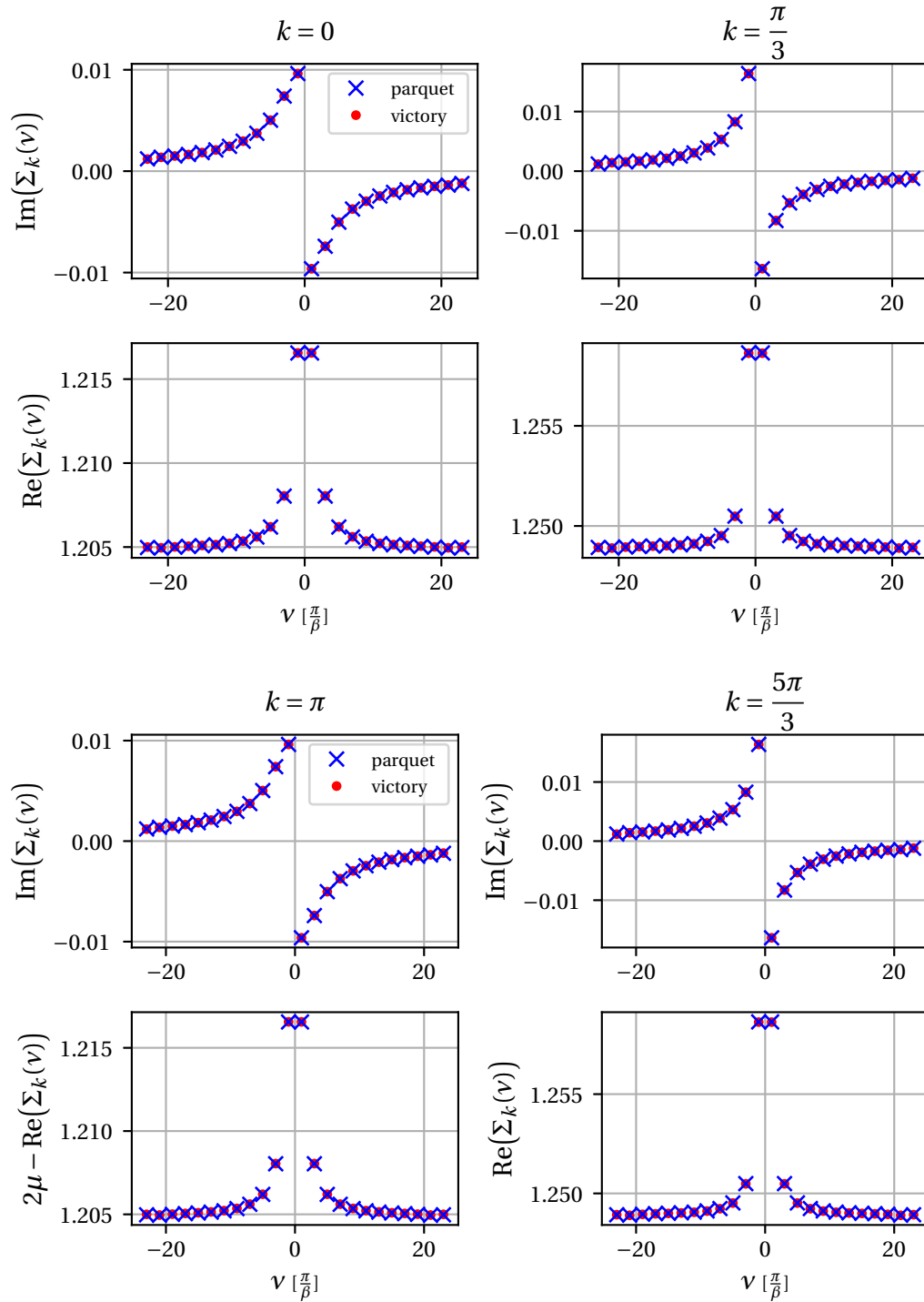


Figure 4.8: $\Sigma_k(\nu)$ with $k=0$ (top, left) and $k=\frac{\pi}{3}$ (top, right), $k=\pi$ (bottom, left) and $k=\frac{5\pi}{3}$ (bottom, right) for $\beta=2.0$, with interaction terms scaled by a factor 0.1.

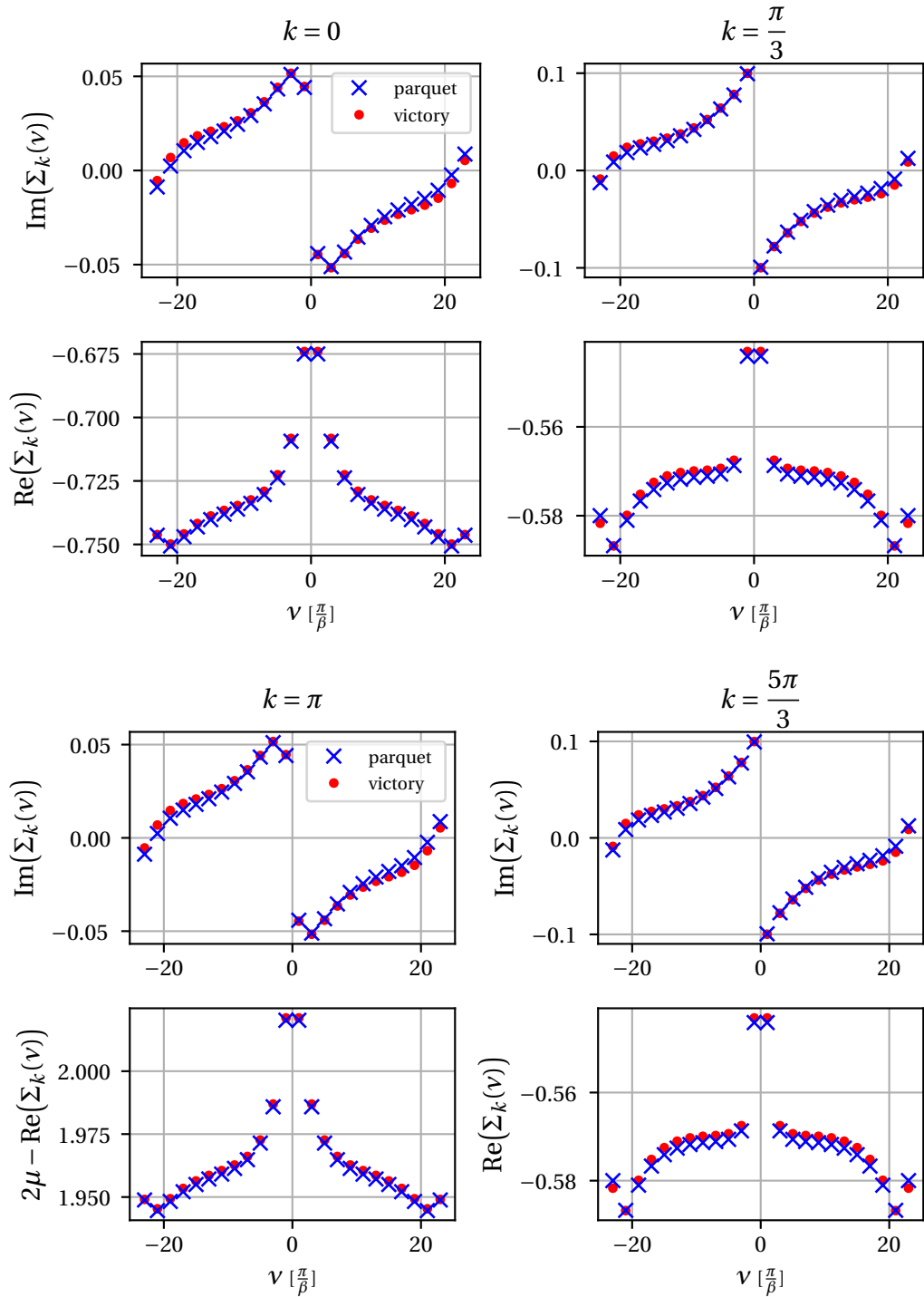


Figure 4.9: $\Sigma_k(\nu)$ with $k = 0$ (top, left) and $k = \frac{\pi}{3}$ (top, right), $k = \pi$ (bottom, left) and $k = \frac{5\pi}{3}$ (bottom, right) for $\beta = 3.0$, with interaction terms scaled by a factor 0.5.

CHAPTER 5

OUTLOOK

As described in the previous lines, we have developed a parquet solver for multi-orbital Hubbard models and applied it to two simple benchmark problems, the Hubbard model in the atomic limit and the benzene molecule.

Before tackling bigger problems with non-local correlations, though, \mathbf{k} -dependence of the vertices has to be implemented in a memory-efficient way. This is feasible with the truncated unity approximation, which was already implemented for a single-orbital parquet solver by [5]. The Schwinger-Dyson equation has to be rewritten to yield contributions not only for the ph-, but also for all other channels – the explicit formulas with asymptotic corrections can be found in appendix A and it is already programmed in multi-orbital-parquet.

The truncated unity approximation assumes that the vertices, for example $\Phi^{\text{ph},\mathbf{k}\mathbf{k}'\mathbf{q}}$ do not depend strongly on \mathbf{k}, \mathbf{k}' , but only on the transfer momentum \mathbf{q} . Another possibility would be to generalize the code to treat all momenta without approximations as in [13]. This would be straightforward: one had to introduce another multi-index with both frequencies ν and momenta \mathbf{k} , with all equations staying the same, except for addition of momenta – here one has to ensure that the sum is always restricted to the first Brillouin zone. Though this generalization can be achieved with not much effort, the truncated unity approximation would be preferable, because the memory requirements for real systems with “full” momentum treatment is out of scope for current hardware.

Concerning memory, there are several ways to make our code more efficient in this regard: one possibility would be the exploitation of the SO(3) symmetry of systems and the usage of the resulting symmetry relations for Green’s functions and vertices in orbital indices.

As we have seen in figure 4.1, correct treatment of the asymptotic frequency-behaviour of vertices in the parquet equation is crucial for convergence. Recently, [25]

proposed a parametrization scheme for high-frequency asymptotics based on diagrammatic analysis. This scheme could replace the scan-edge method in our code, ensuring a consistent frequency treatment in the asymptotic regime.

APPENDICES



Die approbierte gedruckte Originalversion dieser Diplomarbeit ist an der TU Wien Bibliothek verfügbar
The approved original version of this thesis is available in print at TU Wien Bibliothek.

APPENDIX A

CHANNEL-WISE SCHWINGER-DYSON EQUATION

Note that the Schwinger-Dyson equation (3.39) depends only on the full interaction vertex F in the ph-channel, whereas $\overline{\text{ph}}$ - and pp-channels do not contribute. In order to implement the truncated unity scheme for multi-orbital-parquet in a possible future version, a Schwinger-Dyson equation with equal contributions from all channels would be desirable to get non-local contributions also from $\overline{\text{ph}}$ - and pp-channels [4, pp.53–54]. Therefore, we will derive in this appendix expressions for what we call *channel-wise Schwinger-Dyson equation*.

A.1 Time-translation symmetry*

We take equation (3.39) and insert for F^{ph} the parquet equation equation (3.33). Then we get six contributions to self-energy:

$$\Sigma_{i_1 i_2}(\nu) = \Sigma_{i_1 i_2}^{\text{bubble}} + \Sigma_{i_1 i_2}^{U^2}(\nu) + \Sigma_{i_1 i_2}^{\Lambda}(\nu) + \Sigma_{i_1 i_2}^{\text{ph}}(\nu) + \Sigma_{i_1 i_2}^{\overline{\text{ph}}}(\nu) + \Sigma_{i_1 i_2}^{\text{pp}}(\nu). \quad (\text{A.1})$$

The correction terms $\Sigma_{i_1 i_2}^{\text{bubble}}$ (frequency independent) and $\Sigma_{i_1 i_2}^{U^2}(\nu)$ are the same as equations (3.36) and (3.38). For the Λ -contribution we subtract U , as it has the same asymptotics as F , thus we have

$$\Sigma_{i_1 i_2}^{\Lambda}(\nu) = -\frac{1}{2\beta^3} \sum_{\nu', \nu'', \omega} U_{i_1 i_3 i_4 i_5} G_{i_3 i_8}(\nu + \omega) X_{0(i_4 i_5 | i_6 i_7)}^{\text{ph}, \nu' \nu'' \omega} \left(\Lambda_{(i_6 i_7 | i_8 i_2)}^{\text{ph}, \nu'' \nu \omega} - (U_{i_6 i_7 i_8 i_2})_{\nu'' \nu \omega} \right), \quad (\text{A.2})$$

For the ph-contribution we obtain

$$\Sigma_{i_1 i_2}^{\text{ph}}(\nu) = -\frac{1}{2\beta^3} \sum_{\nu', \nu'', \omega} U_{i_1 i_3 i_4 i_5} G_{i_3 i_8}(\nu + \omega) X_{0(i_4 i_5 | i_6 i_7)}^{\text{ph}, \nu' \nu'' \omega} \Phi_{(i_6 i_7 | i_8 i_2)}^{\text{ph}, \nu'' \nu \omega}, \quad (\text{A.3})$$

whereas for the $\overline{\text{ph}}$ -contribution we get

$$\begin{aligned}\Sigma_{i_1 i_2}^{\overline{\text{ph}}}(\nu) &= \frac{1}{2\beta^3} \sum_{\nu', \nu'', \omega} U_{i_1 i_3 i_4 i_5} G_{i_3 i_8}(\nu + \omega) X_{0(i_4 i_5 | i_6 i_7)}^{\text{ph}, \nu' \nu'' \omega} \Phi_{(i_6 i_2 | i_8 i_7)}^{\text{ph}, \nu''(\nu'' + \omega)(\nu - \nu'')} \\ &= \frac{1}{2\beta^3} \sum_{\nu', \nu'', \omega} U_{i_1 i_3 i_4 i_5} G_{i_3 i_8}(\nu + \omega) X_{0(i_4 i_5 | i_6 i_7)}^{\text{ph}, \nu' \nu'' \omega} \Phi_{(i_8 i_7 | i_6 i_2)}^{\text{ph}, (\nu + \omega)\nu(\nu'' - \nu)},\end{aligned}\quad (\text{A.4})$$

where crossing symmetry (3.14a) was used. After relabelling summation indices, we get the same contribution as for ph-channel, therefore we can write

$$\Sigma_{i_1 i_2}^{\text{ph}}(\nu) + \Sigma_{i_1 i_2}^{\overline{\text{ph}}}(\nu) = -\kappa_{\text{ph}} \frac{1}{\beta^3} \sum_{\nu', \nu'', \omega} U_{i_1 i_3 i_4 i_5} G_{i_3 i_8}(\nu + \omega) X_{0(i_4 i_5 | i_6 i_7)}^{\text{ph}, \nu'' \nu \omega} \Phi_{(i_6 i_7 | i_8 i_2)}^{\text{ph}, \nu'' \nu \omega}. \quad (\text{A.5})$$

Finally for the pp-contribution we have

$$\Sigma^{\text{pp}} = -\kappa_{\text{pp}} \frac{1}{\beta^3} \sum_{\nu', \nu'', \omega} U_{(i_1 i_3 | i_4 i_5)}^{\text{pp}} G_{i_8 i_3}(\omega - \nu) X_{0(i_4 i_5 | i_6 i_7)}^{\text{pp}, \nu' \nu'' \omega} \Phi_{(i_6 i_7 | i_8 i_2)}^{\text{pp}, \nu'' \nu \omega}, \quad (\text{A.6})$$

after relabelling summation indices and defining $U_{(i_1 i_2 | i_3 i_4)}^{\text{pp}} := U_{i_1 i_3 i_2 i_4}$.

A.2 SU(2) symmetry*

For additional SU(2) symmetry we proceed as in the section before, but we start now from equation (3.56) and use parquet equations (3.50) and (3.51). The correction terms $\Sigma_{i_1 i_2}^{\text{bubble}}$ and $\Sigma_{i_1 i_2}^{U^2}(\nu)$ are the same as the first and second line in equation (3.56).

For the contribution stemming from the irreducible vertex Λ we get

$$\begin{aligned}\Sigma_{i_1 i_2}^{\Lambda}(\nu) &= -\frac{1}{4\beta^3} \sum_{\nu', \nu'', \omega} G_{i_3 i_8}(\nu + \omega) X_{0(i_4 i_5 | i_6 i_7)}^{\text{ph}, \nu' \nu'' \omega} \\ &\quad \times \left(U_{i_1 i_3 i_4 i_5, \uparrow \uparrow} \left(\Lambda_{(i_6 i_7 | i_8 i_2)}^{\text{d}, \nu'' \nu \omega} + \Lambda_{(i_6 i_7 | i_8 i_2)}^{\text{m}, \nu'' \nu \omega} - 2(U_{i_6 i_7 i_8 i_2, \uparrow \uparrow})^{\nu'' \nu \omega} \right) \right. \\ &\quad \left. + U_{i_1 i_3 i_4 i_5, \uparrow \downarrow} \left(\Lambda_{(i_6 i_7 | i_8 i_2)}^{\text{d}, \nu'' \nu \omega} - \Lambda_{(i_6 i_7 | i_8 i_2)}^{\text{m}, \nu'' \nu \omega} - 2(U_{i_6 i_7 i_8 i_2, \uparrow \downarrow})^{\nu'' \nu \omega} \right) \right).\end{aligned}\quad (\text{A.7})$$

Contributions to ph- and $\overline{\text{ph}}$ -channels have the same form after applying eq. (3.14a):

$$\begin{aligned}\Sigma_{i_1 i_2}^{\text{ph}}(\nu) + \Sigma_{i_1 i_2}^{\overline{\text{ph}}}(\nu) &= -\frac{1}{4\beta^3} \sum_{\nu', \nu'', \omega} G_{i_3 i_8}(\nu + \omega) X_{0(i_4 i_5 | i_6 i_7)}^{\text{ph}, \nu' \nu'' \omega} \left(U_{i_1 i_3 i_4 i_5, \uparrow \uparrow} \left(2\Phi_{(i_6 i_7 | i_8 i_2)}^{\text{d}, \nu'' \nu \omega} + 4\Phi_{(i_6 i_7 | i_8 i_2)}^{\text{m}, \nu'' \nu \omega} \right) \right. \\ &\quad \left. + U_{i_1 i_3 i_4 i_5, \uparrow \downarrow} \left(\Phi_{(i_6 i_7 | i_8 i_2)}^{\text{d}, \nu'' \nu \omega} - 3\Phi_{(i_6 i_7 | i_8 i_2)}^{\text{m}, \nu'' \nu \omega} \right) \right).\end{aligned}\quad (\text{A.8})$$

Finally, for pp-channel we obtain the contribution

$$\begin{aligned} \Sigma_{i_1 i_2}^{\text{pp}}(\nu) = \frac{1}{4\beta^3} \sum_{\nu', \nu'', \omega} G_{i_8 i_3}(\omega - \nu) X_{0(i_4 i_5 | i_6 i_7)}^{\text{pp}, \nu' \nu'' \omega} \left(U_{(i_1 i_3 | i_4 i_5), \uparrow \uparrow}^{\text{pp}} 2\Phi_{(i_6 i_7 | i_8 i_2)}^{t, \nu'' \nu \omega} \right. \\ \left. + U_{(i_1 i_3 | i_4 i_5), \uparrow \downarrow}^{\text{pp}} \left(\Phi_{(i_6 i_7 | i_8 i_2)}^{t, \nu'' \nu \omega} + \Phi_{(i_6 i_7 | i_8 i_2)}^{s, \nu'' \nu \omega} \right) \right). \end{aligned} \quad (\text{A.9})$$

A.3 Asymptotic corrections*

All contributions to channel-wise Schwinger-Dyson equation have the form

$$\frac{1}{\beta^2} \sum_{\omega} G_{i_3 i_8}(\nu + \omega) U_{i_1 i_3 i_4 i_5} \sum_{\nu'} \tilde{\Phi}_{(i_4 i_5 | i_8 i_2)}^{r, \nu' \nu \omega} \quad (\text{A.10})$$

with

$$\tilde{\Phi}_{(i_1 i_2 | i_3 i_4)}^{r, \nu' \nu \omega} = \frac{1}{\beta} \sum_{\nu''} X_{0(i_1 i_2 | i_5 i_6)}^{\text{ph}, \nu' \nu'' \omega} \Phi_{(i_5 i_6 | i_3 i_4)}^{r, \nu'' \nu \omega} \quad (\text{A.11})$$

for channels $r = \text{ph}$ or $r = (\text{d}, \text{m})$ and similiary for the other channels.

We can treat asymptotics for the ν' -summation in the same as we did already for F and Λ with the U^2 -term. To this end we consider $\tilde{\Phi}_{(i_1 i_2 | i_3 i_4)}^{r, \nu \omega} = \Phi_{(i_1 i_2 | i_3 i_4)}^{r, (\nu'' \rightarrow \infty) \nu \omega}$, which can be obtained by Kernel functions (see section 3.5) and replace the reducible vertices in the Schwinger-Dyson equation, which gives us terms of the form

$$\frac{1}{\beta^2} \sum_{\omega} G_{i_3 i_8}(\nu + \omega) U_{i_1 i_3 i_4 i_5} \sum_{\nu'} G_{i_5 i_6}(\nu') G_{i_7 i_4}(\nu' + \omega) \tilde{\Phi}_{(i_6 i_7 | i_8 i_2)}^{r, \nu \omega}. \quad (\text{A.12})$$

As the asymptotic irreducible vertex does not depend on ν' , we can derive an expression for the ν' -summation of the two Green's functions for the ph-channel:

$$\frac{1}{\beta} \sum_{\nu'} G_{i_5 i_6}(\nu') G_{i_7 i_4}(\nu' + \omega) = - \int_0^\beta d\tau e^{i\omega\tau} G_{i_5 i_6}(\tau) G_{i_7 i_4}(\beta - \tau) =: \tilde{X}_{(0 i_4 i_5 | i_6 i_7)}^{\text{ph}, \omega}. \quad (\text{A.13})$$

This a Fourier transformation of two multiplied Green's functions with respect to a bosonic Matsubara frequency ω . After a similar calculation, taking account of the different frequency argument of $G_{i_7 i_4}$ and switched indices, we find for the pp-channel

$$\tilde{X}_{0(i_4 i_5 | i_6 i_7)}^{\text{pp}, \omega} := - \int_0^\beta d\tau e^{-i\omega\tau} G_{i_5 i_6}(\tau) G_{i_4 i_7}(\tau). \quad (\text{A.14})$$

Therefore, we can take account of the asymptotic behaviour of Φ in the channel-

wise Schwinger-Dyson equation for $r = \text{ph}$ or $r = (\text{d}, \text{m})$ by writing

$$\begin{aligned}
& \frac{1}{\beta^2} \sum_{\omega} G_{i_3 i_8}(\nu + \omega) U_{i_1 i_3 i_4 i_5} \sum_{\nu'} \tilde{\Phi}_{(i_4 i_5 | i_8 i_2)}^{r, \nu' \nu \omega} \\
&= \frac{1}{\beta^3} \sum_{\omega} G_{i_3 i_8}(\nu + \omega) U_{i_1 i_3 i_4 i_5} \sum_{\nu' \nu''} X_{0(i_4 i_5 | i_6 i_7)}^{\text{ph}, \nu' \nu'' \omega} (\Phi_{(i_6 i_7 | i_8 i_2)}^{r, \nu'' \nu \omega} - (\bar{\Phi}_{(i_6 i_7 | i_8 i_2)}^{r, \nu \omega})_{\nu''}) \\
&+ \frac{1}{\beta} \sum_{\omega} G_{i_3 i_8}(\nu + \omega) U_{i_1 i_3 i_4 i_5} \tilde{X}_{(0 i_4 i_5 | i_6 i_7)}^{\text{ph}, \omega} \bar{\Phi}_{(i_6 i_7 | i_8 i_2)}^{r, \nu \omega}
\end{aligned} \tag{A.15}$$

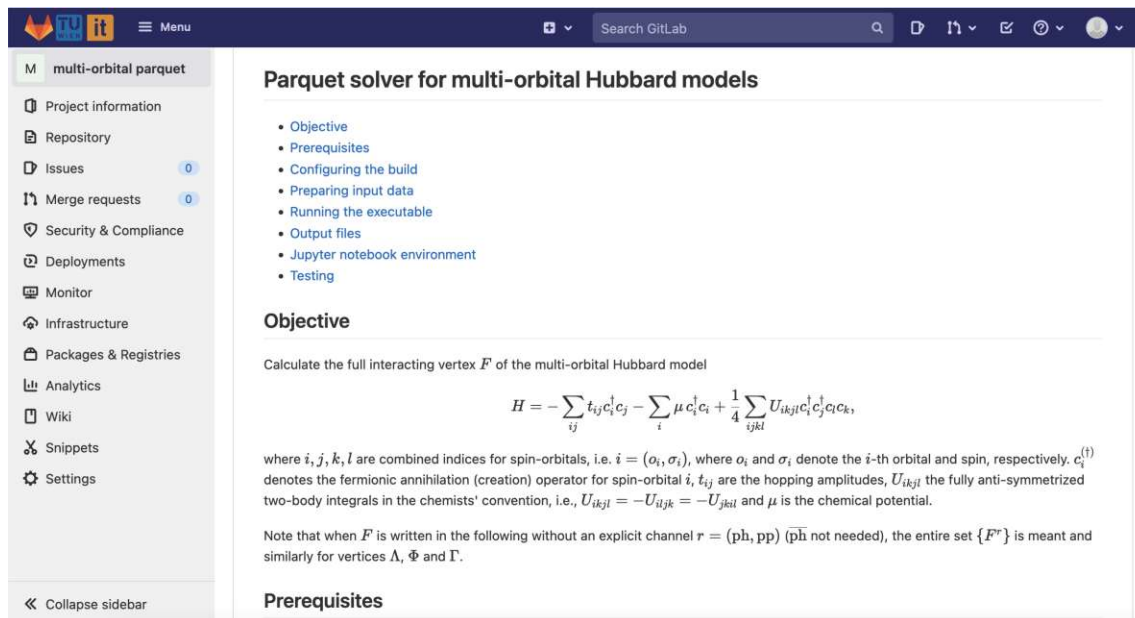
and likewise for $r = \text{pp}$ or $r = (\text{t}, \text{s})$:

$$\begin{aligned}
& \frac{1}{\beta^2} \sum_{\omega} G_{i_8 i_3}(\omega - \nu) U_{(i_1 i_3 | i_4 i_5)}^{\text{pp}} \sum_{\nu'} \tilde{\Phi}_{(i_4 i_5 | i_8 i_2)}^{r, \nu' \nu \omega} \\
&= \frac{1}{\beta^3} \sum_{\omega} G_{i_8 i_3}(\omega - \nu) U_{(i_1 i_3 | i_4 i_5)}^{\text{pp}} \sum_{\nu' \nu''} X_{0(i_4 i_5 | i_6 i_7)}^{\text{pp}, \nu' \nu'' \omega} (\Phi_{(i_6 i_7 | i_8 i_2)}^{r, \nu'' \nu \omega} - (\bar{\Phi}_{(i_6 i_7 | i_8 i_2)}^{r, \nu \omega})_{\nu''}) \\
&+ \frac{1}{\beta} \sum_{\omega} G_{i_8 i_3}(\omega - \nu) U_{(i_1 i_3 | i_4 i_5)}^{\text{pp}} \tilde{X}_{0(i_4 i_5 | i_6 i_7)}^{\text{pp}, \omega} \bar{\Phi}_{(i_6 i_7 | i_8 i_2)}^{r, \nu \omega}.
\end{aligned} \tag{A.16}$$

APPENDIX B

GITLAB DOCUMENTATION

In this appendix we reproduce the README .md on the TUGitLab repository from March 16, 2022 (see figure B.1), in which information about installing and compiling the software multi-orbital-parquet is provided. Furthermore, input and output storage conventions and advanced parameters are explained.



The screenshot shows the GitLab interface for the repository 'multi-orbital-parquet'. The main content area displays the README for the 'Parquet solver for multi-orbital Hubbard models'. The README includes a table of contents with links to sections: Objective, Prerequisites, Configuring the build, Preparing input data, Running the executable, Output files, Jupyter notebook environment, and Testing. The 'Objective' section is expanded, showing the text: 'Calculate the full interacting vertex F of the multi-orbital Hubbard model' followed by the equation
$$H = - \sum_{ij} t_{ij} c_i^\dagger c_j - \sum_i \mu c_i^\dagger c_i + \frac{1}{4} \sum_{ijkl} U_{ijkl} c_i^\dagger c_j^\dagger c_l c_k,$$
 and a paragraph explaining the variables. The 'Prerequisites' section is also visible at the bottom.

Figure B.1: (a) Part of README .md as rendered on the TUGitLab repository.

Parquet solver for multi-orbital Hubbard models

- Objective
- Prerequisites
- Configuring the build
- Preparing input data
- Running the executable
- Output files
- Jupyter notebook environment
- Testing

Objective

Calculate the full interacting vertex F of the multi-orbital Hubbard model

$$H = - \sum_{ij} t_{ij} c_i^\dagger c_j - \sum_i \mu c_i^\dagger c_i + \frac{1}{4} \sum_{ijkl} U_{ijkl} c_i^\dagger c_j^\dagger c_l c_k,$$

where i, j, k, l are combined indices for spin-orbitals, i.e. $i = (o_i, \sigma_i)$, where o_i and σ_i denote the i -th orbital and spin, respectively. $c_i^{(\dagger)}$ denotes the fermionic annihilation (creation) operator for spin-orbital i , t_{ij} are the hopping amplitudes, U_{ijkl} the fully anti-symmetrized two-body integrals in the chemists' convention, i.e., $U_{ijkl} = -U_{iljk} = -U_{jkil}$ and μ is the chemical potential.

Note that when F is written in the following without an explicit channel $r = (\text{ph}, \text{pp})$ ($\overline{p\hbar}$ not needed) or with $\text{SU}(2)$ symmetry $r = (\text{d}, \text{m}, \text{s}, \text{t})$, the entire set $\{F^r\}$ is meant and similarly for vertices Λ , Φ and Γ .

Prerequisites

- HDF5
- LAPACK
- MPI
- CMake (>3.15.1)
- Python (>3.8)

The `hdf5_wrapper` by Matthias Pickem is already provided in `src/hdf5_wrapper` and will be installed automatically.

See `HowToVSC.md` for detailed instructions for how to use the solver on the VSC cluster.

Configuring the build

Build in the project root directory with

```
1 $ cd multi-orbital-parquet
2 $ cmake -B build -DCMAKE_BUILD_TYPE=Release
3 $ cmake --build build
```

The generated executable can be found in `bin/`. To enable compiler options for debugging use `-DCMAKE_BUILD_TYPE=Debug` instead.

Preparing input data

The solver reads the `parameters.ini` and HDF5 files as input from `input/`. There are helper scripts and notebooks in that folder that allow to generate the input files based on different preconfigured setups. A Python environment is necessary for using them. Setting up a Python environment is explained below.

Following model parameters must be set in `parameters.ini`:

Parameter name	Type	Description	Condition
<code>N_ORBITAL</code>	<code>int32</code>	# orbitals	<code>> 0</code>
<code>N_F</code>	<code>int32</code>	# fermionic Matsubara frequencies	even, <code>> 0</code>
<code>N_B</code>	<code>int32</code>	# bosonic Matsubara frequencies	integer multiple of <code><n_tasks></code> , <code>> 0</code>
<code>MAX_ITE</code>	<code>int32</code>	maximum # iterations	<code>> 0</code>
<code>BETA</code>	<code>real64</code>	inverse temperature β	<code>>= 1.0e-16</code>
<code>MU</code>	<code>real64</code>	chemical potential μ	

Following advanced parameters can be set in `parameters.ini` (if not set, default values are taken):

Parameter name	Type	Description	Default value
<code>SU2_BOOL</code>	<code>logical</code>	flag for calculating with SU(2) symmetry	<code>.true.</code>

Parameter name	Type	Description	Default value
ALL_SELF_ENERGIES_BOOL	logical	output flag for storing Σ for every iteration step permanently	.false.
ALL_G_TAU_BOOL	logical	output flag for storing $G_{i,j}(\tau_i, \tau_j)$ for every iteration step permanently	.false.
READ_IN_LAMBDA_PHI_BOOL	logical	input flag for Λ and Φ	.false.
READ_IN_LAMBDA_ONLY_BOOL	logical	input flag for Λ only	.false.
ABS_TOL_SIGMA_MEAN	real64	convergence parameter for Σ	1.0e-8
ABS_TOL_SIGMA_MAX	real64	convergence parameter for Σ	1.0e-7
REL_TOL_SIGMA	real64	convergence parameter for Σ	1.0e-6
ABS_TOL_F	real64	convergence parameter for F	1.0e-7
REL_TOL_F	real64	convergence parameter for F	1.0e-6
ALPHA_MIX	real64	mixing parameter for Φ	0.4

<n_tasks> (and N_TASKS) denotes the number of processes launched when calling `mpirun` (see also below).

From these values the following constants are calculated:

$$\begin{aligned}
N_SPIN &= 2, \\
N_SPIN_EFFECTIVE &= 2 \text{ or } 1, \text{ depending on } SU2_BOOL, \\
CHUNK_SIZE &= \frac{N_B}{N_TASKS}, \\
N_SO &= N_SPIN_EFFECTIVE \times N_ORBITAL, \\
N_SO2 &= N_SO \times N_SO, \\
N_MAX &= N_SO2 \times N_F.
\end{aligned}$$

Note that `N_SPIN_EFFECTIVE` denotes the effective number of spins. When the calculations are performed with $SU(2)$ symmetry, this number is set to 1 and the memory consumption is considerably smaller.

Furthermore, the arrays `u_matrix` and `h0` always have to be provided. They have to be stored as `u_matrix_input.hdf5` and `h0_input.hdf5` respectively, in the convention described in the next sections. Input arrays `u_matrix` and `h0` always have the same size, regardless of `SU2_BOOL`. Note that all input arrays have to be stored in *column-major order*.

Input convention for `u_matrix_input.hdf5`

`u_matrix_input.hdf5` contains the dataset `u_matrix` which consists of a `complex(128)` $((N_ORBITAL \times N_SPIN)^2, (N_ORBITAL \times N_SPIN)^2)$ -array. `u_matrix` stores the interaction matrix U_{ikjl} of the multi-orbital Hubbard model. To store U_{ikjl} as a two-dimensional array `u_matrix`, combined indices $i' = g(i, k)$ and $j' = g(j, l)$ are introduced (which are not tuples, but ordinary integers). We use them to construct a matrix $\tilde{U}_{i'j'}$ which has the same structure as `u_matrix`. Remember that the indices i, j, k, l are spin-orbital indices and therefore tuples, so $i' = g((o_i, \sigma_i), (o_k, \sigma_k))$ and analogously for j' . The function g is defined by

$$\begin{aligned}
g((o_i, \sigma_i), (o_k, \sigma_k)) &= \sigma_i + N_SPIN(o_i - 1) \\
&+ N_SPIN \times N_ORBITAL((\sigma_k - 1) + N_SPIN(o_k - 1)).
\end{aligned}$$

Here, spins were replaced as $\uparrow = 1$ and $\downarrow = 2$. Thus,

$$\begin{aligned}
g((1, \uparrow), (1, \uparrow)) &= 1, \\
g((1, \downarrow), (1, \uparrow)) &= 2, \\
g((2, \uparrow), (1, \uparrow)) &= 3, \\
&\vdots \\
g((1, \uparrow), (1, \downarrow)) &= N_SO + 1
\end{aligned}$$

and so on. There exists also an inverse function with $g_i^{-1}(i') = i$ and $g_k^{-1}(i') = k$. $\tilde{U}_{i'j'} = U_{g_i^{-1}(i')g_k^{-1}(i')g_j^{-1}(j')g_l^{-1}(j')}$ is stored in `u_matrix`.

Input convention for `h0_input.hdf5`

`h0_input.hdf5` contains the dataset `h0` which consists of a `complex(128)` ($N_ORBITAL \times N_SPIN, N_ORBITAL \times N_SPIN$)-array. `h0` stores the hopping matrix t_{ij} of the multi-orbital Hubbard model. Remember that i, j are spin-orbital indices and thus tuples, i.e. $i = (o_i, \sigma_i)$. Formally we introduce again combined indices $i' = h(i)$ and $j' = h(j)$, where h is defined by

$$h((o_i, \sigma_i)) = \sigma_i + N_SPIN(o_i - 1).$$

There exists also the inverse function with $h^{-1}(i') = i$ and $h^{-1}(j') = k$. $\tilde{t}_{i'j'} = t_{h^{-1}(i')h^{-1}(j')}$ is finally stored in `h0`.

Input flags

Depending on the set input flags, one has to provide additional `.hdf5`-files as input. The self-energy is always initialized as $\Sigma = 0$.

Case 1: `READ_IN_LAMBDA_PHI_BOOL` and `READ_IN_LAMBDA_ONLY_BOOL` both set to `.false.` No further input files needed. The vertices are initialized as

- F as lowest-order approximation
- $\Lambda = F$,
- $\Phi = 0$,
- $\Gamma = F$.

Case 2: READ_IN_LAMBDA_ONLY_BOOL set to .true. When this flag is activated, Λ (possibly obtained from a DGA calculation) has to be additionally provided. The size of these input arrays depends on SU2_BOOL.

SU2_BOOL set to false Here, $\Lambda_{(ij|lp)}^{\text{ph}, \nu_n \nu'_m \omega_k}$ and $\Lambda_{(ij|lp)}^{\text{pp}, \nu_n \nu'_m \omega_k}$ are distributed in ω_k -chunks between the launched processes. Therefore, every launched process with MPI identifier $\langle \text{id} \rangle$ (or in mathematical notation $\text{ID} = 0, \dots, \text{N_TASKS} - 1$) must be provided with a file `lambda_input- $\langle \text{id} \rangle$.hdf5` with datasets `lambda_ph` and `lambda_pp`, where $\langle \text{id} \rangle$ needs to be formatted as a three-digit integer. Every dataset consists of a `complex(128)` (`N_MAX, N_MAX, CHUNK_SIZE`)-array and stores a portion of the full vertex, $\Lambda_{(ij|lp)}^{\text{ph/pp}, \nu_n \nu'_m \omega_{\tilde{k}}}$ for `CHUNK_SIZE` values $\omega_{\tilde{k}}$, where

$$\tilde{k} = \text{CHUNK_SIZE} \times \text{ID}, \dots, \text{CHUNK_SIZE} \times (\text{ID} + 1) - 1.$$

As an example, take `N_B = 10` and `N_TASKS = 5`, then `CHUNK_SIZE = 2`. According to the formula above, the process with `ID = 0` has to be provided with `lambda_input-000.hdf5` which stores $\Lambda_{(ij|lp)}^{\text{ph/pp}, \nu_n \nu'_m \omega_{\tilde{k}}}$ with $\tilde{k} = 0, 1$ (all other indices n, m, i, j, l, p span their full range), and similarly for the remaining four processes.

Note that $\omega_k = \frac{2k}{\beta} \pi$ and $\nu_n = \frac{2n - \text{N_F} - 1}{\beta} \pi$, which is different from the usual definition of the fermionic Matsubara frequency.

To store the vertices with as three-dimensional arrays, we introduce the index $k' = f(\tilde{k})$ and the combined indices $i' = s(i, j, \nu_n)$ and $j' = s(l, p, \nu'_m)$, with

$$\begin{aligned} f(\tilde{k}) &= \tilde{k} - \text{CHUNK_SIZE} \times \text{ID} + 1, \quad \text{and} \\ s((o_i, \sigma_i), (o_j, \sigma_j), \nu_n) &= \sigma_i + \text{N_SPIN_EFFECTIVE}(o_i - 1) \\ &\quad + \text{N_SO}((\sigma_j - 1) + \text{N_SPIN_EFFECTIVE}(o_j - 1) + \text{N_SO}(n - 1)). \end{aligned}$$

Also the corresponding inverse functions exist with $s_i^{-1}(i') = i$, $s_k^{-1}(j') = j$, $s_n^{-1}(j') = n$ and $f^{-1}(k') = \tilde{k}$. $\tilde{\Lambda}_{i'j'k'}^{\text{ph}} = \Lambda_{(s_i^{-1}(i')s_j^{-1}(j')|s_l^{-1}(j')s_p^{-1}(j'))}^{\text{ph}, \nu_{s_n^{-1}(i')} \nu'_{s_m^{-1}(j')} \omega_{f^{-1}(k')}}$ is stored in `lambda_ph`, and analogously the vertex for the pp-channel.

The remaining vertices are initialized as

- $\Gamma = \Lambda$,
- F as lowest-order approximation,
- Φ with the Bethe-Salpeter equation.

SU2_BOOL set to .true. As written in the previous section, the vertices $\Lambda_{(ij|lp)}^{r, \nu_n \nu'_m \omega_k}$, $r = d, m, s, t$) are distributed in ω_k -chunks between the launched processes. Again, every process with MPI identifier $\langle id \rangle$ must be provided with a file `lambda_input- $\langle id \rangle$.hdf5`, but now with datasets `lambda_d`, `lambda_m`, `lambda_s` and `lambda_t`.

In the $SU(2)$ -symmetric case, `N_SPIN_EFFECTIVE = 1` and we no longer have to take spin variables σ_i into account. Therefore, spin-orbital indices are no longer tuples, but scalars (they are just the orbital indices). Consequently, we have to modify the function $s(i, j, \nu_n) = s(o_i, o_j, \nu_n)$ such that

$$s(o_i, o_j, \nu_n) = o_i + N_ORBITAL((o_j - 1) + N_ORBITAL(n - 1)).$$

to store the vertices as three-dimensional arrays in the $SU(2)$ -symmetric case, whereas $f(\vec{k})$ remains unchanged. By means of the inverse functions, which can be defined in the same manner as in the previous section, the vertices have to be stored in datasets `lambda_d`, `lambda_m`, `lambda_s` and `lambda_t`. The initialization of the remaining vertices is the same as described above.

Case 3: READ_IN_LAMBDA_PHI_BOOL set to .true. Here, $\Lambda_{(ij|lp)}^{ph, \nu_n \nu'_m \omega_k}$, $\Lambda_{(ij|lp)}^{pp, \nu_n \nu'_m \omega_k}$, $\Phi_{(ij|lp)}^{ph, \nu_n \nu'_m \omega_k}$ and $\Phi_{(ij|lp)}^{pp, \nu_n \nu'_m \omega_k}$ must be provided as datasets `lambda_ph` and `lambda_pp` in files `lambda_input- $\langle id \rangle$.hdf5` as well as `phi_ph` and `phi_pp` in files `phi_input- $\langle id \rangle$.hdf5`, and analogously for the channels in the $SU(2)$ -symmetric case. The storage convention depends again on `SU2_BOOL` and is the same as described in the previous section.

The remaining vertices are initialized as

- F with the Parquet equation,
- $\Gamma = F - \Phi$.

Convergence parameters

Convergence is attained when the following conditions are fulfilled:

$$\begin{aligned} \langle |\Sigma^{(i)} - \Sigma^{(i-1)}| \rangle &< \text{ABS_TOL_SIGMA_MEAN}, \\ \max(|\Sigma^{(i)} - \Sigma^{(i-1)}|) &< \text{ABS_TOL_SIGMA_MAX}, \\ \max\left(\frac{|\Sigma^{(i)} - \Sigma^{(i-1)}|}{|\Sigma^{(i)}|}\right) &< \text{REL_TOL_SIGMA}, \\ \max_{\text{ID}}(|\max(F_{\text{ID}}^{r(i)}) - \max(F_{\text{ID}}^{r(i-1)})|) &< \text{ABS_TOL_F}, \\ \max_{\text{ID}}\left(\frac{|\max(F_{\text{ID}}^{r(i)}) - \max(F_{\text{ID}}^{r(i-1)})|}{|\max(F_{\text{ID}}^{r(i)})|}\right) &< \text{REL_TOL_F}, \end{aligned}$$

for the i -th iteration step and $r = (\text{ph}, \text{pp})$ or $(\text{d}, \text{m}, \text{s}, \text{t})$, $\langle \cdot \rangle$ being the mean value and $|\cdot|$ the element-wise absolute value. When all elements of $\Sigma^{(i)}$ or $F^{r(i)}$ are close to zero, then convergence is determined only by absolute tolerances.

Mixing parameter

After the Bethe-Salpeter equation is performed, the newly obtained Φ is mixed with the one from the previous iteration step, such that for the i -th iteration step

$$\Phi^{(i)} \leftarrow \text{ALPHA_MIX} \times \Phi^{(i-1)} + (1 - \text{ALPHA_MIX}) \times \Phi^{(i)}.$$

Mixing improves the convergence of the algorithm. It is recommended to use similar values for ALPHA_MIX as the default one.

Running the executable

Run the executable in the project root directory with suitable `<n_tasks>` (must be commensurate with `N_B`) by

```
1 $ mpirun -np <n_tasks> ./bin/multi-orbital-parquet.out
```

All paths in the code are set relative to the project root directory. The generated output is written to `output/`.

Output files

General data

After reading in `parameters.ini`, the program saves the following parameters to `general_data.hdf5`:

Parameter	Dataset name	Type
N_ORBITAL	general/n_orbital	int32
N_F	general/n_f	int32
N_B	general/n_b	int32
BETA	general/beta	real64

Parameter	Dataset name	Type
MU	general/mu	real64
N_TASKS	general/n_tasks	int32

Vertices

After every iteration, the newest calculated vertices F and Φ are stored as `f-<id>.hdf5` and `phi-<id>.hdf5` respectively, where every process with MPI identifier `<id>` (formatted as three-digit integer) writes a file for a certain ω_k -chunk. Vertices of the previous iteration step are moved to `f-old-<id>.hdf5` and `phi-old-<id>.hdf5`. If the calculation is interrupted, this output scheme guarantees that the calculation can be continued with the latest vertex (and self-energy values).

Every file contains datasets `f/f_ph` and `f/f_pp` or `phi/phi_ph` and `phi/phi_pp` respectively (or for SU(2) symmetry the corresponding channels `d, m, s, t`), each consisting of a `complex(128)` (`N_MAX, N_MAX, CHUNK_SIZE`)-array.

The storage convention for the vertices F and Φ is the same as for the irreducible ones.

In addition to that, every `.hdf5` file also contains attributes `f/ite` or `phi/ite` respectively, which store the iteration step as an `integer`.

Self-energy

The self-energy $\Sigma_{ij}(\nu_n)$ is stored after every iteration in a similar fashion as the vertices. If `ALL_SELF_ENERGIES_BOOL` is set to `.true.`, the self-energy is stored permanently for every iteration step `<ite>` (formatted as three-digit integer) as `sigma-<ite>.hdf5` and the last one is stored as `sigma.hdf5`.

In contrast to the vertices, the self-energy is not split-up in chunks, but comprises the full fermionic Matsubara range $\nu_n = \frac{2n-N_F-1}{\beta}\pi$, with $n = 1, \dots, N_F$. Therefore, the files contain a dataset `sigma` which consists of a `complex128` (`N_SO, N_SO, N_F`)-array.

The storage convention for the first two dimensions is the same as for `h0_input.hdf5`, so we introduce again combined indices $i' = h(o_i, \sigma_i)$ and $j' = h(o_j, \sigma_j)$ with h defined as above, i and j are again spin-orbital indices. For the third dimension we leave the index n unchanged. Thus, $\Sigma_{i'j'n}$ is finally stored in `sigma`.

Additionally, the self-energy `.hdf5` files also contain an attribute `sigma/ite`, which stores the iteration step as an `integer`.

One-particle Green's function

The one-particle Green's function $G_{i,j}(\tau_i, \tau_j)$, i, j denoting spin-orbital indices, is stored after every iteration in a similar fashion to the self-energy. If `ALL_G_TAU_BOOL` is set to `.true.` $G_{i,j}(\tau_i, \tau_j)$ is stored permanently for every iteration step `<ite>` (formatted as three-digit integer) as `g_tau-<ite>.hdf5` and the last one is stored as `g_tau.hdf5`.

The file contains a dataset `g_tau` which consists of a `complex128` (`N_SO, N_SO, N_F`)-array. The storage convention is the same as for the self-energy. The third dimension is to be seen as the values for $\tau = \frac{l-1}{N_F-1}\beta$, with $l = 1, \dots, N_F$. Additionally, the one particle Green's function's `.hdf5` files also contain an attribute `g_tau/ite`, which stores the iteration step as an `integer`.

$G_{i,j}(\tau_i, \tau_j)$ is related to the occupation number n_l for a given spin-orbital l via

$$n_l = \langle [c_l^\dagger(\tau)c_l(\tau)] \rangle = -G_{l,l}(\beta^-) = \frac{1}{\beta} \sum_{\nu} e^{-i\nu\tau} \tilde{G}_{l,l}(\nu).$$

Jupyter notebook environment

To use the Python scripts and Jupyter notebooks included in `input` and `notebooks/` a Python environment with the packages specified in `pip-requirements.txt` needs to be configured and enabled.

For Python venv:

```
1 $ python -m venv path/to/my_venv
2 $ source path/to/my_venv/bin/activate
3 $ pip install -r pip-requirements.txt
```

For anaconda:

```
1 $ conda create -n my_venv python --file pip-requirements.txt
2 $ conda activate my_venv
```

Testing

Tests are provided which check the code against the atomic limit (single-site, single-orbital Hubbard model). The user has to set the internal flag `TEST_B00L` in `parameters.f90` to `.true.`, then special test parameters located in `test/` are used, which should not be changed and the user is asked in terminal, if tests should be performed with $SU(2)$ symmetry. Furthermore, for both symmetry settings notebooks for visualization and checking symmetries are included in `notebooks/atomic_limit_comparison`. The numerical results of the core solver are checked against the analytic results of Phys. Rev. B, 98, 235107 (2018) in the notebooks.



Die approbierte gedruckte Originalversion dieser Diplomarbeit ist an der TU Wien Bibliothek verfügbar
The approved original version of this thesis is available in print at TU Wien Bibliothek.

BIBLIOGRAPHY

- [1] K. Astleithner, A. Kauch, T. Ribic, and K. Held, “Parquet dual fermion approach for the Falicov-Kimball model”, *Phys. Rev. B*, vol. 101, no. 165101, 16 Apr. 2020. DOI: [10.1103/PhysRevB.101.165101](https://doi.org/10.1103/PhysRevB.101.165101). [Online]. Available: <https://link.aps.org/doi/10.1103/PhysRevB.101.165101> (cit. on p. 2).
- [2] C. De Dominicis and P. C. Martin, “Stationary entropy principle and renormalization in normal and superfluid systems. II. Diagrammatic formulation”, *J. Math. Phys.*, vol. 5, no. 1, pp. 31–59, 1964. DOI: [10.1063/1.1704064](https://doi.org/10.1063/1.1704064) (cit. on pp. I, III, 2, 40).
- [3] I. T. Diatlov, V. V. Sudakov, and K. A. Ter-Martirosian, “Asymptotic meson-meson scattering theory”, *Soviet Phys. JETP*, vol. 5, Nov. 1957. [Online]. Available: <https://www.osti.gov/biblio/4338008> (cit. on pp. I, III, 2).
- [4] C. J. Eckhardt, “Making the parquet equations feasible – Truncated unity method with application to the 2D Hubbard model”, M.S. thesis, RWTH Aachen, 2019 (cit. on pp. 40, 41, 59).
- [5] C. J. Eckhardt, C. Honerkamp, K. Held, and A. Kauch, “Truncated unity parquet solver”, *Phys. Rev. B*, vol. 101, no. 155104, 15 Apr. 2020. DOI: [10.1103/PhysRevB.101.155104](https://doi.org/10.1103/PhysRevB.101.155104). [Online]. Available: <https://link.aps.org/doi/10.1103/PhysRevB.101.155104> (cit. on pp. 2, 55).
- [6] A. Galler, P. Thunström, P. Gunacker, J. M. Tomczak, and K. Held, “Ab initio dynamical vertex approximation”, *Phys. Rev. B*, vol. 95, no. 115107, 11 Mar. 2017. DOI: [10.1103/PhysRevB.95.115107](https://doi.org/10.1103/PhysRevB.95.115107). [Online]. Available: <http://link.aps.org/doi/10.1103/PhysRevB.95.115107> (cit. on p. 1).
- [7] A. Georges, G. Kotliar, W. Krauth, and M. J. Rozenberg, “Dynamical mean-field theory of strongly correlated fermion systems and the limit of infinite dimensions”, *Rev. Mod. Phys.*, vol. 68, pp. 13–125, 1 Jan. 1996. DOI: [10.1103/RevModPhys.68](https://doi.org/10.1103/RevModPhys.68).

13. [Online]. Available: <https://link.aps.org/doi/10.1103/RevModPhys.68.13> (cit. on p. 1).
- [8] H. Hafermann, E. G. C. P. van Loon, M. I. Katsnelson, A. I. Lichtenstein, and O. Parcollet, “Collective charge excitations of strongly correlated electrons, vertex corrections, and gauge invariance”, *Phys. Rev. B*, vol. 90, no. 235105, 23 Dec. 2014. DOI: [10.1103/PhysRevB.90.235105](https://doi.org/10.1103/PhysRevB.90.235105). [Online]. Available: <https://link.aps.org/doi/10.1103/PhysRevB.90.235105> (cit. on p. 1).
- [9] A. Kauch, P. Pudleiner, K. Astleithner, P. Thunström, T. Ribic, and K. Held, “Generic optical excitations of correlated systems: π -tons”, *Phys. Rev. Lett.*, vol. 124, no. 047401, 4 Jan. 2020. DOI: [10.1103/PhysRevLett.124.047401](https://doi.org/10.1103/PhysRevLett.124.047401). [Online]. Available: <https://link.aps.org/doi/10.1103/PhysRevLett.124.047401> (cit. on p. 2).
- [10] J. Kaufmann, C. Eckhardt, M. Pickem, M. Kitatani, A. Kauch, and K. Held, “Self-consistent ladder dynamical vertex approximation”, *Physical Review B*, vol. 103, no. 3, Jan. 2021, ISSN: 2469-9969. DOI: [10.1103/physrevb.103.035120](https://doi.org/10.1103/PhysRevB.103.035120). [Online]. Available: <http://dx.doi.org/10.1103/PhysRevB.103.035120> (cit. on p. 40).
- [11] J. Kuneš, “Efficient treatment of two-particle vertices in dynamical mean-field theory”, *Phys. Rev. B*, vol. 83, no. 085102, 8 Feb. 2011. DOI: [10.1103/PhysRevB.83.085102](https://doi.org/10.1103/PhysRevB.83.085102). [Online]. Available: <https://link.aps.org/doi/10.1103/PhysRevB.83.085102> (cit. on p. 1).
- [12] —, “Wannier functions and construction of model Hamiltonians”, in *The LDA+DMFT approach to strongly correlated materials*, E. Pavarini, E. Koch, D. Vollhardt, and A. Lichtenstein, Eds., ser. Modeling and Simulation, Forschungszentrum Jülich, vol. 1, 2011 (cit. on p. 6).
- [13] G. Li, A. Kauch, P. Pudleiner, and K. Held, “The victory project v1.0: An efficient parquet equations solver”, *Comput. Phys. Commun*, vol. 241, pp. 146–154, 2019, ISSN: 0010-4655. DOI: <https://doi.org/10.1016/j.cpc.2019.03.008>. [Online]. Available: <http://www.sciencedirect.com/science/article/pii/S0010465519300864> (cit. on pp. I, III, 2, 43, 50, 55).

- [14] N. Lin, E. Gull, and A. J. Millis, “Two-particle response in cluster dynamical mean-field theory: Formalism and application to the Raman response of high-temperature superconductors”, *Phys. Rev. Lett.*, vol. 109, no. 106401, 10 Sep. 2012. DOI: [10.1103/PhysRevLett.109.106401](https://doi.org/10.1103/PhysRevLett.109.106401). [Online]. Available: <https://link.aps.org/doi/10.1103/PhysRevLett.109.106401> (cit. on p. 1).
- [15] J. Otsuki, H. Hafermann, and A. I. Lichtenstein, “Superconductivity, antiferromagnetism, and phase separation in the two-dimensional Hubbard model: A dual-fermion approach”, *Phys. Rev. B*, vol. 90, no. 235132, 23 Dec. 2014. DOI: [10.1103/PhysRevB.90.235132](https://doi.org/10.1103/PhysRevB.90.235132). [Online]. Available: <https://link.aps.org/doi/10.1103/PhysRevB.90.235132> (cit. on p. 1).
- [16] P. Pudleiner, P. Thunström, A. Valli, A. Kauch, G. Li, and K. Held, “Parquet approximation for molecules: Spectrum and optical conductivity of the Pariser-Parr-Pople model”, *Phys. Rev. B*, vol. 99, no. 125111, 12 Mar. 2019. DOI: [10.1103/PhysRevB.99.125111](https://doi.org/10.1103/PhysRevB.99.125111). [Online]. Available: <https://link.aps.org/doi/10.1103/PhysRevB.99.125111> (cit. on p. 2).
- [17] P. Pudleiner, “One- and two-particle vertex functions within Monte Carlo and parquet calculations of correlated electron systems”, Ph.D. dissertation, Technische Universität Wien, 2019. DOI: [10.34726/hss.2019.35565](https://doi.org/10.34726/hss.2019.35565) (cit. on p. 50).
- [18] P. Pudleiner, A. Kauch, K. Held, and G. Li, “Competition between antiferromagnetic and charge density wave fluctuations in the extended Hubbard model”, *Phys. Rev. B*, vol. 100, no. 075108, 7 Aug. 2019. DOI: [10.1103/PhysRevB.100.075108](https://doi.org/10.1103/PhysRevB.100.075108). [Online]. Available: <https://link.aps.org/doi/10.1103/PhysRevB.100.075108> (cit. on p. 2).
- [19] G. Rohringer, “New routes towards a theoretical treatment of nonlocal electronic correlations”, Ph.D. dissertation, Technische Universität Wien, 2013. DOI: [10.34726/hss.2013.21498](https://doi.org/10.34726/hss.2013.21498) (cit. on pp. 5, 10, 12, 13, 14, 23, 25, 27).
- [20] G. Rohringer, A. Valli, and A. Toschi, “Local electronic correlation at the two-particle level”, *Phys. Rev. B*, vol. 86, no. 125114, 12 Sep. 2012. DOI: [10.1103/PhysRevB.86.125114](https://doi.org/10.1103/PhysRevB.86.125114). [Online]. Available: <https://link.aps.org/doi/10.1103/PhysRevB.86.125114> (cit. on p. 1).

- [21] K.-M. Tam, H. Fotso, S.-X. Yang, T.-W. Lee, J. Moreno, J. Ramanujam, and M. Jarrell, “Solving the parquet equations for the Hubbard model beyond weak coupling”, *Phys. Rev. E*, vol. 87, no. 013311, 1 Jan. 2013. DOI: [10.1103/PhysRevE.87.013311](https://doi.org/10.1103/PhysRevE.87.013311). [Online]. Available: <https://link.aps.org/doi/10.1103/PhysRevE.87.013311> (cit. on pp. 43, 45).
- [22] P. Thunström, O. Gunnarsson, S. Ciuchi, and G. Rohringer, “Analytical investigation of singularities in two-particle irreducible vertex functions of the Hubbard atom”, *Physical Review B*, vol. 98, no. 23, 2018. DOI: [10.1103/PhysRevB.98.235107](https://doi.org/10.1103/PhysRevB.98.235107) (cit. on pp. 45, 47).
- [23] M. Wallerberger, A. Kauch, H. Shinaoka, and J. Mangott, “Parquet equations in the multi-orbital case”, Oct. 2021 (cit. on pp. 2, 8, 10, 23, 27, 30).
- [24] M. Wallerberger, H. Shinaoka, and A. Kauch, “Solving the Bethe-Salpeter equation with exponential convergence”, *Phys. Rev. Research*, vol. 3, no. 033168, 3 Aug. 2021. DOI: [10.1103/PhysRevResearch.3.033168](https://doi.org/10.1103/PhysRevResearch.3.033168). [Online]. Available: <https://link.aps.org/doi/10.1103/PhysRevResearch.3.033168> (cit. on pp. 45, 46).
- [25] N. Wentzell, G. Li, A. Tagliavini, C. Taranto, G. Rohringer, K. Held, A. Toschi, and S. Andergassen, “High-frequency asymptotics of the vertex function: Diagrammatic parametrization and algorithmic implementation”, *Physical Review B*, vol. 102, no. 8, 2020. DOI: [10.1103/PhysRevB.102.085106](https://doi.org/10.1103/PhysRevB.102.085106) (cit. on pp. 36, 43, 55).

ACKNOWLEDGEMENTS

I want to thank my supervisor Univ. Prof. Dr. Karsten Held for giving me the opportunity to write my diploma thesis in his group.

Many thanks to Univ. Ass. Dr. Anna Kauch for her close supervision, her commitment and contagious enthusiasm for solid-state physics. I am also grateful for her critical reading of this thesis.

I had the honor to co-supervise the project thesis of my fellow student Kayran Schmidt. Thank you for the excellent work and the many fruitful discussions.

Thanks to Patrick Kappl for giving me a course in drawing Feynman diagrams with Inkscape.

The computational results presented in section 4.2 have been achieved using the Vienna Scientific Cluster (VSC).

Last but not least, I owe my family a great debt of gratitude for their support and advice.